1987

Computer Simulation of Hydrostatic Co-Extrusion of Bimetallic Compounds.

Mohammad Mohammad abadi Dehghani
Louisiana State University and Agricultural & Mechanical College

INFORMATION TO USERS

The most advanced technology has been used to photograph and reproduce this manuscript from the microfilm master. UMI films the original text directly from the copy submitted. Thus, some dissertation copies are in typewriter face, while others may be from a computer printer.

In the unlikely event that the author did not send UMI a complete manuscript and there are missing pages, these will be noted. Also, if unauthorized copyrighted material had to be removed, a note will indicate the deletion.

Oversize materials (e.g., maps, drawings, charts) are reproduced by sectioning the original, beginning at the upper left-hand corner and continuing from left to right in equal sections with small overlaps. Each oversize page is available as one exposure on a standard 35 mm slide or as a 17" × 23" black and white photographic print for an additional charge.

Photographs included in the original manuscript have been reproduced xerographically in this copy. 35 mm slides or 6" × 9" black and white photographic prints are available for any photographs or illustrations appearing in this copy for an additional charge. Contact UMI directly to order.

Accessing the World's Information since 1938

300 North Zeeb Road, Ann Arbor, MI 48106-1346 USA

Order Number 8811402

Computer simulation of hydrostatic co-extrusion of bimetallic compounds

Dehghani, Mohammad Mohammad Abadi, Ph.D.

The Louisiana State University and Agricultural and Mechanical Col., 1987

U·M·I
300 N. Zeeb Rd.
Ann Arbor, MI 48106

PLEASE NOTE:

In all cases this material has been filmed in the best possible way from the available copy. Problems encountered with this document have been identified here with a check mark __✓__.

1. Glossy photographs or pages _____
2. Colored illustrations, paper or print _____
3. Photographs with dark background _____
4. Illustrations are poor copy _____
5. Pages with black marks, not original copy _____
6. Print shows through as there is text on both sides of page _____
7. Indistinct, broken or small print on several pages ✓
8. Print exceeds margin requirements _____
9. Tightly bound copy with print lost in spine _____
10. Computer printout pages with indistinct print _____
11. Page(s) _____ lacking when material received, and not available from school or author.
12. Page(s) _____ seem to be missing in numbering only as text follows.
13. Two pages numbered _____. Text follows.
14. Curling and wrinkled pages _____
15. Dissertation contains pages with print at a slant, filmed as received _____
16. Other _____

_____

_____

COMPUTER SIMULATION OF HYDROSTATIC CO-EXTRUSION OF BIMETALLIC COMPOUNDS

A Dissertation

Submitted to the Graduate Faculty of the
Louisiana State University and
Agricultural and Mechanical College
in partial fulfillment of the
requirements for the degree of
Doctor of Philosophy

in

The Department of Mechanical Engineering

by
Mohammad M. Dehghani
B.S.M.E., Louisiana State University, 1980
M.S.M.E., Louisiana State University, 1982
December, 1987

ACKLOWLEDGMENTS

I would like to express my sincere appreciation to my major professor, Dr. Craig S. Hartley, for his invaluable advice, direction, and encouragement in the course of this research. His support was unfailing and endured throughout this work, even in his absence.

For consultation and help on various aspects of this work, I am grateful to the members of my committee, namely Dr. Mehdi Sabbaghian, Dr. George Voyajis, and Dr. Haravill Eaton.

I also would like to extend my gratitude to those institutions which have contributed in different ways to this study: to the staff and fellow students of the Mechanical Engineering Department at Louisiana State University for providing the opportunity and the environment necessary for this work; to the Westinghouse Laboratories for providing the extrusion press and the extruded materials; to the United States Air Force Material Laboratories for the assistance in preparing the test materials; and to the Louisiana Department of Transportation and Development for provision of the computational equipment, without which the completion of this work was in jeopardy.

For valuable suggestions and contacts, I am indebted to Professor Raghu Sirtenvasson of Wright State University, to Dr. Man. Iyer of Westinghouse Laboratories, and to Dr. Ramzy Adams of the Louisiana Department of Transportation and Development.

My further thanks go to Mrs. Dot Sterling of the Computer Division of the Louisiana Department of Transportation and Development for her devoted and effective assistance whenever needed and for her enduring patience.

Finally, the whole owes its coherent existence to Ms. Libbye Morris, who kept track of a stream of disconnected material and buttoned up the loose ends. She is also the recipient of the credit for editing and typing the entire manuscript.

TABLE OF CONTENTS

LIST OF TABLES

LIST OF FIGURES

ABSTRACT

A study of hydrostatic co-extrusion of a hard-core/soft-clad bi-metallic compound has been conducted. The research employs the Sachs' boring-out technique to determine the residual stress distribution in a hydrostatically co-extruded copper-clad Glidcop® composite. A parallel simulation of the residual stress distribution in such composites extruded to extrusion ratios of 2.25, 4.0, and 7.5 was conducted using the ABAQUS finite element code. The version of the code employed uses an elastic-plastic constitutive law for material behavior and does not simulate deformation heating effects. Data for the mechanical properties were obtained experimentally by constant true strain-rate tests on material identical to that used in the extrusion experiments.

The results indicate that the extrusion pressure varies linearly with the natural logarithm of the extrusion ratio. The simulation results obtained for this pressure, however, are generally higher than those found in experiments. Comparison of the experimental and numerical results of the residual stresses indicate that although the two results are qualitatively similar, they are quantitatively different. In all cases, the experimental results were much lower than those of numerical calculations, implying that some recovery has occurred during the extrusion process.

The investigation shows, however, that finite element analysis in conjunction with experimental measurements can be applied successfully to predict and verify the qualitative residual stress patterns developed in hydrostatically extruded products.

Dedicated to the memory of my father and to my mother.

CHAPTER 1

INTRODUCTION

1.1 General Principles

1.1.1 The Extrusion Process

Extrusion is essentially a deformation process by which a billet or slug of material is converted into a continuous product of uniform cross-section by being forced through a suitably shaped die.* The principle is quite simple: a billet, originally in a closed container, is squeezed through a die so that its cross-section is altered in size and shape. The schematic diagram in Figure 1.1 illustrates the essential principle of the simplest form of the extrusion process, in which the load is transmitted to the billet through an intermediate dummy block via a mechanically or hydraulically driven ram.

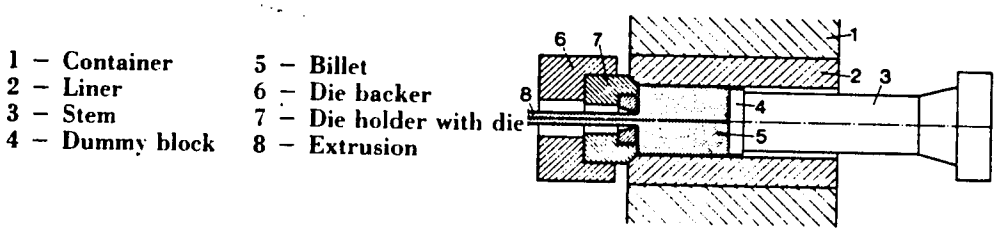

Figure 1.1. Schematic diagram of the extrusion process.

---

* To "extrude" means literally to thrust or force out (L. extrudere). The New English Dictionary gives as one definition of "extrusion": the act of expulsion by mechanical force.

The remarkable developments in extrusion techniques and equipment have aided every related sector of industry. The extrusion process provides a practical fabricating method for producing a limitless variety of parallel surfaced shapes to meet almost any design demand. Cross-sections of varying geometry and complexity can be extruded. Hollow, solid, thick, thin, simple, or intricate sections of any size can be produced at room temperature or at higher temperatures, depending on the material, die configuration, press size, and method. In fact, there is virtually no shape that cannot be produced with the easily extruded alloys. However, diverse sections, naturally associated with varying degrees of difficulty, have been classified systematically according to their shapes.

An additional merit of extrusion is that it affords an invaluable means of working certain alloys that are not processed satisfactorily by other forming methods, such as rolling or forging. Powders and some tender materials are good examples of such alloys.

From the metallurgical point of view, perhaps the main contribution has been made outside the extrusion process, in the development of new alloys for use in extrusion; in improved tool steels; in providing more homogeneous and sound billets; etc.

Generally, the advances made in extrusion have resulted largely from progress in engineering design and construction materials, combined with the gradual acquisition of technical experience.

1.1.2 Historical Development

The famous British hydraulic engineer Joseph Bramah most likely had

the earliest perception of the principles of extrusion. It has been noted that Bramah, in a patent granted in 1797, described a press, shown in Figure 1.2, "for making pipes of lead or other soft metals of all dimensions and of any given length without joints" [*101*].

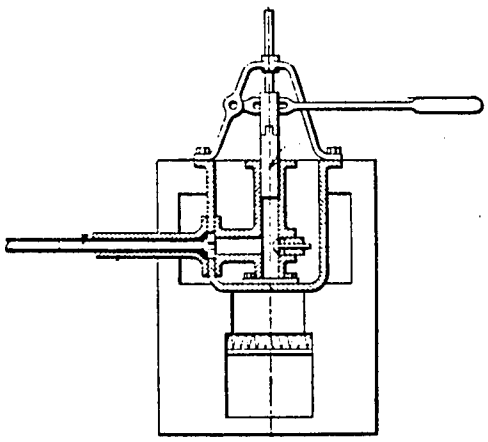

Figure 1.2. Bramah's lead-pipe machine.

In Bramah's press, lead was maintained in its molten state in an iron pot with a fire beneath and was forced into a long, projecting tube by a pump. The projecting tube served as a die, and a tapered mandrel was supported concentrically by a bridge at its end.

Although it is doubtful that Bramah's machine was devised to make pipes in its original composition, records show that it was the first machine to embody the concept of extrusion [*101*]. Bramah's idea was not developed immediately, and the earlier methods of making lead pipes

continued to be used. It was not until 1820 that the manufacture of lead pipes by extrusion came into actual operation, when Thomas Burr constructed his hydraulically powered press (Figure 1.3). Burr's machine consisted of a strong cylindrical container, a steel die, a fitting plunger, and a mandrel rod.

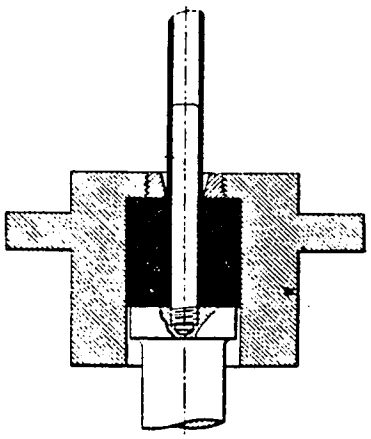

Figure 1.3. Thomas Burr's hydraulically powered press.

After withdrawing the plunger to its fullest extent, lead was poured into the container through the die orifice and, after an interval of solidification of the metal, the lead was forced up through the die by the hydraulic ram [*101*].

In 1837, J. and C. Hanson made a modified press that avoided the awkwardness of the previous refilling method by making a hole in the upper part of the container wall, which was sealed by the plunger at the beginning of the working stroke. The lead container in the new design was made the moveable part by being mounted on top of the main ram of a

hydraulic press. The plunger, however, was made the stationary part by being attached to the head of the press ram. These arrangements are shown in Figure 1.4 [*101*].

The new design introduced two features to improve concentricity in the pipes. The first was the use of a form of bridge die, which replaced the long mandrel with a short one held in a support. This arrangement eliminated the problem of non-uniform wall thickness in the pipe, which was attributed to the fact that the long mandrel bar tended to bend and subsequently to lie out of center of the die.

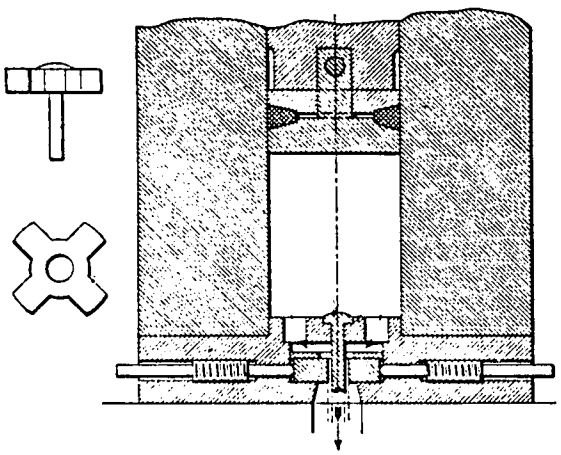

Figure 1.4. J. and C. Hansons' modified press.

The second feature was a capability of centering the die by four adjusting screws. By the careful arrangement of the die and the support plate combined with the short mandrel, the stream of lead was divided so that it would reunite before actually entering the die. This action controlled the amount of lead that flowed into the die on each side of

the mandrel [101].

By mid-century, the process of lead extrusion had become firmly established. At this time, however, the problem of corrosion became obvious. The next noteworthy developments arose from the interest then being taken in the production of tin-lined pipes to overcome the danger of lead poisoning that occurs when lead pipes are used to convey certain waters and other liquids. Running molten tin inside lengths of extruded pipe was one simple solution often practiced.

In 1863, Shaw used a press in which precast hollow billets of lead, with an internally cast sleeve of tin, were charged into the container to produce a bi-metallic pipe [101]. A difficulty was encountered in arriving at the exact shape of sleeve to produce a uniform lining of tin in the pipe. Four years later, in 1867, Hamon invented a remarkable press in France that overcame the problem of corrosion by incorporating many advanced features.

Hamon's machine was the first example of a heated container which, through ducts in its outer jacket, allowed circulation of steam or hot gases to raise its temperature to 210°C. Although the hydraulic accumulator had been invented earlier, Hamon was the first to introduce it into the extrusion press [101].

The next stage in the evolution of the process was the introduction in 1870 of the indirect, or inverted, method of extrusion. It was introduced, simultaneously, by two independent sources--Haines and J. and W. Weems. The new technique made it possible to produce a more uniform coating of tin in the pipe. This was because the relative displacement of the billet and the container walls was avoided; therefore, the metal remained undisturbed except in the vicinity of the die.

With the rapid development of the electrical industry came the need for a protective envelope that would shield cables against mechanical damage and would enable them to be submerged in water. Lead seemed to be the ideal material for the task. It was relatively immune to corrosion and was soft and pliable enough to be used in the laying operations. In fact, by 1879 the first methods of extruding a lead sheath directly onto cables were devised in France and Germany by Borel and Wesslan, respectively. They used vertical extrusion presses to extrude hollow-cast billets of lead over an insulated conductor in the form of a tubular sheath. The conductor was passed into the press through a hollow mandrel and then was issued through the tubular ram [*101*].

The next notable modification of the extrusion presses originated in America with the design of a vertical press for sheathing continuous lengths of cables. This was Eaton's ingenious adaptation of the ordinary pipe press in 1880. In Eaton's press, as shown in Figure 1.5, a

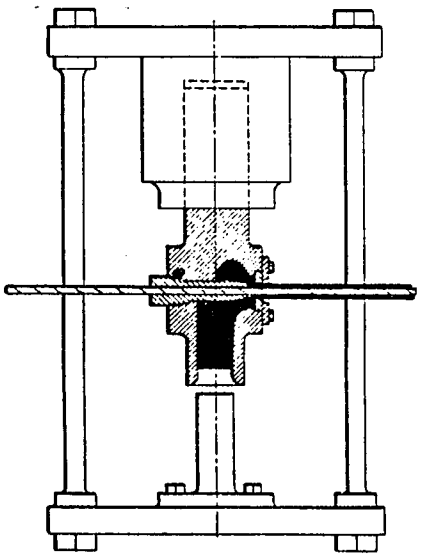

Figure 1.5. Eaton's vertical press.

charge of lead was cast and solidified in the container made to flow circumferentially around a mandrel over the cable that was threaded through the mandrel. The mandrel was at a right angle to the axis of the container [101]. While the development of the vertical press ensued, the evolution of the horizontal press continued. In its modern form, the horizontal press has almost entirely surpassed other types.

The outstanding achievements brought about by extrusion in the service of the lead industry directed attention to the possible utilization of the process for metals with better mechanical properties, such as brass. Records show that several efforts to extrude brass alloys were made during the 19th century, but the difficulties proved to be too great, and the lead presses used for experiments were unsuitable [102].

The major problem with extruding brass, as compared with lead, was that even the brasses most feasible for hot work had to be heated to a temperature of at least 600°C before they became plastic enough to undergo the heavy deformation involved in extrusion. Therefore, the problem was not only that of providing a powerful press, but also of providing containers, dies, and other press components that could withstand the severe thermal and stress conditions required of the extrusion operation.

Few special steels had been developed in the 1800s, however, and soft dies continued to be deformed along with the billets in the extrusion of hard brasses. It is therefore had to overestimate the achievement of Alexander Dick in overcoming the obstacles involved. His decisive invention in 1883 laid the foundation of the modern hot extrusion process, which now has been extended far beyond its original

limitations to a stage at which it has become one of the major metal working processes in the field. Figure 1.6 shows a schematic diagram of Dick's original design in which the horizontal press frame was braced together by four tie-rods. A pair of jaws held a heavy cross-head on

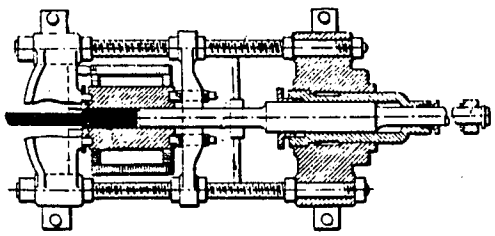

Figure 1.6. Dick's horizontal extrusion press.

one end of the press, and a pair of set-screws held and centered the container, which was surrounded by a furnace jacket. The billet was fed into the container from the front and was heated to a plastic state by coke or gas. By locating a separate dummy block in front of the extrusion stem, Dick prevented wedging of the ram caused by slippage of the metal past its sides [*101*].

At the same time that Alexander Dick was developing his versatile press, the idea of employing hydrostatic pressure in metal forming was being conceived in England. In fact, the first patent was granted to Robertson in 1894, the same year that Dick obtained the first patent for his horizontal press [*101*]. Experimental results of the hydrostatic extrusion, however, were not obtained until 1949, when Bridgman invented

his high-pressure seal. Then he found himself in a unique position to study the high-pressure effects on materials, and he spent the rest of his life doing experiments which led to a mountain of research papers on the subject [103]. The first high-pressure unit bearing Bridgman's name was manufactured by Harwood Engineering Company of Newhall, England [104]. At the same time, a similar type of press was produced by the Pressure Technology of America, headed by Bobrowsky [105].

Systematic hydrostatic extrusion of materials was started in England by Pugh at the National Engineering Laboratory in Glasgow. He developed the process of hydrostatic extrusion to the extent of industrial production [106]. In the Soviet Union, Vereshehayin of the High Pressure Laboratory of The Academy of Sciences began the study of high pressure, and the first results appeared in 1957 [107].

The first seminar on hydrostatic metal working processes was held at Battelle Columbus Laboratories in 1967 [108]. This first exclusive conference indicates the great progress in high-pressure engineering that was made in the 1960s. Today, after two decades of research and development, the techniques of hydrostatic extrusion have progressed to such a level that they are now established as an industrial process. The process has been applied successfully to copper tubings, copper-clad aluminum wire, fine wires of noble metals, tubings of aluminum alloys, and so forth.

1.1.3 Comparison with Other Deformation Processes

The most significant advantage of the extrusion process is that it provides an invaluable means of forming certain alloys that can be

deformed only slightly by other techniques. This is because of the favorable compressive state of stress reached in the material during the extrusion process; this indicates a high capacity for deformation far beyond the ability of other methods. In fact, in the classification of deformation processes, extrusion is listed under the heading of "compressive deformation." Referring to the general state of stress in the deformation zone of a deforming material, stress components occur in each of the three directions in the planes normal to each other. There are two shear stresses: τ, and a normal stress σ, perpendicular to one another, as shown in Figure 1.7. By choosing the coordinate system

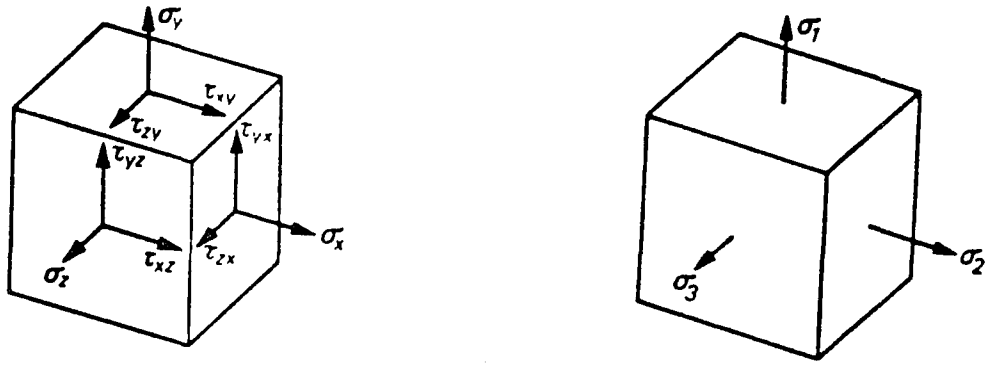

Figure 1.7. General state of stress and principal stresses.

properly, the stresses can be represented by the three normal stresses σ_1, σ_2, and σ_3, shown in Figure 2.4. These are, of course, the principal stresses, with tensile stresses positive in sign and of negative compressive stresses. The start of deformation or plastic flow occurs when the difference between the maximum and minimum principal stresses

exceeds a certain value called flow stress k_p. If σ_1 is the maximum principal stress and σ_3 the minimum, then, according to Tresca's yield criterion, the plastic flow initiates when

$$\sigma_1 - \sigma_3 = k_f.$$

Therefore, as long as the stress gradient is maintained at the value of flow stress, the deformation process will continue to occur whether the stresses are compressive or tensile. However, an important feature of extrusion is that all three principal stresses are compressive, in contrast to most other deformation processes. The tangential and radial stresses have approximately the same magnitude but are less than σ_1, which is the maximum principal stress.

The advantage of plastic deformation under a state of multiaxial compression is the very high strain that can be attained in extrusion. Even though the yield stress according to Tresca is independent of the state of stress, the workability increases with increasing mean or hydrostatic pressure:

$$\sigma m = 1/3\ (\sigma_1 + \sigma_2 + \sigma_3).$$

This very important fact makes the process of hydrostatic extrusion even more advantageous over other extrusion techniques.

Figure 1.8 shows a schematic diagram of the deformability of the extrusion process in comparison with other forming techniques and with deformation to the point of fracture in tension, compression and torsion testing [*109*].

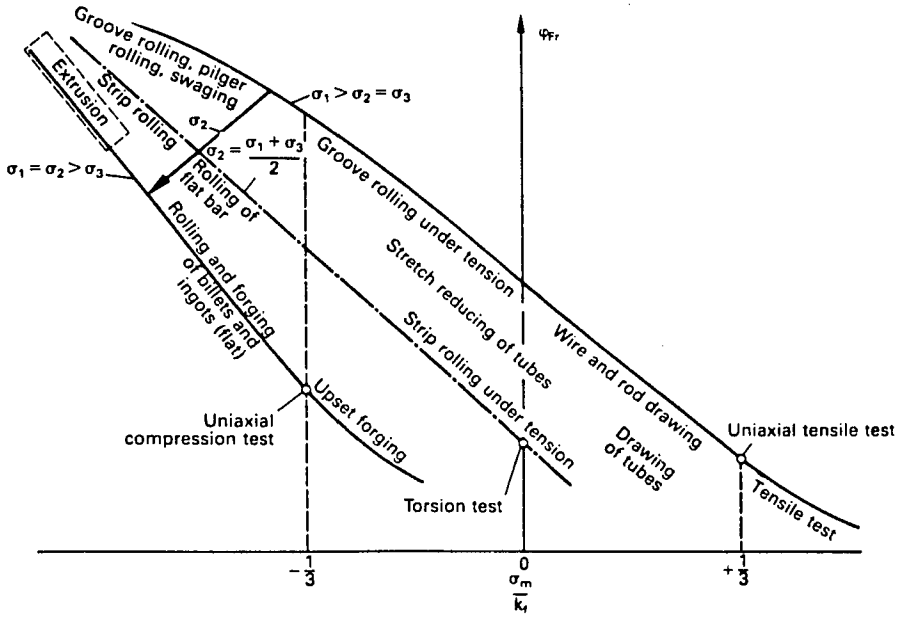

Figure 1.8. Deformability σ_{Fr} in various deformation processes.

The extrusion process, like every other forming method, is not without its shortcomings. The effect of friction can lead to the development of a tensile stress exceeding the tensile strength at the surface of the material which, in turn, can cause surface defects. Thus, the extrudability of many metals is limited. Fortunately, because there is little or no friction between the billet and the die in hydrostatic extrusion, the result is a more uniform deformation of the extruded product.

1.2 Types of Extrusion

The properties and, in particular, the quality of extruded products are influenced by the manner in which the metal has been extruded to take up its final dimensions and form. In fact, the complex relationship between the extrusion parameters and the flow characteristics of various alloys makes it impossible to use the same method for all materials. Different methods are associated with different materials. According to the typical flow behavior of a given alloy, a special method of operation is implemented to ensure the optimum quality of the product. Figure 1.9 is a schematic diagram of the three basic methods of extrusion--direct, indirect, and hysrostatic.

Figure 1.9. Basic methods of extrusion: (a) direct extrusion, (b) indirect extrusion, (c) hydrostatic extrusion.

1.2.1 Direct Extrusion

The conventional direct extrusion is perhaps the most common production method in use. In this process, a billet or slug of material is converted into a continuous product of uniform cross-section by being forced through a suitably shaped die. The billets, placed within a strong-walled enclosure, are caused to extrude through the die under the powerful pressure exerted by a ram, actuated hydraulically or mechanically (Figure 1.10).

An important use of direct extrusion is in the manufacturing of products with gradual cross-section variations along the length of the extrusion. This is achieved by interrupting the extrusion stroke after a certain ram displacement, then changing the die. Stepped posts for

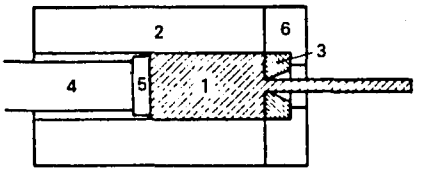

1 – Billet
2 – Container
3 – Die
4 – Extrusion stem
5 – Dummy block
6 – Die holder

Figure 1.10. Conventional direct extrusion.

street lamps, for example, are produced by starting the extrusion with the smallest cross-section; then the die is replaced by a larger one, the ram stroke is continued, and the process is repeated as long as necessary. Figure 1.11 is a schematic illustration of this process. It

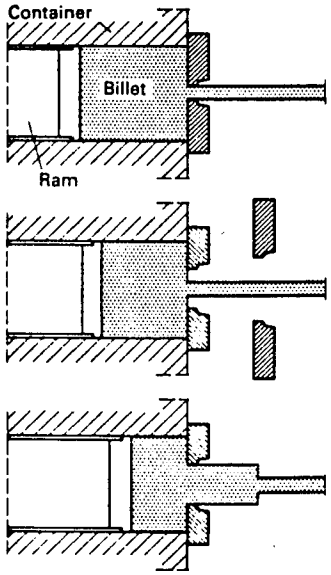

Figure 1.11. Extrusion of step product.

must be noted that dies also have been developed to cause a continuous increase or decrease in the size of the aperture and to allow conical sections to be extruded.

In the process of direct extrusion, the surface of the billet slides along the container wall; thus, part of the extrusion load is expended in overcoming the friction between the billet and the container. If the material has a strong tendency to adhere to the con-

tainer wall, then the peripheral layer of the material adjacent to the wall moves slower than the inner material, resulting in a nonuniform flow pattern. This nonuniformity of the flow can cause product defects such as central bursting and voids.

The direct extrusion process can be conducted with or without a lubricant. The use of the lubricated process naturally results in a lower extrusion load and makes possible the extrusion of some very difficult alloys. In comparison with the production methods using no lubricant, the presence of a good lubricant between the billet and the container results in a relatively uniform strain rate over most of the cross-section of the billet. Therefore, the entire billet is more uniformly deformed, and the billet surface also forms the surface of the extruded product--with the advantage that the impurities on the surface, such as oxides, are not drawn into the product. The lubricant used varies from alloy to alloy. For extrusion of steel, for example, the container and the die have to be well-lubricated, whereas for copper the self-lubricating oxide layer is sufficient.

In spite of the potential advantages, the lubricants can be harmful if used improperly. Several noted cases of surface defects have been caused by an excess or shortage of lubricant; these cases are not encountered in the usual method of unlubricated extrusion [110]. Numerous papers have been published in the area of lubrication in extrusion; some of these are listed in References 104-112.

1.2.2 Indirect Extrusion

In indirect extrusion, the die is placed on the end of the ram,

which is bored out to allow the passage of the extruded product. The hollow stem moves relatively to the container, but there is no relative displacement between the billet and the container (Figure 1.12). The

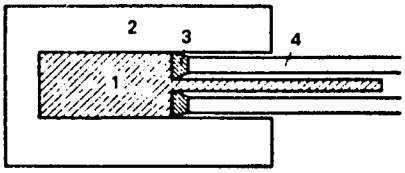

1 – Billet
2 – Container
3 – Die
4 – Extrusion stem
5 – Dummy block
6 – Die holder

Figure 1.12. Indirect extrusion.

main advantage of the indirect extrusion process is the absence of friction between the billet surface and the container. The required load therefore is decreased. Figure 1.13 shows a typical shape of the

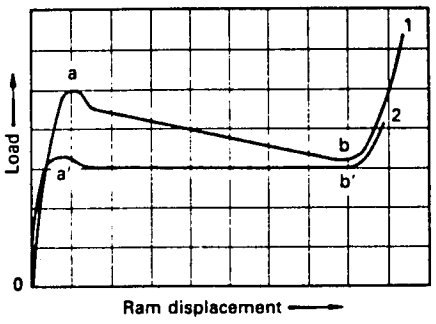

Figure 1.13. Comparison of the pressure variation for direct and indirect extrusion.

extrusion load ram displacement diagram for direct and indirect extrusion. The difference in the two peak values of pressure in direct and indirect processes is attributed to the significant friction between the surface of the billet and the container wall [113]. In fact, in the case of an aluminum rod, an average savings of 30 percent in the load requirements, compared to that of direct extrusion, has been reported [114]. Another distinguishing feature of the indirect extrusion process is also contributed to the absence of friction at the container wall--this feature is that the only limitation of the billet length is the length of the stem and, therefore, much longer containers can be used. This, in turn, means that longer products can be extruded by the indirect method.

The processes of direct and indirect extrusion can be combined to take advantage of the features of indirect extrusion with the mechanical capabilities of direct presses. Figure 1.14 shows a schematic diagram of such arrangements.

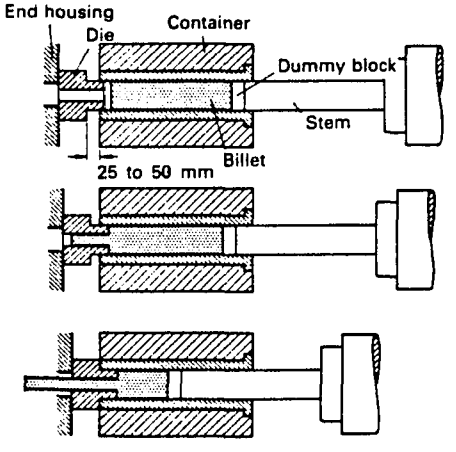

Figure 1.14. Combined direct and indirect extrusion.

The process begins with indirect extrusion and therefore avoids the initial peak load associated with the direct process. During this stage, the container is free to move axially 20 to 50 mm before it reaches a stop on the die holder. At this point, the normal direct extrusion takes over, and the remainder of the process is completed.

1.2.3 Hydrostatic Extrusion

Hydrostatic extrusion is essentially the process by which a billet is extruded through a die by a high-pressure liquid acting as a pressure medium, instead of by direct application of force by a ram, as in conventional direct extrusion. Figure 1.15 shows a schematic comparison of hydrostatic extrusion with conventional extrusion.

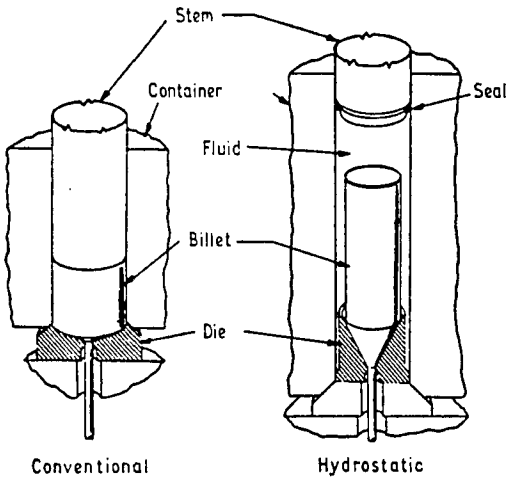

Figure 1.15. Comparison of hydrostatic extrusion with conventional direct extrusion.

Also known as ramless, fluid, or hydraulic extrusion, hydrostatic extrusion is one of the most prominent metal-working processes upon which considerable research has been done in recent years. Although the idea was patented by J. Robertson in 1893, it was not unitl about thirty years ago that the process was proposed as a new lubricated extrusion process. From that time on, the process has been applied to metals, special alloys, and composite materials, with the results of diverse research and development justifying its vast utilization in industry. Today many hydrostatic extrusion presses up to 40 MN are in use world-wide as research and production presses [101].

One of the significant features of the hydrostatic extrusion process is that there is no friction between the billet and the container wall; thus, the length of the billet is not limited as it is in conventional extrusion. Superior lubrication, a favorable stress condition for metal deformation, and better quality products are also advantages of hydrostatic extrusion over conventional extrusion.

1.2.3.1 Method of operation

In the process of hydrostatic extrusion, the billet is forced through the die from a high-pressure chamber into an atmospheric-pressure or a low-pressure chamber. In conventional extrusion, the material maintains contact with three components: the die, chamber, and the ram or dummy block. In hydrostatic extrusion, on the other hand, the material is surrounded by the liquid and is in contact with the die only. In fact, when hydrodynamic lubrication prevails, even contact with the die is avoided.

High-pressure seals are used at the die and at the ram to seal off the pressure-transmitting fluid of the container. Extrusion begins as soon as the hydrostatic pressure is high enough, depending on the flow stress of the material, die angle, and extrusion ratio. One way to provide this pressure is with the ram of a press forced into the extrusion chamber (Figure 1.16). Another is to provide the pressure through a pump, with or without a pressure intensifier (Figure 1.17).

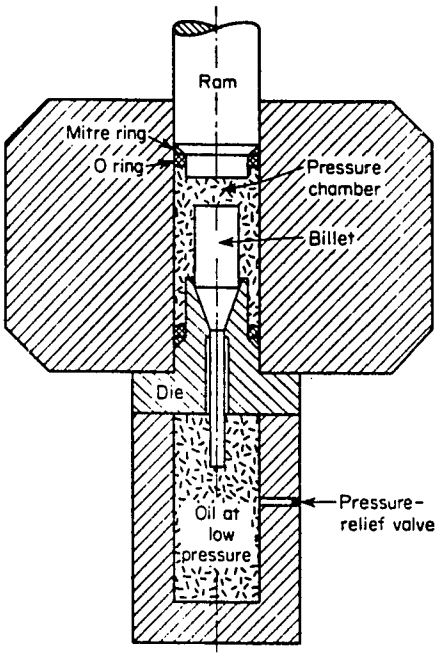

Figure 1.16. Ram-type extrusion chamber.

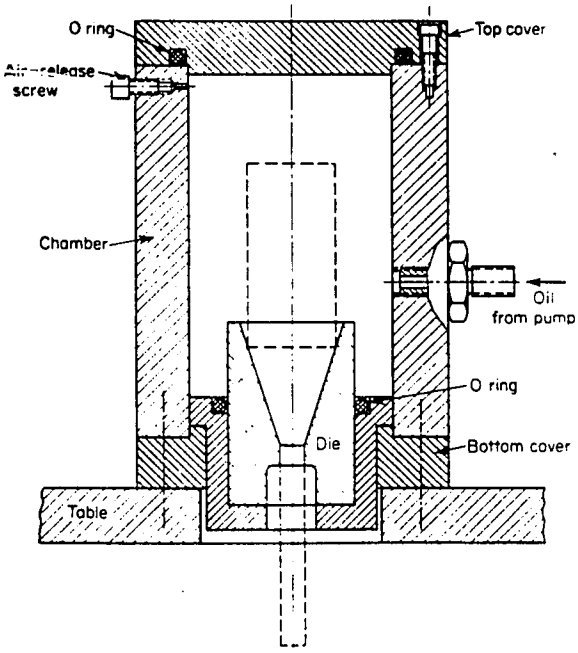

Figure 1.17. Pump-type extrusion chamber.

The use of conical dies allows a film of lubricant to develop. At the die opening, the pressure is lower than the extrusion pressure. Subsequently, a resultant force is exerted on the material, forcing it to flow out through the die.

One disadvantage of hydrostatic extrusion that every billet has to

be prepared laboriously to match the die angle so that a seal is formed at the start of the extrusion process. Another disadvantage is that at low extrusion ratios, surface defects reappear in an elongated form on the surface of the product. At low ratios, therefore, the entire surface of the billet generally has to be machined.

1.2.3.2 Simple hydrostatic extrusion

In simple hydrostatic extrusion, just as in conventional direct extrusion, the material is extruded through the die into the atmosphere. This basic process is perfectly suitable for extruding metals of average or good ductility at high extrusion ratios. Some examples of commonly extruded products are aluminum and copper wires, copper tubes and sections, and steel tubes with high surface quality. Extrusion of very long billets is also feasible by this method, providing that the extrusion press is slightly rearranged (Figure 1.18).

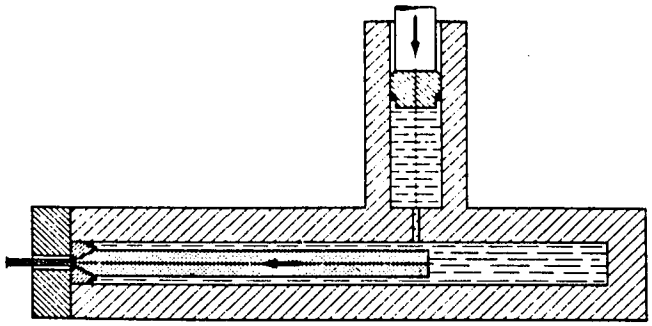

Figure 1.18. Hydrostatic extrusion of long billets.

Materials can fracture during simple hydrostatic extrusion because the hydrostatic pressure falls toward zero at the die exit. One remedy is to use the fluid-to-fluid hydrostatic extrusion technique.

1.2.3.3 Fluid-to-fluid hydrostatic extrusion

Products that are produced by simple hydrostatic extrusion are sometimes defective because many brittle materials are susceptible to circumferential and longitudinal surface cracking during hydrostatic extrusion. These cracks first occur in the rear section of the die, immediately before the exit plane, and are attributed mainly to the sharp drop in hydrostatic pressure at the die exit. These cracks can be reduced or prevented by using a differential-pressure, fluid-to- fluid extrusion process. In this process, as shown in Figure 1.19, the

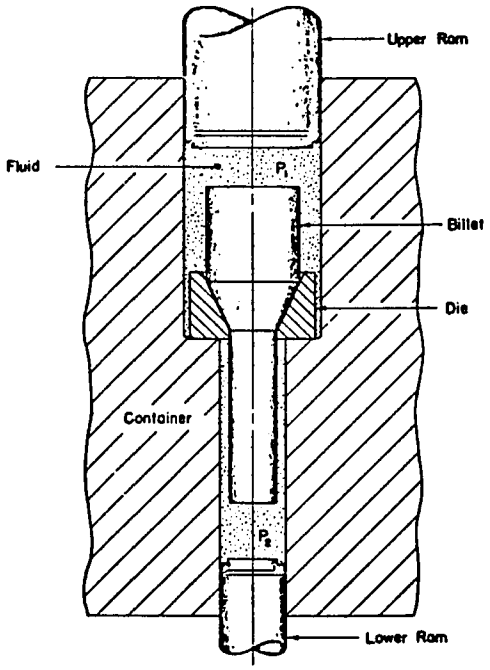

Figure 1.19. Fluid-to-fluid hydrostatic extrusion.

product is extruded into a hydraulic pressure chamber containing a sufficiently high back pressure, instead of into the atmosphere as in simple hydrostatic extrusion.

Although this method provides a reasonable solution, it has several disadvantages that limit its application as a production technique. The main setback is higher tooling and operational cost of the secondary pressure chamber. The billet length that can be used is also severely limited by the length of the back pressure container.

1.2.3.4 Augmented hydrostatic extrusion

In an attempt to obtain a large extrusion ratio with low hydrostatic pressure, modifications to the basic process have been developed [*115*]. In augmented hydrostatic extrusion, for example, a supplementary mechanical force is applied which improves the displacement of the billet or of the product. Depending on the manner in which the additional axial load is applied, the process is classified as either billet-augmented hydrostatic extrusion or product-augmented hydrostatic extrusion (Figure 1.20). In the former, the supplementary load is transmitted onto the back end of the billet by a ram. In the latter, this additional axial load is a tensile force applied to the front end of the product by a cable.

An important feature of augmented extrusion is that it stabilizes the process by preventing the stick-slip phenomenon, a source of problems in some cases of pure hydrostatic extrusion. The process suffers from the disadvantage of the complexity of the system, especially in the billet-augmented process.

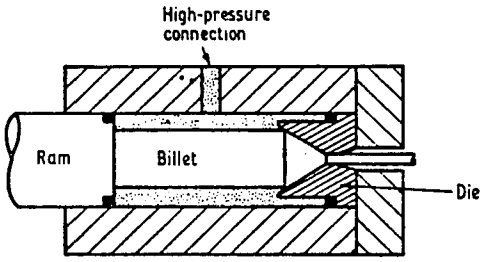

Figure 1.20. Billet augmented hydrostatic extrusion.

1.2.3.5 Continuous and semi-continuous hydrostatic extrusion

Semi-continuous hydrostatic extrusion is the process by which continuous billets of any length are extruded in steps or intervals. The principle of operation is the same as in the pressure augmentation process, in which the augmenting pressure is transmitted to the billet by a sealed clamping system, shown in Figure 1.21. The high pressure in the chamber, combined with the augmenting pressure, extrudes the billet progressively. At regular intervals, however, the process is interrupted to reposition the clamping jaws and is continued as long as necessary.

In continuous hydrostatic extrusion, the mechanical augmenting pressure of the clamping system is replaced by the dragging effect of a viscous liquid that is forced to flow along the rod and in the direction of extrusion. The necessary pressure drop in the viscous fluid is

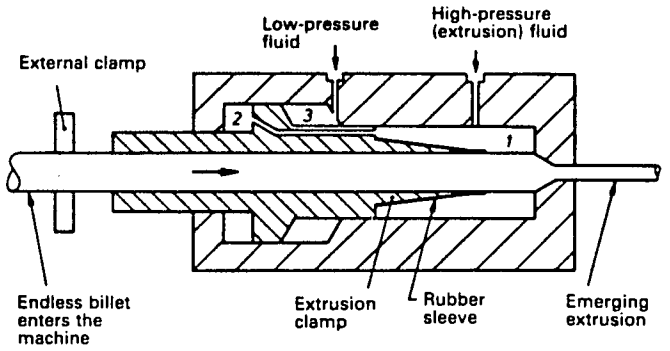

Figure 1.21. Semi-continuous hydrostatic extrusion.

established throughout the extruder press by utilizing a flow reversal design schematically illustrated in Figure 1.22. Control of this pressure drop through the machine is necessary to balance the radial and axial stresses on the rod to avoid bending, yielding, or rod pinch-off.

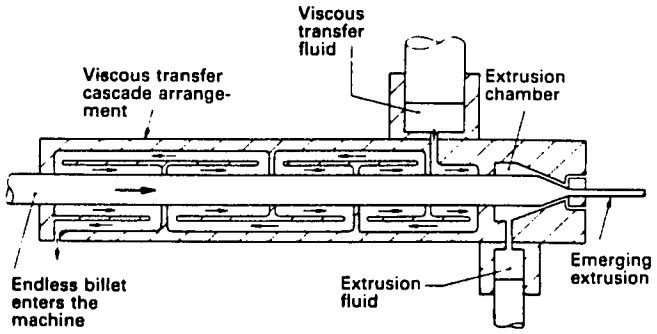

Figure 1.22. Continuous hydrostatic extrusion.

1.2.4 Hydrostatic Co-extrusions

Implementation of bi- or multi-metallic compounds in industry has drawn a great deal of attention to the manufacturing and production of composite products by hydrostatic extrusion and other techniques. Application of such products range from ordinary thermostats to multi-filamentary superconductors. Introduction of such products was the result of the realization that metallic compounds consisting of two or more metals can achieve physical and mechanical properties that cannot be obtained by their individual constituents alone. The high-strength but corrosion-sensitive base alloys, for example, are covered with non-corrosive materials such as pure aluminum. A wide variety of copper sections clad with silver are produced by the hydrostatic extrusion process for use in the electronic industry. Recent increases in the use of high-performance superconducting magnets for nuclear fusion research and other applications demand a reliable method for mass production, and the hydrostatic extrusion process is effective and reliable for the manufacture of such composite wires [116].

Even though the hydrostatic extrusion process is not the only co-extrusion technique available, clad metals made by this process achieve a very high degree of dimensional uniformity. This is because of the uniform flow that can be maintained during the hydrostatic extrusion, due to the absence of container friction.

Another application of co-extrusion is in the forming process of brittle materials and powder compacts. These materials generally are difficult to process by themselves, and extrusion attempts to deform such alloys usually result in defective products. Using co-extrusion,

however, a softer, more deformable metal surrounds the difficult-to-extrude material, and the matrix is jointly extruded to form the desired configuration. The product then is machined and, upon removal of the clad, the final product is revealed.

Clad-composite metals generally are extruded in two dispositions of their individual constituents: soft-core, hard-clad composites, such as copper-clad aluminum bars, or hard-core, soft-clad products, such as aluminum wires clad with soft lead. In general, due to the diffusion that takes place during hydrostatic extrusion, clad-composite metals produced by this technique possess a strong bonding between their components. However, in extreme cases, such as those of large flow stress ratio, slippage of the inner and outer layers can occur at the interface, causing defects in the product. These defects vary depending on whether the billet structure is soft-core, hard-clad or hard-core, soft-clad. In the case of the former, for example, clad fracture may occur as the soft core is extruded only when slipping occurs and compression at the die corresponds to the fracture stress of the outer layer. In the latter situation, however, the soft clad is extruded while the hard core may act as a mandrel on the pipe extrusion.

Each configuration, therefore, has its range of processing parameters over which successful extrusions can be obtained. With proper choice of independent parameters, such as extrusion ratio, die angle, and volume fraction of the billet constituents, the product is a sound, solid rod.

1.3 Advantages and Disadvantages of Different Methods of Operation

The complex relationship between the extrusion parameters and the flow characteristics of various alloys, together with the desired quality of the extruded products, dictates the extrusion method adopted for each case. There are distinct advantages and disadvantages associated with each method. In direct extrusion, simplicity is the main advantage. Higher extrusion load is needed, however, to overcome the friction between the surface of the billet and the container wall. Therefore, if the material has a strong tendency to adhere to the container wall, the result is a nonuniform flow pattern, which can cause product defects such as central bursting and voids.

The main advantage of the indirect extrusion process is the absence of friction between the billet surface and the container. The required load therefore is decreased. The disadvantage of the process is that the cross-sectional area of the product is limited by the size of the hollow stem. Also, the defects or impurities on the billet surface affect the surface of the product. Therefore, an additional machining operation is needed to obtain the best results.

The most significant advantage characterizing the hydrostatic extrusion process is the complete elimination of friction between the billet and the container wall. The load at the start of extrusion is much lower, and billets of any length can be used. Superior lubrication, a favorable stress condition for metal deformation, and better quality products also are advantages of hydrostatic extrusion over conventional extrusion.

Hydrostatic extrusion has its disadvantages. Design and manufac-

turing of high-pressure chambers and seals are difficult and expensive. Also, repeated high pressurization of the chamber can cause fatigue and failure. Another disadvantage is the laborious preparation of the billets. The lead end of every billet must be tapered to match the die angle in order to form a seal at the start of the process. Also, the entire surface of the billets generally has to be machined to remove surface defects which would reappear in an elongated form on the extruded product.

1.4 Defects and Preventive Measures

Extrusion defects generally are the result of nonuniform deformation of the material. There are two kinds of defects--internal defects, such as central bursting, and external defects, such as surface cracking.

Central bursting occurs when the product fractures along the centerline (Figure 1.23). This is explained by the occurrence of a

Figure 1.23. Central bursting defect in extruded products.

state of hydrostatic tension (triaxial tension) near the axis of the billet. Hydrostatic tension is the result of formations at high ratios of billet diameter to the deformation contact zone. Therefore, the phenomenon is most likely to occur in extrusions with high die angles and low extrusion ratios.

Surface cracking, or snake skin defect, occurs in the extrusion of many brittle materials. It is caused by sudden elastic recovery of the metal upon exiting the die, Figure 1.24.

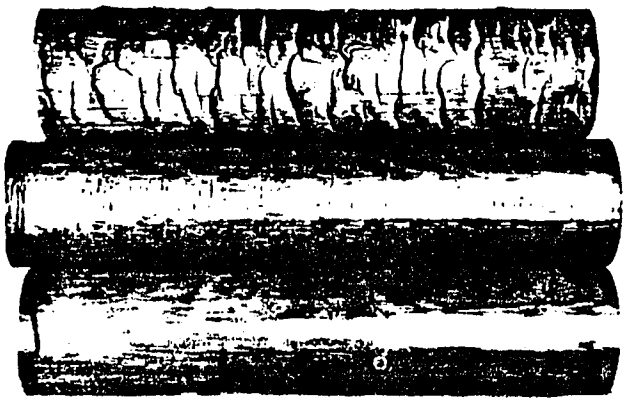

Figure 1.24. Snake skin defect in extruded products.

It is known that such cracking in hydrostatic extrusion can be prevented by using differential-pressure fluid-to-fluid extrusion chambers. In this technique, the billet is extruded from one pressurized fluid into another at a lower pressure, and thus the sudden stress drop at the die exit is eliminated.

Another approach in prevention of the surface defect is extrusion by using a double-reduction die. In this approach, the major billet reduction takes place at the first land and a small reduction at the second land. The second reduction imposes a counterpressure in the form of a longitudinal compressive elastic stress to the extruding product upon exit from the first die. This prevents circumferential cracks by reducing the axial tensile stesses in the outer fibers of the product.

1.5 Scope of the Study

This investigation is a study of hydrostatic co-extrusion of bi-metallic compounds of hard-core, soft-clad materials. Specifically, the research investigates the extrusion of copper-clad copper alloys and consists of two phases--analytical and experimental.

The analytical phase of the investigation is the computer simulation of the extrusion process. A nonlinear elastoplastic finite element program (ABAQUS) is used to investigate the effects of die angle, extrusion ratio, and volume fraction of the core on the extrusion pressure, deformed geometry, and the residual stress distribution in the product. Die angles of 45° and 60° are used. Three extrusion ratios (2.25, 4.0, and 7.5) are simulated. Billets of 100 percent copper and 100 percent copper alloys, along with composites of 50 percent and 75 percent core, also are investigated.

The experimental phase of the study includes the hydrostatic extrusion of billets and composites of copper and copper alloys, as well as the electrochemical material-removing experiment of residual

stress determination in the extruded specimens. The results of the two phases then are compared to yield conclusions concerning the entire investigation and to calibrate the numerical simulation. The calibrated finite element program then can be used to predict the proper arrangements of process variables for products of better quality.

CHAPTER 2

LITERATURE SURVEY

Even though the idea of employing hydrostatic pressure for metal-working was first introduced in the nineteenth century, experimental proofs of the pressure-induced ductility in materials were not available until Bridgman's extensive study of the subject. The results of his investigation of the behavior of metals under pressure were published in the form of a monograph [201] in 1949. He invented the high-pressure seal, which put him in a uniquely advantageous position to study the effects of high pressure on the metals. As a result, he devoted the rest of his life to the study of the fascinating world of high pressure, and the results of his work later were compiled into a seven-volume monograph titled Collected Experimental Papers of P. W. Bridgman [202]. With the assistance of Abbot, former research assistant of Bridgman, the Harwood Engineering Company of Newhall, Scotland manufactured the first high-pressure unit called the Bridgman Press. Shortly thereafter, the Pressure Technology Corporation of America, headed by Bobrowsky, produced a similar type of press [203].

The first report on hydrostatic extrusion out of the Soviet Union appeared in 1957 [204]. The work had been initiated there by Vereshchagin of the high-pressure laboratory of the Academy of Sciences.

In Great Britain, meanwhile, systematic work on the hydrostatic extrusion of materials was started at the National Engineering Laboratory in Glasgow by H. H. D. Pugh [205]. He and his assistants developed the technique of hydrostatic extrusion to today's level of industrial

production.

M. Nishihara's early recognition of the importance of the effects of hydrostatic pressure on the mechanical properties of materials led to a series of research at room temperature [206,207] and at elevated temperatures [208,209] at Doshisha University in Kyoto, Japan. He determined the strength and ductility of carbon steel, magnesium, titanium, and zinc at pressures up to 5 kilobars and temperatures up to 600°C [210].

In industry, there were four pioneers who used the new technology on a commercial basis--ASEA in Sweden, Lips BV of Holland, the Western Electric Company in the United States, and Kobe Steel in Japan [211]. The main advantage of the new technique for commercial production was the extremely high reduction ratios obtained in one single pass. The disadvantage was the limitation of being a batch technique. It is not without reason, therefore, that the decade of the 1970s saw an increase in the commercial use of the batch-type production unit on one hand, and of research and development of a continuous process on the other. Numerous ideas on the continuous process were conceived, and some of them were subjected to experimentation.

Continuous extrusion was introduced first by Fuchs [212]. His viscous drag extrusion marked the beginning of a series of attempts to use the technique in forms other than batch production. Other novel methods were proposed as well, such as "continuous extrusion forming," or so-called "conforming," by Green [213]; "linear continuous extrusion," or "linex," by Black and Voorhes [214]; "extrolling" by Avitzur [215]; and "hydrostatic extrusion with continuous feed" by Kobe Steel [216].

Great progress also has been reported with regard to the theory of hydrostatic extrusion. Analytical methods that had been used in

conjunction with metalforming processes prior to the hydrostatic extrusion technique were brought into the analysis of the new process. Specifically, the slab method, or free-body approach, was the most frequently employed. Other techniques such as "extremum principles," the "slip line field theory," and especially the "upper bound approach" also have been quite successful [217]. Analytical formulas made it possible to predict the pressure required to extrude materials with a prescribed amount of deformation which, in turn, was useful in determining the optimum shape of the die and the selection of other process parameters.

More recently, however, numerical techniques such as finite differences and finite elements have been applied to analyze the stress and strain distributions in the products. The mathematical tools, however, require the accurate, constitutive equation of the billet material to be known as the basis of the calculation.

2.1 THEORETICAL BACKGROUND

2.1.1 Introduction

Because of the simplicity in handling, some of the analytical methods have been applied to many of the forming processes. In the case of hydrostatic extrusion, the slab method, the lower bound theory, and the upper bound theory have been employed to estimate the stresses as well as the extrusion pressure [218]. The slip line field method presents an accurate solution for plane strain problems with rigid, perfectly plastic materials. Various slip line fields for extrusion are

cited by Johnson and Kudo [219]. Other theoretical methods such as Ewing's series method [220] and Collins' matrix method [221] were proposed later. These methods, however, are limited to plane strain problems and do not seem to be usable in practical situations.

In recent years, on the other hand, a new and more accurate numerical analysis of the extrusion process has been obtained by employing the finite element technique. The finite element method is a numerical technique for solving differential equations governing engineering problems by dividing the material into many hypothetical elements interconnected at nodal points. For analysis of metal forming, there are two schemes of the finite element method, i.e., an elastic-plastic one and a rigid-plastic one. In later sections, the abovementioned theories, as well as the finite element method, are discussed in more detail.

2.1.2 Basic Concepts

To express the equations of mechanics in Cartesian coordinates in simple forms, it is convenient to use the stress tensor:

$$\sigma_{ij} = \begin{pmatrix} \sigma_{xx} & \sigma_{xy} & \sigma_{xz} \\ \sigma_{yx} & \sigma_{yy} & \sigma_{yz} \\ \sigma_{zx} & \sigma_{zy} & \sigma_{zz} \end{pmatrix} = \begin{pmatrix} \sigma_x & \tau_{xy} & \tau_{xz} \\ \tau_{yx} & \sigma_y & \tau_{yz} \\ \tau_{zx} & \tau_{zy} & \sigma_z \end{pmatrix} \qquad (2.1)$$

where the first subscript of a stress component refers to the direction of the normal to the area, and the second subscript refers to the direction of the force component, Figure 2.1.

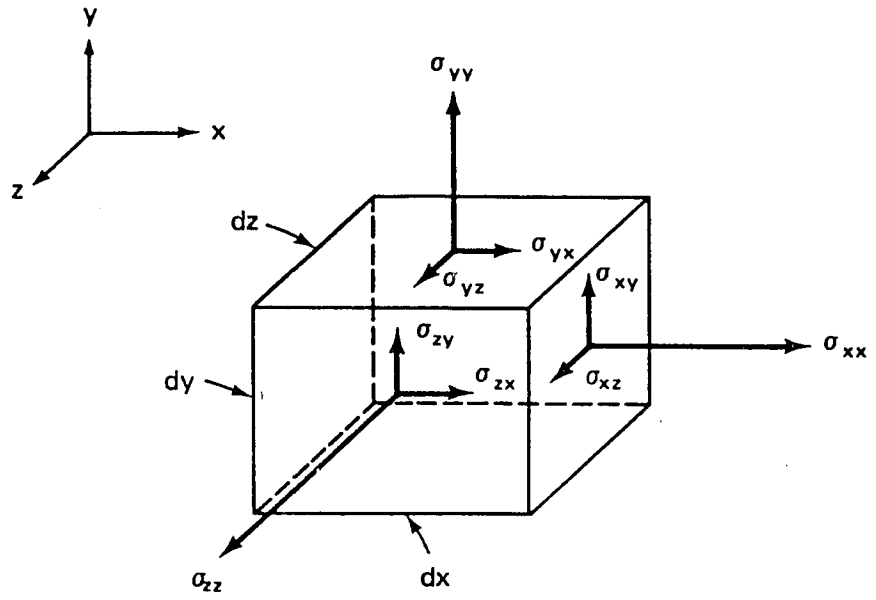

Figure 2.1 Stress element for a homogeneous state of stress.

Equilibrium implies the absence of rotational effects around any axis, so:

$$\sigma_{xy} = \sigma_{yx} \tag{2.2}$$

or, more generally,

$$\sigma_{ij} = \sigma_{ji} \tag{2.3}$$

The stress components should satisfy the equations of equilibrium in the body. Therefore,

$$\frac{\partial \sigma_x}{\partial x} + \frac{\partial \tau_{xy}}{\partial y} + \frac{\partial \tau_{xz}}{\partial z} + F_x = 0,$$

$$\frac{\partial \tau_{yx}}{\partial x} + \frac{\partial \sigma_y}{\partial y} + \frac{\partial \tau_{yz}}{\partial z} + F_y = 0, \qquad (2.4)$$

$$\frac{\partial \tau_{zx}}{\partial x} + \frac{\partial \tau_{zy}}{\partial y} + \frac{\partial \sigma_z}{\partial z} + F_z = 0$$

where F_x, F_y, and F_z are components of body forces per unit volume. Tensorial representation of the above equations is:

$$\frac{\partial \sigma_{ij}}{\partial x_j} + Fi = 0. \qquad (2.5)$$

The hydrostatic stress component is the average value of normal stress components:

$$\sigma_m = (\sigma_x + \sigma_y + \sigma_z)/3 = \sigma_{ii}/3. \qquad (2.6)$$

The deviatoric stress tensor, often used in the theory of plasticity, is defined as:

$$\sigma'_{ij} = \sigma_{ij} - \delta_{ij}\sigma_m \qquad (2.7)$$

where δ_{ij} is the Kronecker delta, which is 1 when i=j and 0 when i≠j. The strain at a point of the body is defined by the tensor:

$$\varepsilon_{ij} = \frac{1}{2}\left(\frac{\partial u_j}{\partial x_i} + \frac{\partial u_i}{\partial x_j}\right) \qquad (2.8)$$

where u_i and u_j are the components of displacement.

The strain rate is defined as the rate at which the strain changes with respect to time. So:

$$\dot{\varepsilon}_{ij} = \frac{d\varepsilon_{ij}}{dt} = \frac{1}{2}\left[\frac{\partial v_j}{\partial x_i} + \frac{\partial v_i}{\partial x_j}\right] \tag{2.9}$$

where v_i and v_j are the components of velocity. It should be noted that the engineering shear strain rate, i.e., $\dot{\gamma}_{xy}$, is double the tensor component of shear strain, i.e., $\dot{\varepsilon}_{xy}$:

$$\begin{aligned}\dot{\gamma}_{xy} &= \dot{\varepsilon}_{xy} + \dot{\varepsilon}_{yx} = 2\dot{\varepsilon}_{xy}\\ \dot{\gamma}_{xz} &= \dot{\varepsilon}_{xz} + \dot{\varepsilon}_{zx} = 2\dot{\varepsilon}_{xz}\\ \dot{\gamma}_{yz} &= \dot{\varepsilon}_{yz} + \dot{\varepsilon}_{zy} = 2\dot{\varepsilon}_{yz}.\end{aligned} \tag{2.10}$$

Also, the volumetric strain rate is defined by:

$$\dot{\varepsilon}_v = \dot{\varepsilon}_x + \dot{\varepsilon}_y + \dot{\varepsilon}_z = \dot{\varepsilon}_{ii}. \tag{2.11}$$

In many of the analyses of metal forming problems, the material is assumed to obey von Mises' yield criterion:

$$(\sigma_x-\sigma_y)^2 + (\sigma_y-\sigma_z)^2 + (\sigma_z-\sigma_x)^2 + 6(\tau_{xy} + \tau_{xz} + \tau_{yz}) - 2\bar{\sigma}^2 = 0 \tag{2.12}$$

where $\bar{\sigma}$ is the yield, or flow stress.

Mises' yield criterion is expressed in terms of deviatoric stress tensor as:

$$3\sigma'_{ij}\,\sigma'_{ij} - 2\bar{\sigma}^2 = 0. \tag{2.13}$$

In the "rigid-plastic" assumption of the materials, the elastic deformation is neglected, and the relation between deviatoric strain rate and stress components is given by the Levy-Mises equation as:

$$\dot{\varepsilon}_{ij} = \frac{3}{2}\frac{\dot{\bar{\varepsilon}}}{\bar{\sigma}}\sigma'_{ij} \tag{2.14}$$

where $\dot{\bar{\varepsilon}}$ is the equivalent strain rate and is expressed as:

$$\dot{\bar{\varepsilon}} = \left(2/9\left[(\varepsilon_x - \varepsilon_y) + (\varepsilon_x - \varepsilon_z) + (\varepsilon_y - \varepsilon_z) + 3/2\,(\gamma_{xy} + \gamma_{yz} + \gamma_{yz})\right]\right)^{1/2}$$

$$= \left(3/2\ \dot{\varepsilon}_{ij}\dot{\varepsilon}_{ij}\cdot\right)^{1/2} \tag{2.15}$$

This flow rule implicitly includes the incompressibility condition of:

$$\dot{\varepsilon}_v = \dot{\varepsilon}_x + \dot{\varepsilon}_y + \dot{\varepsilon}_z$$

$$= \frac{3}{2}\frac{\dot{\bar{\varepsilon}}}{\bar{\sigma}}(\sigma'_x + \sigma'_y + \sigma'_z) = 0. \tag{2.16}$$

The equivalent strain is obtained by integrating the equivalent strain rate in terms of time. Therefore:

$$\bar{\varepsilon} = \int \dot{\bar{\varepsilon}}dt. \tag{2.17}$$

The equivalent strain is used as a measure of the degree of work-hardening. Finally:

$$\bar{\sigma} = H(\bar{\varepsilon}). \tag{2.18}$$

In the elastic-plastic behavior, however, the relations between the strain rate and stress rate is given by Prandtl-Reuss' equation. Strain rate components are expressed in terms of elastic strain rate which, in turn, is related to stress rate through Hooke's law:

$$\begin{aligned} \dot{\varepsilon}_{ij} &= \frac{\partial \dot{\sigma}'_{ij}}{2G} + \delta_{ij} \frac{\dot{\sigma}_m}{3K} + \frac{3\dot{\bar{\varepsilon}}}{2\bar{\sigma}} \sigma'_{ij} \\ &= \frac{\dot{\sigma}'_{ij}}{2G} + \delta_{ij} \frac{\dot{\sigma}_m}{3K} + \frac{3\dot{\bar{\sigma}}}{2\bar{\sigma}H'} \sigma'_{ij} \end{aligned} \tag{2.19}$$

where

$$H' = \frac{d\bar{\sigma}}{d\bar{\varepsilon}}. \tag{2.20}$$

The inversion of the above equations has been carried out by Hill [ ] as:

$$\dot{\sigma}_{ij} = 2G \left(\dot{\varepsilon}_{ij} + \frac{\nu}{1-2\nu} \delta_{ij} \dot{\varepsilon}_{ii} - \sigma'_{ij} \frac{\sigma'_{k\ell}\dot{\varepsilon}_{k\ell}}{s}\right) \tag{2.21}$$

where

$$s = \frac{2}{3} \bar{\sigma}^2 \left(1 + \frac{1}{3G} H'\right) \tag{2.22}$$

The plastic work per unit volume up to an equivalent strain $\bar{\varepsilon}$, is given by the relation:

$$w = \int_0^{\bar{\varepsilon}_1} \bar{\sigma} d\bar{\varepsilon}. \tag{2.23}$$

This corresponds to the area under the flow curve shown in Figure 2.2.

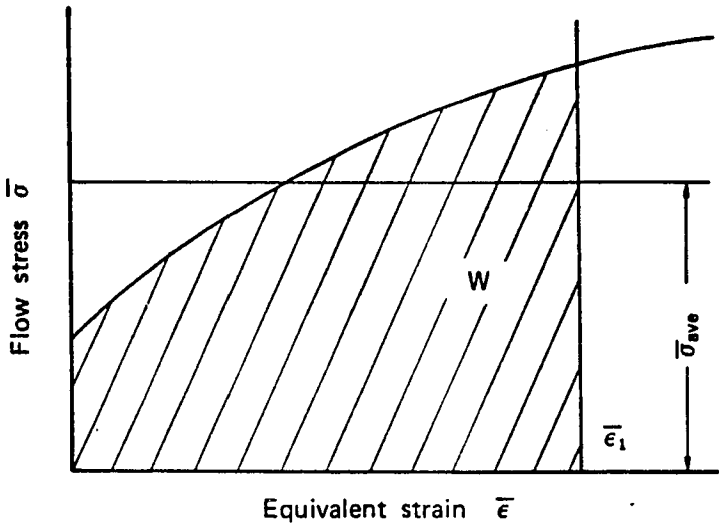

Figure 2.2. Flow curve.

On the other hand, the work done by the fluid pressure, P, in extruding a billet of length l_b and cross-sectional area A_b is given by:

$$W_{pressure} = P l_b A_b. \tag{2.24}$$

If it is assumed that all of this work is dissipated in plastic deformation and has caused an equivalent strain $\bar{\varepsilon}_1$ in the product, then:

$$W_{deformation} = \ell_b A_b \int_0^{\bar{\varepsilon}_1} \bar{\sigma} d\bar{\varepsilon}. \tag{2.25}$$

Comparing equations (2.24) and (2.25) reveals that the extrusion pressure and the strain, ε, in the product are related by:

$$P = \int_0^{\bar{\varepsilon}_1} \bar{\sigma} d\bar{\varepsilon}. \tag{2.26}$$

In calculating the adiabetic temperature rise in the product, almost all of the plastic work is assumed to have been converted into heat. Due to this complete conversion, the temperature rise ΔT then is calculated from the relation:

$$\Delta T = W/J\rho c, \tag{2.27}$$

where W is the plastic work, J is the mechanical equivalent of heat, and ρ and c are the density and specific heat of the material, respectively.

Not all of the extrusion pressure is spent on uniform deformation. In fact, this pressure is considered to consist of three components: 1) the pressure to overcome the frictional force between the billet and the die, 2) the pressure for uniform deformation of the material, and the pressure for redundant deformation. The frictional force depends on the contact area between the die surface and the work piece. Therefore, for a given extrusion ratio and a constant coefficient of friction, the pressure required to overcome this force increases as the die angle

decreases. The uniform deformation is the minimum deformation necessary to change the outside dimensions of the billets and hence the pressure required to cause such deformation increases with an increase in the reduction ratio and die angle. Finally, the redundant deformation, which increases with the die angle, is the additional internal shearing that occurs in the product. Figure 2.3 is a schematic comparison of ideal and actual deformation.

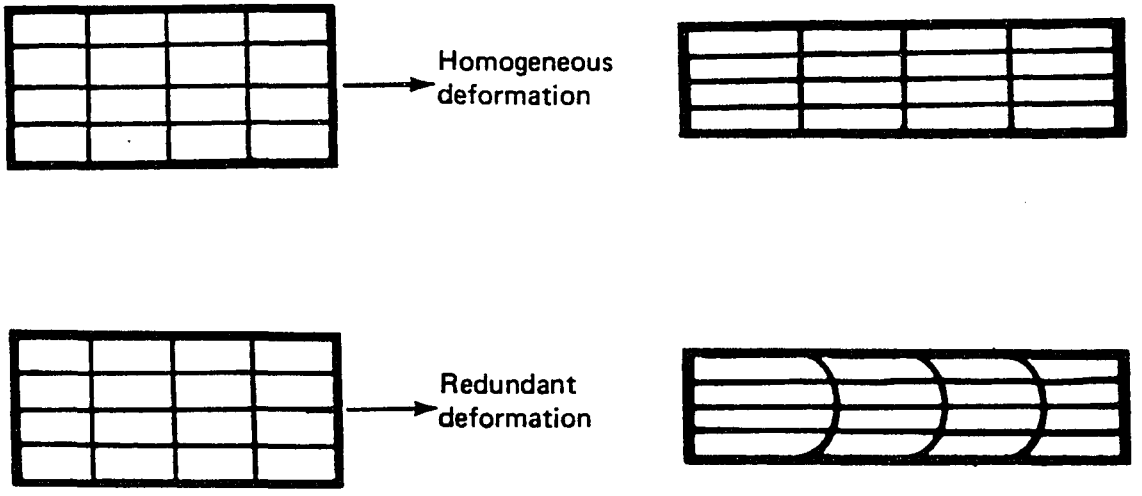

Figure 2.3. Comparison of ideal and actual deformation.

Since the frictional force decreases with an increase in the die angle, and the redundant work increases with an increase in die angle, there must be an optimum value of die angle in order to minimize the extrusion pressure. Indeed, in practice this optimum value of die angle has been established to be in the range of 30 to 60 degrees for hydrostatic extrusion [222].

Theoretical estimation of hydrostatic extrusion pressure ranges from the ideal extrusion pressure, derived from the equation [223]:

$$P_{ideal} = \int_0^{\ln R} \bar{\sigma} d\bar{\varepsilon} \qquad (2.28)$$

to the empirical expression [224] of:

$$P = a + b \ln R \qquad (2.29)$$

where R is the extrusion ratio, and a and b are constants. In extrusions with large reduction ratios and small die angles, the value of a is small compared with b ln R. Therefore, the above equation may be approximated by [225]:

$$P = c \ln R, \qquad (2.30)$$

where c is a constant for a given material, depending on the various theories, some of which are discussed in more detail later. The constants of equation (2.29) will assume different values.

2.1.3 Co-extrusion

As indicated in Chapter 1, metallic compounds consisting of two or more metals have a wide variety of use, and such products have been produced and implemented in almost every sector of industry. Extrusion

in general and hydrostatic extrusion in particular provide efficient means of producing such products and, therefore, numerous investigations have been carried out by researchers in the past [226,227,228,229,230].

The analysis of co-extrusion of bimetallic compounds has been categorized by the dispositions of their individual constituents, namely soft-core, hard-clad composites, or hard-core, soft-clad products. Copper-clad aluminum bars are an example of the former, while Glidcop® (hard copper alloys) clad with copper represent the latter. Current investigation is of the hard-core, soft-clad composite.

The theoretical investigations of co-extrusion have ranged from empirical techniques [231,232] to complex upper bound analyses [233] with computer-aided numerical simulation techniques appearing in recent years [234,235,236].

In order to obtain estimates of the extrusion pressure for composite billets, Alexander and Hartley [237] made extensions to the analysis developed for homogeneous materials. They established an upper bound on extrusion pressure by choosing particular velocity fields. The pressure expression used was of the form in equation 2.29, and the coefficients a and b were related to the volume fraction of the constituents. Alexander and Hartley also established a lower bound on the extrusion pressure simply by determining the weighted average of the lower bounds for a solid cylindrical core surrounded by an annular sheath.

The interfacial strength of copper-clad aluminum rodes were investigated by Lugosi, et. al [238], and it was found that severe fluctuations of extrusion pressure were associated with billets with low interfacial strength. This was because of the faster extrusion of

aluminum cores compared to a copper sheath adhering to the die and acting as a die orifice.

In the study of the hydrostatic co-extrusion of aluminum and copper, Hartley and Srinivasan [239] investigated the development of stresses during extrusions under different processing conditions of die angle, extrusion ratio, and volume fraction of the core. They concluded that lower die angles in general promote a more uniform metal flow and lower residual stress magnitudes.

In their analysis of hydrostatic co-extrusion of bimetallic compounds, Avitzur et. al [240,241] concluded that, in general, fracture of the hard constituent is more probable than of the softer one, the smaller the range of safe extrusion parameters. The conclusions are valid regardless of the arrangement of the constituents as soft-core, hard-clad, or vice versa.

Another interesting investigation of the bimetallic compounds with hard cores was reported by Osakada et. al [242]. They studied three different modes of deformation of such composites, depending on the ratio of yield and the strength of the two materials. Uniform deformation was referred to the products in which both materials deformed to the same reduction. Cladding, however, occurred when the clad material was much softer than the core. In this case, no deformation of the core occurred, and the softer clad deformed to cover the hard core fractures due to tensile necking.

2.2 PREVAILING THEORIES

2.2.1 Analytical Approaches

One of the major concerns regarding any forming operation is the prediction of the externally-applied loads required to cause the metal to flow and deform to the desired configuration. Due to the uncertainties introduced during complex deformations, such factors as friction, non-homogeneous deformation, strain hardening, and exact values of load requirements are seldom predictable. Nevertheless, by imposing pertinent assumptions, several techniques have been developed which enable an approximation of these loads. Generally, however, these techniques do not provide a means for predicting other information, such as the mechanical properties of the product. Some of the prevailing analytical techniques for force prediction are explained briefly in the next section.

2.2.1.1 Energy method

The deformation energy method is the simplest method for prediction of external loads. This technique assumes that the process is ideal in the sense that external work is completely utilized to cause deformation only, i.e., there are no frictional losses or redundant work. In reality, however, frictional work is consumed at the interface of the work piece and the die. Redundant work also exists and is caused by internal distortion [243].

To illustrate the technique, consider an element Δl of the billet shown in Figure 2.4. The initial diameter of the billet is D_o and the

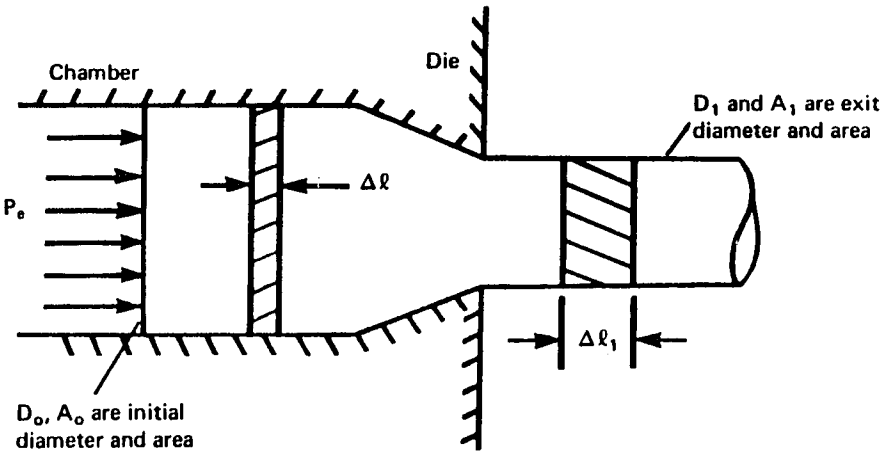

Figure 2.4. Schematic diagram of direct extrusion.

final diameter D_1. Due to the incompressibility of the material as it flows through the converging die, a volume of metal $A_o \Delta l$ must exit as $A_1 l_1$ and the total external work done by the pressure is given by:

$$W = P_e A_o \Delta l. \tag{2.31}$$

The deformation energy expended in deforming the volume $A\Delta l$ to a strain ε is given as:

$$E_d = \left(\int_0^{\bar{\varepsilon}} \bar{\sigma} d\bar{\varepsilon} \right) \quad A_o \Delta l_1. \tag{2.32}$$

Since the mean flow stress σ_{ave} is given by:

$$\sigma_{ave} = \frac{1}{\varepsilon_1} \int_0^{\varepsilon} \sigma d\varepsilon \qquad (2.33)$$

then:

$$E_d = (\sigma_{ave} \quad \overline{\varepsilon}) \quad A_{o\delta\ell}. \qquad (2.34)$$

Also, since the deformation is assumed to be ideally uniform, the equivalent strain in the product is:

$$\overline{\varepsilon}_{ideal} = \ln R. \qquad (2.35)$$

Therefore:

$$E_d = (\sigma_{ave} \ln R)\, A_o\, \delta\ell \qquad (2.36)$$

by equating the external work to the energy consumed in deforming the workpiece, this equation results:

$$P_e = \sigma_{ave} \ln R. \qquad (2.37)$$

It relates the external pressure of the deforming material to the extrusion ratio and to the average stress of deformation. As mentioned earlier, this simplistic approach neglects friction and provides no details regarding metal flow.

2.2.1.2 Slab analysis

The slab method, also called the free body equilibrium approach, was developed to calculate stresses and loads by integrating the differential equation of equilibrium under a simplified stress state. The assumption of planar sections remaining planar is made and, therefore, the deformation is considered to be homogeneous in regard to the determination of induced strain. Moreover, although the effects of surface friction are included in the force balance, they don't influence the internal distortion of the material or of the orientation of principal directions.

Because of its simplicity, the slab method has been applied to many forming processes. Osakada and Mellor [244] showed that the required pressure for extrusion of a material with yield stress σ_y through a conical die of an included angle α at an extrusion ratio R is expressed as:

$$P = \sigma_y \left(1 + \frac{1}{\mu \mathrm{Cot}\alpha}\right)\left(R^{\mu \mathrm{Cot}\alpha} - 1\right) + \frac{4\alpha}{3\sqrt{3}} \qquad (2.38)$$

where μ is the friction coefficient between the die and the workpiece. For small die angles, where $\mu \mathrm{Cot}\alpha < 1$, the above equation is simplified to:

$$P = \sigma_y \left\{(1 + \mu \mathrm{Cot}\alpha)\ln R + \frac{4\alpha}{3\sqrt{3}}\right\} \qquad (2.39)$$

2.2.1.3 Lower bound analysis

This method was developed on the basis of the variational principle and some constraining conditions. The contribution of friction, for example, is entirely ignored. As the name suggests, the analysis provides an underestimate of the exact load from a statically admissible stress field. The detailed description of this theorem is lengthy and beyond the scope of this study. The reader, however, is referred to a book by Prager and Hodge [245], in which the lower bound theorem is presented as:

"Among all statically admissable stress fields, the actual one maximizes the expression:

$$I = \int_{S_v} T_i v_i ds \tag{2.40}$$

where I is the computed power supplied by the tool over surfaces over which velocity is prescribed."

In the above equation, T_i are the normal components of surface traction over which velocity is prescribed, i.e., the interface between the ram and the billet in direct extrusion. The v_i is the ram velocity in that case.

2.2.1.4 Upper bound analysis

The upper bound analysis is another technique based on the varia-

tional principle which predicts a load that is at least equal to or greater than the exact load needed to cause plastic flow. This approach, unlike the lower bound technique, does not regard stress equilibrium. Instead, the method focuses upon satisfying a yield criterion and upon assuming that the velocity field is kinematically admissible. Avitzur [246] assumed a special velocity field with the material within the die flowing toward the apex. He derived the following expression for the load:

$$P = \sigma_y \{(f(\alpha) + \frac{m}{\sqrt{3}} \text{Cot}\alpha)\ln R + \frac{2}{\sqrt{3}} (\frac{\alpha}{\sin^2\alpha} - \text{Cot}\alpha)\}$$

where σ_y is the effective flow stress of the material, α the semi-cone angle, and $f(\alpha)$ as the following: (2.42)

$$f(\alpha) = \frac{1}{\sin^2\alpha} (1-\text{Cos}\alpha\sqrt{1-\frac{11}{12}\sin^2\alpha} + \frac{1}{\sqrt{132}} \ln \frac{1+\sqrt{11/12}}{\sqrt{11/12\ \text{Cos}\alpha} + \sqrt{1-(11/12)\sin^2\alpha}}$$

By employing the above expressions, it is possible to determine critical die angles for extrusion of a given material with an extrusion ratio of R.

2.2.2 Numerical Approaches

Numerical approaches to the metalforming analysis are relatively new techniques which have made great progress parallel to that of electronic computers. The finite element method, specifically, tackles the problem of metalforming by dividing the continuum into an assemblage

of discrete, quadrilateral regions called elements. This numerical method which has been used in this study is the subject of the next chapter.

CHAPTER 3

FINITE ELEMENT ANALYSIS OF METAL FORMING PROCESSES

3.1 INTRODUCTION

The underlying idea of the finite element method is that any continuous quantity can be approximated by a set of piecewise continuous functions defined over a number of components assembled to represent the quantity. The discretization of continuum can be done intuitively by creating an analogy between real discrete elements and finite portions of the continuum domain. In fact, the concept of the finite element analysis was conceived in the early 1940s when McHenry [301], Hrenikoff [302], and Newmark [303] showed that adequate solutions to a continuum problem could be obtained by substituting an arrangement of simple elastic bars for small portions of the continuum. Therefore, it is from the view of engineering analogy that the term "finite element" has come about.

The method had its birth in the aerospace industry in the early 1950s and was first presented in the publication by Turner, Clough, Martin, and Topp [304]. In fact, Clough [305] was the first to use the term "finite element," which he defines as "a standard methodology applicable to discrete systems." The publication by Turner, et. al in 1956 stimulated other researchers and resulted in several technical articles that discussed the application of the method to structural and solid mechanics.

In 1963, Melosh [306] showed that the finite element was actually a

variation of the well-known Raleigh-Ritz procedure. This was an important theoretical contribution and helped numerous other researchers to better understand and apply the technique in their respective fields of study.

The connection of the finite element method with a minimization procedure quickly led to its extensive use in structural problems in which the method produced a set of equilibrium equations by minimizing the potential energy of the system. The publications by Zienkiewicz and Cheung [307], Wilson and Nickell [308], and Visser [309] were first in showing the application of the finite element method to heat transfer problems. The application to fluid mechanics, particularly to the flow through a porous medium, followed immediately [310].

Today a great number of numerical analysts have turned to finite elements, and the technique itself has advanced from a procedure for solving structural problems to a general numerical method for solving a differential equation or systems of differential equations. This advancement has been accomplished in a short period of time and has been assisted by the development of high-speed digital computers. Currently, there are a number of general purpose finite element programs available that are capable of handling problems of any magnitude in virtually every sector of the engineering discipline. In this work, a non-linear, large deformation, elasto-plastic finite element code, ABAQUS [311], has been used to simulate the hydrostatic co-extrusion of bi-metallic compounds, the analysis of which is presented in the sections that follow.

3.2 THEORY

In the analysis of metal forming, there are two schemes of the finite element method. The first is the "rigid-plastic," or "flow" analysis, which assumes that the metal is a non-Newtonian fluid having a visco-plastic or rigid-plastic behavior [312]. The second scheme is the solid approach, or the elastic-plastic analysis [313,314,315,316]. The rigid-plastic assumption is not feasible for the analysis in which the residual stresses are concerned. This is due to the fact that in this approach the elastic deformations are neglected, and the strain or strain rate components are only plastic ones [317]. Large metal deformations, however, are elastic-plastic in nature and are generally non-linear both in material properties and in geometry. The non-linearities in such deformations are associated with large displacements involving rigid body motions and strains [318].

Lee and McMeeking [319, 320] showed that in most cases of elastic-plastic metal deformation, the elastic response is essentially unchanged by plastic deformation, and the two behaviors can be considered uncoupled. This is because the elastic properties depend on the arrangement of atoms in the bulk and are basically unaffected by moderate plastic flow, which is due to the movement of dislocations [321]. Therefore, since elastic and plastic deformations are due to different processes in the lattice, it is justifiable to separate them in the constitutive equations governing the elastic-plastic deformation of metals. Before proceeding with these equations, however, a brief summary of the continuum mechanics is due, and the following sections of this chapter are devoted to this purpose.

3.2.1 Basic Mechanics

3.2.1.1 Displacements

In any continuum mechanics problem, the analyst describes the initial configuration of the body and is interested in its deformation throughout the history of loading. The material particle initially located at some position x in space will move to a new position z, Figure 3.1. Since we assume that material cannot appear or disappear,

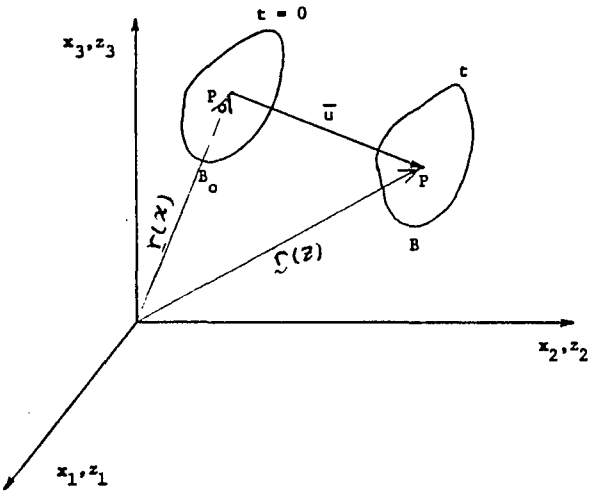

Figure 3.1 Coordinate systems and description of displacement.

there will be a one-to-one correspondence between x and z, so that we can always write the history of the location of a particle as:

$$z = z(x,t) \tag{3.1}$$

and this relationship can be inverted, i.e., we know x when we know z and t. Therefore,

$$x_i = x_i(z_1,z_2,z_3,t) \qquad i = 1,2,3 \qquad (3.2)$$

and

$$z_i = z_i(x_1,x_2,x_3,t) \qquad i = 1,2,3 \qquad (3.3)$$

The above transformations are assumed to be single-value and continuous, provided that:

$$0 < \det. \frac{\partial z_i}{\partial x_j} < \infty \qquad (3.4)$$

where the $\frac{\partial z_i}{\partial x_j}$ is the Jacobian.

Now, depending on whether or not the displacement vector is associated with a point in the original or deformed configuration, the components of the displacement vector are given by the following relations:

$$u_i(x_1,x_2,x_3) = z_i(x_1,x_2,x_3) - x_i \qquad (3.5)$$

$$u_i(z_1,z_2,z_3) = z_i - x_i(z_1,z_2,z_3) \qquad (3.6)$$

The material description of the velocity vector is simply the time derivative of the displacement vector; thus,

$$v_i = \frac{\partial u_i(x,t)}{\partial t} \qquad i = 1,2,3 \qquad (3.7)$$

3.2.1.2 Strain Measures

The description of strain or the change in distance between any two points on the body is the key to the analysis of deformation. Consider an infinitesimal line segment connecting two neighboring particles, located at x and at x+dx in the initial configuration, Figure 3.2.

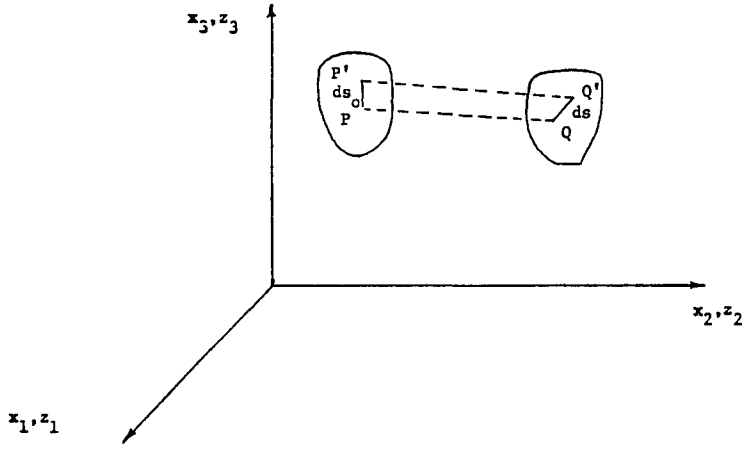

Figure 3.2 Deformation of a continuum.

In the original and current configurations, we must have, respectively:

$$dx_i = \frac{\partial x_i}{\partial z_j} dz_j \qquad (3.8)$$

and

$$dz_i = \frac{\partial z_i}{\partial x_j} dx_j \tag{3.9}$$

Also, in the initial and current configuration, we can write:

$$ds_o^2 = dx_1^2 + dx_2^2 + dx_3^2 \tag{3.10}$$

and

$$ds^2 = dz_1^2 + dz_2^2 + dz_3^2 \tag{3.11}$$

or simply:

$$ds_o^2 = dx^T \cdot dx \tag{3.12}$$

and

$$ds^2 = dz^T \cdot dz \tag{3.13}$$

It is usually important to distinguish rigid body motion and straining motion. Therefore, the stretch of the infinitesimal gauge length ds_o is defined as:

$$\lambda = \frac{ds}{ds_o} = \left[\frac{dz^T \cdot dz}{dx^T \cdot dx}\right]^{\frac{1}{2}} \tag{3.14}$$

and if $\lambda = 1$, there is no strain involved--the gauge length has undergone rigid body motion only. If $\lambda \neq 1$, however, there is strain, and in order to define this motion, we may rewrite expressions (3.10) and (3.11), using the Kronecker delta, as:

$$ds_o = \delta_{ij} dx_i dx_j = \delta_{ij} \frac{\partial x_i}{\partial z_r} \frac{\partial x_j}{\partial z_s} dz_r dz_s \tag{3.15}$$

and

$$ds = \delta_{ij} dz_i dz_j = \delta_{ij} \frac{\partial z_i}{\partial x_r} \frac{\partial z_j}{\partial x_s} dx_r dx_s \tag{3.16}$$

Useful results are obtained by subtracting the expressions (3.10) and (3.11) from one another; therefore,

$$ds^2 - ds_o^2 = \left(\delta_{rs} \frac{\partial z_r}{\partial x_i} \frac{\partial z_s}{\partial x_j} - \delta_{ij}\right) dx_i dx_j \tag{3.17}$$

or

$$ds^2 - ds_o^2 = \left(\delta_{ij} - \delta_{rs} \frac{\partial x_r}{\partial z_i} \frac{\partial x_s}{\partial z_j}\right) dz_i dz_j \tag{3.18}$$

We define the strain tensors:

$$e_{ij} = \tfrac{1}{2} \left(\delta_{rs} \frac{\partial z_a}{\partial x_i} \frac{\partial z_b}{\partial x_j} - \delta_{ij}\right) \tag{3.19}$$

and

$$h_{ij} = \tfrac{1}{2} \left(\delta_{ij} - \delta_{rs} \frac{\partial x_r}{\partial z_i} \frac{\partial x_s}{\partial z_j}\right) \tag{3.20}$$

so that:

$$ds^2 - ds_o^2 = 2e_{ij}\, dX_i dX_j \tag{3.21}$$

and

$$ds^2 - ds_o^2 = 2h_{ij}\, dz_i dz_j \tag{3.22}$$

The strain tensor e_{ij} is the material description of a strain tensor and is known as Green's strain tensor, while h_{ij} is the spatial form of the strain tensor and is called Cauchy's or Almansi's strain tensor.

Using the components of the displacement vector u, and the relations:

$$\frac{\partial z_r}{\partial x_i} = \frac{\partial u_r}{\partial x_i} + \delta_{ri}, \qquad \frac{\partial x_r}{\partial z_i} = \delta_{ri} - \frac{\partial u_r}{\partial x_i} \tag{3.23}$$

these forms of the strain tensors may be written as:

$$e_{ij} = \tfrac{1}{2}\left[\frac{\partial u_j}{\partial x_i} + \frac{\partial u_i}{\partial x_j} + \frac{\partial u_a}{\partial x_i}\frac{\partial u_a}{\partial x_j}\right] \tag{3.24}$$

and

$$h_{ij} = \tfrac{1}{2}\left[\frac{\partial u_j}{\partial z_i} + \frac{\partial u_i}{\partial z_j} - \frac{\partial u_a \partial u_a}{\partial z_i \partial z_j}\right] \tag{3.25}$$

In the unabridged notation (x,y,z for x_1,x_2,x_3; and u,v,w for u_1,u_2,u_3), the Green's strain tensor e_{xx} is expressed as:

$$e_{xx} = \frac{\partial u}{\partial x} + \frac{1}{2}\left[\left(\frac{\partial u}{\partial x}\right)^2 + \left(\frac{\partial v}{\partial y}\right)^2 + \left(\frac{\partial w}{\partial z}\right)^2\right] \tag{3.26}$$

Designating e_1 as the measure of extension per unit undeformed length, or

$$e_1 = \frac{ds - ds_o}{ds_o} \tag{3.27}$$

then e_1 can be related to the material strain tensor by the expression:

$$e = (2e_{11} + 1)^{\frac{1}{2}} - 1 \tag{3.28}$$

The volumetric strain $\frac{dv}{dv_o}$ is expressed in terms of the material strain tensor; as

$$\frac{dV}{dV_o} = J \tag{3.29}$$

where J is the Jacobian and is expressed as:

$$J = (1 + 2I_e + 4II_e + 8III_e)^{\frac{1}{2}} \tag{3.30}$$

where I_e, II_e, and III_e are the first, second, and third strain invariants, respectively, and are defined as:

$$\begin{aligned} I_e &= e_{AA} \\ II_e &= 1/2(e_{AA}e_{BB} - e_{CD}e_{CD}) \\ III_e &= 1/6(2e_{AB}e_{BC}e_{CA} - 3e_{EF}e_{EF}e_{MM} + e_{NN}e_{PP}e_{QQ}). \end{aligned} \tag{3.31}$$

3.2.1.3 Strain Rates

The material strain rate tensor is the time derivative of the material strain tensor and is defined as:

$$\dot{e}_{ij} = \frac{\partial e_{ij}}{\partial t} = \frac{1}{2}\left[\frac{\partial v_i}{\partial x_j} + \frac{\partial v_j}{\partial x_i}\right] \tag{3.32}$$

where:

$$\frac{D}{Dt}(ds^2 - ds_o^2) = 2\dot{e}_{ij}\, dx_i dx_j \tag{3.33}$$

Similarly, the spatial strain rate tensor is the time derivative of the spatial strain tensor and is expressed as:

$$\dot{h}_{ij} = \frac{\partial h_{ij}}{\partial t} = \frac{1}{2}\left|\frac{\partial V_i}{\partial z_j} + \frac{\partial V_j}{\partial z_i}\right. \tag{3.34}$$

where:

$$\frac{D}{Dt}(ds^2 - ds_o^2) = 2\dot{h}_{ij}\, dz_i dz_j \tag{3.35}$$

The material and spatial strain rate tensors are related through the expression:

$$\dot{e}_{ij} = \dot{h}_{kl}\frac{\partial z_k}{\partial x_i}\frac{\partial z_l}{\partial x_j} \tag{3.36}$$

3.2.1.4 Stress Measures and Stress Rates

Referring to Figure 3.3, the material stress vector $P_{(n)}$, defined as the surface force per unit area in the undeformed body, may be expressed in terms of $t_{(n)}$ as follows:

$$P_{(n)} = t_{(n)} \frac{dA}{dA_o} \tag{3.37}$$

It is understood that $P_{(n)}$ acts on an area element whose unit normal in the initial state is n_o.

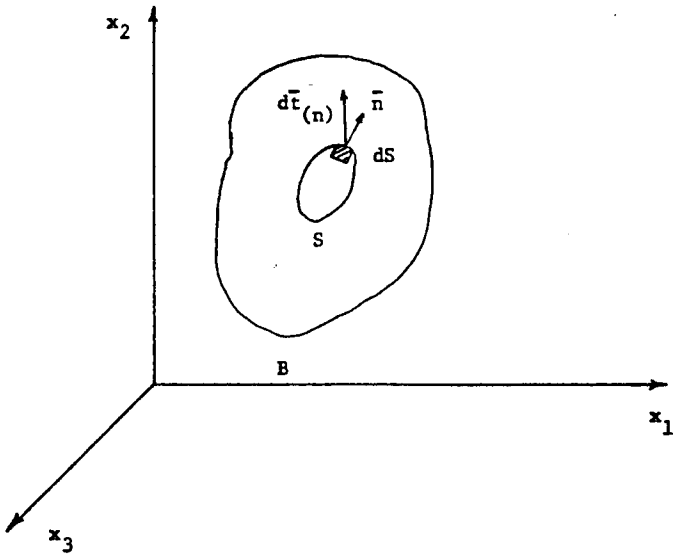

Figure 3.3 Stress principle.

The material, or Piola-Kirchhoff stress tensor, is defined as:

$$S_{AB} = \sigma_{ij} J \frac{\partial x_A}{\partial z_i} \frac{\partial x_B}{\partial z_j} \tag{3.38}$$

where σ_{ij} is the Cauchy stress tensor.

The material stress rate tensor $\dot{S}_{AB}$ is the time derivative of the stress tensor rate, therefore:

$$\dot{S}_{AB} = \frac{\partial S_{AB}}{\partial t} \tag{3.39}$$

3.2.2 Governing Equations for Elasto-plastic Deformation

The fundamental equation which describes the mechanics of elasto-plastic deformation is the Lagrangean description of the rate equation given by the expression

$$\int_{v^\circ} S_{ij}\delta\left(\frac{\partial v_j}{\partial x_i}\right)dv = \int_{s^\circ} f_i \delta v_i ds + \int_{v^\circ} b_i \delta v_i dv \tag{3.40}$$

where [s] is the material rate of the unsymmetric nominal stress tensor or the first Piolo-Kirchhoff stress tensor; {b}, the body force intensity vector; and {f}, the surface traction vector. In the above equation, all integrations are performed in the reference configuration. In the Eulerian description of the deformation, however, the motion is described in terms of true stress and true strain, both of which are defined with respect to an Eulerian or current reference frame. This is a more appropriate way of stating the rate equation since the laws of plasticity are usually formulated with reference to the current configuration ( ). The scheme that is most popular among the researchers in the field of large incremental metal deformation, however, is the "updated Lagrangean" scheme, in which the state at a time t is taken as the reference for displacements that occur at time $t+\Delta t$ ( ). This updated Lagrangean description of equation 3.40, as

formulated by McMeeking and Rice (322), is expressed as

$$\int_V (\tau^\circ_{ij}\delta\varepsilon_{ij} + \sigma_{ij}\delta(\varepsilon_{ik}\varepsilon_{kj} - V_{k,i}V_{k,j}/2))dv = \int_S f_i\delta v_i ds + \int_V b_i\delta v_i dv \tag{3.41}$$

where the suffix ,j refers to partial differentiation with respect to the spatial variable x and summation is implied with respect to repeated suffixes. In the above equation, $[\tau^\circ]$ is the Jaumann rate of the Kirchhoff stress tensor and is given by the equation

$$\tau^\circ_{ij} = \tau_{ij} - W_{ik}\tau_{kj} + \tau_{ik}W_{kj}. \tag{3.42}$$

τ°_{ij} is also related to $[S_{ij}]$ through the expression

$$\tau^\circ_{ij} = S_{ij} + \sigma_{kj}\varepsilon_{ki} + \sigma_{ik}\varepsilon_{kj} - \sigma_{ik}V_{j,k}. \tag{3.43}$$

In the above equation, $[\sigma_{ij}]$ is the Cauchy stress tensor and is related to the Kirchhoff stress tensor τ°_{ij} by the equation

$$\tau^\circ_{ij} = (\rho^\circ/\rho)\sigma_{ij} \tag{3.44}$$

where ρ° and ρ are the material densities in the reference and current configurations. The rate of deformation tensor $[\dot{\varepsilon}_{ij}]$ is given by:

$$\dot{\varepsilon}_{ij} = (v_{i,j} + v_{j,i})/2 \tag{3.45}$$

and the spin tensor, [w], by

$$W_{ij} = (v_{i,j} - v_{j,i})/2. \tag{3.46}$$

Equation ( ) is the well-known formulation of McMeeking and Rice, which was further improved for incremental procedures by Lee and Mallett (323). This improved equation serves as the fundamental formulation of the elasto-plastic incremental procedure used in ABAQUS, and is given as

$$\int_V (\rho/\rho^\circ)(\overset{*}{\tau}_{ij}\delta\varepsilon_{ij} + \tau_{ij}\delta(\varepsilon_{ik}\varepsilon_{kj} - v_{k,i}\, v_{k,j}/2))dv = \int_S f_i\delta v_i ds + \int_V b_i\delta v_i dv. \tag{3.47}$$

3.2.3 Constitutive Equations

A wide variety of metals is encountered in the metal deformation processes, and for any one of these metals there usually exists a range of constitutive models. The ones used in this study, copper and copper alloys, exhibit elastic response as well as inelastic behavior. Classical plasticity theory provides a useful model for these materials and the finite element program used in this work, ABAQUS, considers elastic-plastic and elastic-visco-plastic responses, using classical time-independent and time-dependent theories of plasticity at large strains presented in reference (324).

The mathematical models implemented in the program assume a linear elastic behavior below the yield point, Von Mises yield criterion, and a post-yield behavior. The mathematical description of this combination can be written in terms of the rates of deformation tensors as

$$\varepsilon = \varepsilon^{el} + \varepsilon^{pl}, \tag{3.48}$$

where ε^{el} and ε^{pl} are the elastic and the plastic parts of the total deformation rate, respectively. As shown by Lubarda (325), even though the above decomposition is not kinematically exact, it is quite reasonable for deformation processes in which elastic strains are small compared to plastic strains.

For elastic loading and any unloading, the generalized Hooke's Law can be written

$$\varepsilon_{ij}^{el} = \frac{1+\upsilon}{E} \overset{*}{\tau}_{ij} - \frac{\upsilon}{E} \delta_{ij} \overset{*}{\tau}_{kk}, \tag{3.49}$$

where υ is Poisson's ratio and E Young's modulus. The plastic component of the rate of deformation is given by the Prandtl-Reuss flow law as

$$\varepsilon_{ij}^{pl} = \frac{3}{2} \frac{\tau'_{ij}\, \tau'_{kl}}{h\tau^2} \overset{*}{\tau}_{kl}, \tag{3.50}$$

where h is the instantaneous slope of the flow curve in a simple tension test, and the primes indicate deviatoric tensors; τ^2 is defined by

$$\tau^2 = \frac{3}{2} \tau'_{ij}\, \tau'_{ij}. \tag{3.51}$$

Therefore, equations (3.48) through (3.51) define the stress-strain relationships for a given material, and they can be inverted and

generalized to express the stress rate in terms of the rate of deformation. This was carried out by Yamada et. al (326), who obtained the expression

$$\tau_{ij} = 2G(\varepsilon_{ij} + \frac{\upsilon}{1-2\upsilon}\delta_{ij}\varepsilon_{kk}) + \frac{1}{1+(h/3G)}\frac{3}{2\varepsilon}\frac{\tau'_{ij}\tau'_{kl}}{\tau^2}\varepsilon_{kl}, \tag{3.52}$$

where G is the shear modulus.

3.3 THE FINITE ELEMENT PROGRAM

The finite element program used in this investigation, ABAQUS, is a general-purpose nonlinear, large-deformation, elasto-plastic program designed as a flexible tool for numerical modeling of structures and their response to some form of external loading. Usage of the program requires the generation of an input data file that consists of two sections: model input and history input. Listing 3.1 is a sample of such an input data file and corresponds to a typical input file used for hydrostatic extrusion simulations.

The model input file is the description of both geometry and material of the problem. The geometric definition consists mainly of giving the nodes, elements, and kinematic constraints, as well as the associated parameters.

The history portion of the input file serves to define the variation of external parameters to which the response of the system is sought. Here the program is told to perform a certain type of analysis

LISTING 3.1. THE INPUT FILE FOR A TYPICAL EXTRUSION PROBLEM

```
*HEADING,UNSYMM
TEST PROBLEM FOR EXTRUSION
****
*NODE
1,0.00000000,1.50
2,0.66876644,1.50
3,1.20018500,1.50
.       .       .
.       .       .
.       .       .
*NGEN
1,161,10
2,162,10
3,163,10
.   .   .
.   .   .
.   .   .
*ELEMENT,TYPE=CAX4H,ELSET=ABILLET
1,1,2,12,11
*ELGEN,ELSET=ABILLET
1,4,1,1,42,10,10
*ELEMENT,TYPE=CAX4H,ELSET=BBILLET
5,5,6,16,15
*ELGEN,ELSET=BBILLET
5,4,1,1,42,10,10
*ELEMENT,TYPE=IRS21A,ELSET=RIG
9,9,19
*ELGEN,ELSET=RIG
9,42,10,10
*RIGID SURFACE,ELSET=RIG,TYPE=SEGMENTS,SMOOTH=0.8
START,2.74,4.58
LINE,1.0000,8.75000
LINE,1.0020,16.0000
*NSET,NSET=END,GENERATE
1,9,1
*NSET,NSET=AXIS,GENERATE
1,421,10
*NSET,NSET=PRINT,GENERATE
1,9,1
*NSET,NSET=PRINT,GENERATE
9,429,10
*NSET,NSET=PRINT,GENERATE
421,429,1
*ELSET,ELSET=PRINT
381,388,411,414,418
*ELSET,ELSET=END,GENERATE
1,8,1
*ELSET,ELSET=TOP,GENERATE
8,158,10
```

```
*MATERIAL,ELSET=ABILLET
*ELASTIC
128.0E+9,0.326
*PLASTIC
0.7165000E 08,0.00000000
0.1166904E 09,0.10000000
0.2126390E 09,0.20000000
     .      .      .
     .      .      .
     .      .      .
*MATERIAL,ELSET=BBILLET
*ELASTIC
128.0E+9,0.326
*PLASTIC
0.6320307E 08,0.00000000
0.1562519E 09,0.09999990
0.2259095E 09,0.19999980
     .      .      .
     .      .      .
     .      .      .
*MATERIAL,ELSET=RIG
*FRICTION
0.05
*SURFACE CONTACT
0.001,600000000
*BOUNDARY
AXIS,1
*RESTART,WRITE,FREQUENCY=10
*******
*STEP,AMP=RAMP,NLGEOM,INC=2,CYCLE=10
*STATIC,PTOL=5000.
0.5,1.0
*BOUNDARY
END,2,2,0.0125
*NODE PRINT,FREQ=2,NSET=PRINT
*EL PRINT,FREQ=2,LOADS,ELSET=PRINT
*PLOT,FREQ=2
DISPLACEMENT PLOTTING
*DISPLACED
1,1
*END STEP
*******
*RESTART,WRITE,FREQUENCY=30
*******
*STEP,AMP=RAMP,NLGEOM,INC=500,CYCLE=12
*STATIC,PTOL=3000000,RIKS
0.02,1.000,0.0001,0.3,,421,2,7.2
```

```
*BOUNDARY,OP=NEW
AXIS,1
*DLOAD
END,P1,600000000
TOP,P2,600000000
*PRINT,FREQUENCY=5,RESIDUAL=YES,CONTACT=YES
*EL PRINT,FREQ=50,LOADS,ELSET=PRINT
*NODE PRINT,FREQ=30,NSET=PRINT
*PLOT,FREQ=30
CONTOUR PLOTTING
*DISPLACED
1,1,1
*CONTOUR
1,5
2,5
3,5
. .
. .
. .
*END STEP
```

and/or the type of loading is prescribed. The basic concept of analysis in the program is the division of the problem history into "steps." Typically, a step is simply a change from one procedure and loading to another. Within each step, the program increments and iterates as necessary to analyze a step.

In the problem at hand, a number of steps had to be used, two of which are shown in listing 3.1. In the first step, the billet was moved, using displacement control, for the leading end of the billet to come into contact with the rigid surface which modeled the die. After establishing contact, the hydrostatic pressure loading was applied to the end and the top of the billet. Automatic incrementation of loads was used by which the program takes increments of load according to the rate of convergence. The scheme is based on the convergence rate

observed in the iteration process at each increment. After four iterations, the program checks the convergence rate and estimates if convergence is likely within the maximum number of iterations allowed. If not, the increment size is reduced by a factor of four. If, on the other hand, the convergence is achieved in less than one half of the maximum number of iterations allowed, the increment size is increased by a factor of 1.5. This process is continued until the maximum value of the load is achieved, or until the analysis is completed.

The procedure "input options" of the program provides the definition of the type of analysis needed to obtain the response of any structure under an external loading. Static analysis is used in hydrostatic extrusion problems due to the fact that inertia effects are insignificant. Because of nonlinearity, however, the analysis requires the solution of nonlinear equilibrium equations. This is normally done using Newton's method. In the case of extrusion problems, however, this technique is not efficient and often fails in the neighborhood of critical points. The modified Riks' algorithm, offered by the program, is one way of tracing nonlinear response from the pre-limit into the post-limit range. It chooses increments based on controlling the path length along the load-displacement response curve, and thus obtains solutions regardless of whether the response is stable or unstable. Details of the modified Riks' method are presented in a paper by E. Ramm (329).

3.4 SIMULATION PARAMETERS

The problem was treated axisymmetrically and therefore, half of the

meridian planes of the billets were discretized as the domain of the problem, as shown in Figure 3.4. Three extrusion ratios of 2.25, 4.0,

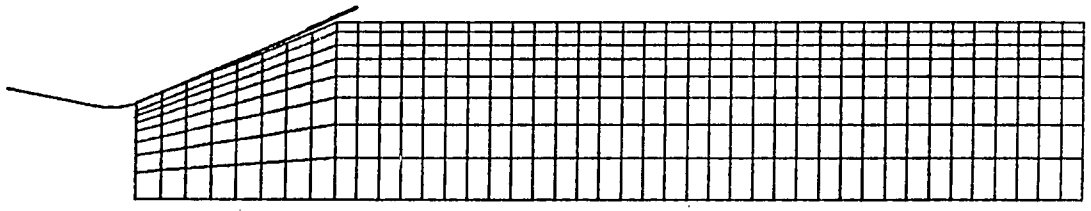

Figure 3.4. Finite element discretization of the domain.

and 7.5 in conjunction with two die angles of 45° and 60° were simulated. Solid copper, solid Glidcop®, 50% Glidcop® core, and 75% Glidcop® core composites were used. These simulation arrangements were in addition to those for which experimental results were available, namely, extrusion ratio of 3.0, die angle of 60°, and composites of 50, 25 and 10 volume percent Glidcop® core clad with copper.

Depending upon the extrusion ratio, the domain was divided into a 42 x 8 grid or a 42 x 6 grid. Eight-node axisymmetric hybrid elements with four integration stations were used, and the dies were simulated as properly-shaped rigid surfaces. A coefficient of friction of 0.05 was used at the die-billet interface, and uniform pressure boundary conditions were imposed on the exposed surfaces of the billets to simulate the hydrostatic fluid pressure.

The material properties of Glidcop® were determined by a series of tests in which samples of the material were machined and tested in a tension machine. A saturation-type equation of the form

$$\sigma = \sigma_s - (\sigma_s - \sigma_m) \exp \left(\frac{-\sigma_m \varepsilon_m}{\sigma_s \sigma_m} \left(\frac{\varepsilon}{\varepsilon_m} - 1\right)\right) \qquad (3.53)$$

was used to obtain the flow curve where σ_s is the saturation stress and σ_m and ε_m are the stress and strain of maximum load. For copper, values of 141.8 Mpa, 115.19 Mpa, and 0.2884 were used for σ_s, σ_m, and ε_m, respectively. Glidcop® and copper have the same modulus of elasticity, and a value of 128 GPA was used for both. Also, Poisson's ratio of both materials was assumed to be 0.326.

CHAPTER 4

HYDROSTATIC EXTRUSION EXPERIMENTS

4.1 INTRODUCTION

Presented in this chapter are a description of the hydrostatic extrusion experiments as well as the residual stress measurements conducted at the Westinghouse Research & Development Center, Pittsburgh, Pennsylvania. The details of these experiments are based on the report by Iyer, Lovic, and Male [*401*]. The residual stress measurements were carried out using Sachs' boring-out method, which assures a controlled metal removal rate without damaging the specimen.

4.2 HYDROSTATIC EXTRUSION EXPERIMENTS

4.2.1 Experimental Facilities

Figure 4.1 shows a schematic diagram of the Bridgman-Birch vertical extrusion press used in the extrusion experiments. The press was equipped with a 38-mm chamber capable of withstanding pressures up to 765 Mpa. Also, a versatile hydraulic system facilitated the use of constant ram velocities of up to 15 mm/sec. The ram velocity was controlled in the experiment by a pressure-compensating system component of the press. This assured "stick slip"-free extrusions. A linear and a pressure transducer input module, a transducer-amplifier, and a limit control output module were among the auxiliary instruments of the press.

Dies used in the experiments were fabricated from A2 tool steel and

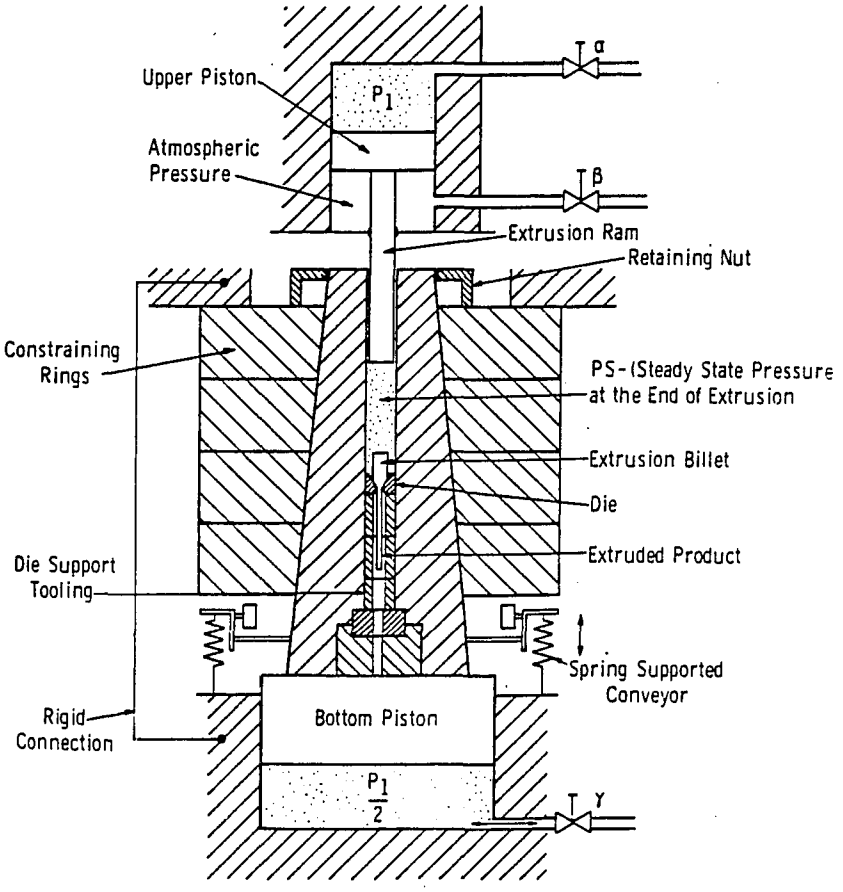

Figure 4.1. Hydrostatic extrusion press.

hardened to Rc 60-62. The geometry of dies consisted of an approach angle which was 120°, 60°, or 45°; a 9mm bearing length; and a 10° included relief angle, Figure 4.2. The approach angles and bearing lengths of all dies were polished to 200μmm. Three dies were used to cover the entire range of extrusion ratios. The dies were positioned at the same location in the high-pressure chamber for all of the experiments.

The materials used for the experiments were OFHC copper and two grades of Glidcop®, namely AL-20 Glidcop® and AL-60 Glidcop®. These

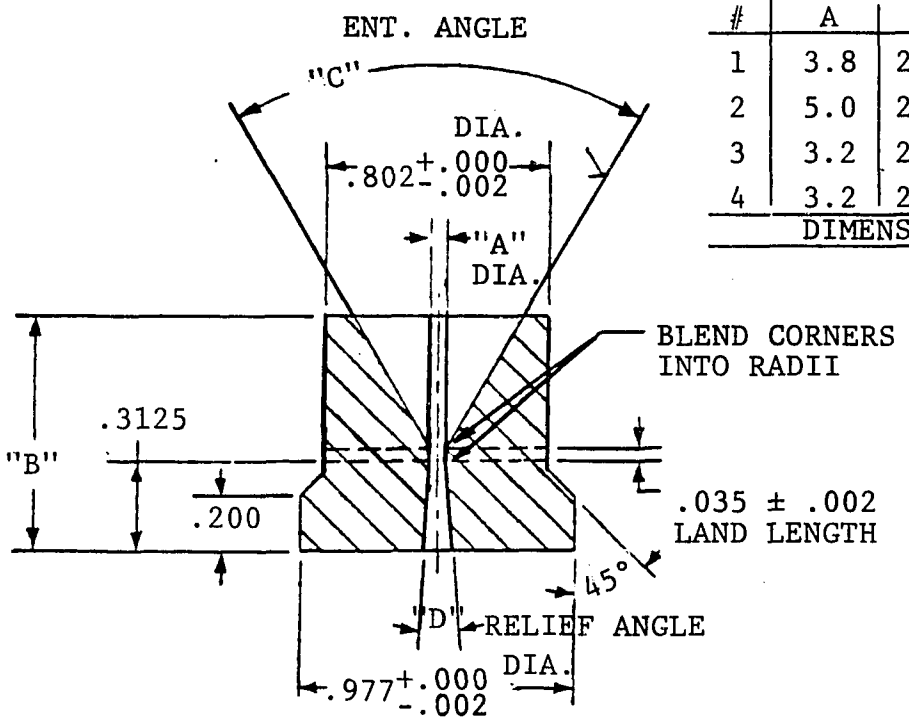

DIE #	DIE DESIGN A	B	C	D
1	3.8	22.4	30°	10°
2	5.0	22.4	60°	10°
3	3.2	22.4	90°	10°
4	3.2	22.4	120°	10°

DIMENSIONS IN mm

Figure 4.2. The extrusion die design.

constitute a class of copper alloys strengthened by various amounts of aluminum oxide dispersions. Four billet configurations were used--solid copper, solid Glidcop®, 25% Glidcop® core/75% copper-clad, and 50% Glidcop®/50% copper-clad composites. These combinations of materials were selected to investigate the extrusion of hard-core/soft-clad (copper-clad/Glidcop® core) configurations, as well as single-component materials (copper and Glidcop®).

surface finish. The billet's leading ends were conical with 30° to 60°

4.2.2 Experimental Procedure

Specimens were prepared by machining 15.25 cm-long billets of 800μ

included nose angles for corresponding die angles in the same range. The slight mismatch of cone angles beneficially influenced the breakthrough pressure. Prior to each experiment, composite samples were prepared by first machining the cores for a sliding fit to ease assembly, Figure 4.3.

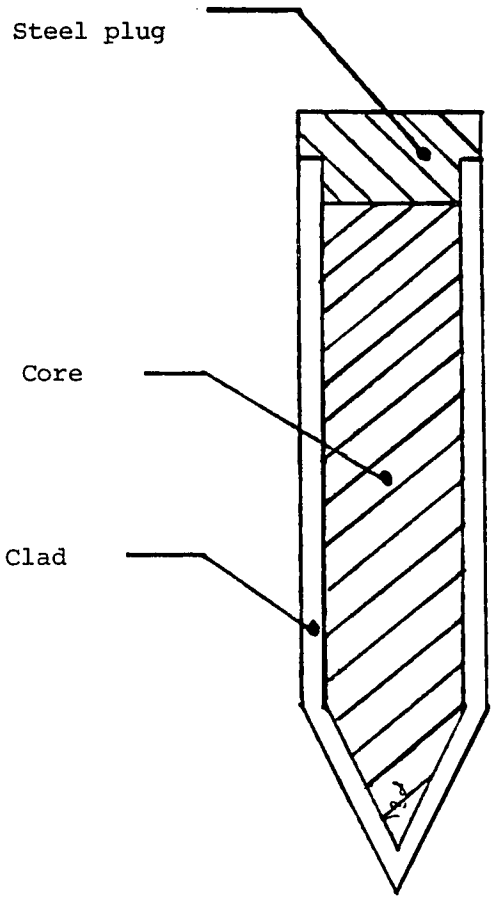

Figure 4.3. Co-extrusion billet.

The billet's surface then was degreased and coated with a light film of lanolin for lubrication. Finally, a steel plug was attached to the back end of the billet to prevent unrestrained extrusion. The billet then was inserted into the die, positioned concentrically, and tapped lightly to

provide a slight seal. Laboratory-grade castor oil was used as the pressurizing fluid.

From the initiation of the billet's movement (breakthrough point), every attempt was made to achieve the same average strain rate by controlling the ram velocity. The process was stopped in time to preserve approximately 50 mm of the unextruded billet. This was done so that the unextruded portion could be used for the interfacial strength studies in which the change in bond strength is investigated between the core and the clad, both prior to and after the extrusion.

The results of extrusion experiments, along with the simulation results, are presented in the next chapter. Table 4.1, however, gives the various billet configurations and extrusion ratios covered in these experiments, along with the extrusion pressures.

TABLE 4.1. EXTRUSION PARAMETER-EXTRUSION PRESSURE DATA

Experiment Number	Material Grade	Extrusion Ratio	Percent Core	Extrusion Pressure (Mpa)
AL-20-1	AL-20	3.0	100	285
AL-20-2	AL-20	2.0	100	270
AL-60-1	AL-60	3.0	100	298
AL-60-2	AL-60	2.0	100	278
AL-20-50	AL-20	3.0	50	260
AL-20-75	AL-20	3.0	75	268
AL-60-90	AL-20	3.0	90	305
AL-60-50	AL-60	3.0	50	283
AL-60-75	AL-60	3.0	75	305
AL-60-90	AL-60	3.0	90	312

Die angle: 60°
Lubricant: Lanolin
Pressurizing Fluid: Castor Oil

4.3 RESIDUAL STRESS MEASUREMENTS

4.3.1 Residual Stresses

Residual stresses are those present in a body in the absence of all external forces. Also called internal or locked-in stresses, these arise from several causes: elastic recovery after non-uniform plastic deformation, phase transformation, thermal expansion, or a combination of the above. Evaluation of these stresses is of interest from both scientific and technological viewpoints since the nature, magnitude, and distribution of such stresses influence the mechanical behavior of the product. Therefore, the design of forming operations, such as hydrostatic extrusion, would benefit from a knowledge of the relationships among internal stress distributions, process geometry, and material properties.

Removal of internally-stressed material from a body causes the remainder of the body to alter its shape in order to maintain equilibrium. Employment of this warping effect is the main concept in many techniques for residual stress measurement. Indeed, by adopting proper boundary conditions, different methods have been developed to measure residual stresses in cylindrical rods, tubes, and composites with axisymmetric, anti-symmetric, and non-symmetric triaxial stresses. Early formulations, however, assumed elastic isotropy and material homogeneity to relate measured strains and stresses. A recent development treats the case of a cylindrical composite having n concentric layers of different materials, all exhibiting cylindrical elastic orthotropy [402].

In this study, Sachs' boring-out technique is employed to determine experimentally the residual stress distributions of extruded products. A

brief description of this method is presented in the next section.

4.3.2 Sachs' Boring-out Technique

Expressions for radial, axial, and tangential components of residual stresses obtained by Lambert [403] are based on Sachs' boring-out technique, in which Sachs [402] proposed a method for determining the residual stresses in axi-symmetric products. In this method, the stress components are obtained by measuring strains on the outer surface of a rod or thick-walled tube, when a thin, uniform layer of stressed material is removed from the center. Isotropic linear elasticity is used to relate the measured strains to residual stresses. The following is a brief description of the derivations of the stress equations used in this thesis. The derivations presented here are based on Lambert's solution to Sachs' boring-out method [403].

4.3.2.1 Radial Stresses

According to the theory of elasticity, tangential stresses at the surface of a thick-walled cylinder subjected to an internal pressure P_i are given by [404]:

$$\sigma_t = 2P_i \frac{r^2}{R^2 - r^2} \tag{4.1}$$

where r and R are the internal and external radii of the cylinder, respectively.

Also, according to the generalized Hooke's Law,

$$\bar{\sigma}_a = \frac{E}{(1-\nu^2)}(e_a + \nu e_t) \tag{4.2}$$

$$\sigma_t = \frac{E}{(1-\nu^2)}(e_t + \nu e_a) \tag{4.3}$$

where e_t and e_a are the tangential and axial strains measured on the outer surface of the cylinder, and E and ν are the Young's modulus and Poisson's ratio, respectively.

Now consider a cylindrical rod that has been bored out to an internal radius r. As a result, a uniform pressure P_i, corresponding and equal to the original radial stress at radius r, has been removed from the inside boundary due to the removal of material containing residual stresses. Therefore,

$$\sigma_r = P_i \tag{4.4}$$

Solving for P_i, equations (4.1) and (4.4) become

$$\bar{\sigma}_r = \frac{R^2 - r^2}{2r^2}\sigma_t \tag{4.5}$$

Substituting for σ_t from equation (4.3) and multiplying the numerator and denominator by π, the above equation becomes

$$\bar{\sigma}_r = \frac{E}{(1-\nu^2)}\frac{A_R - A_r}{2A_r}(e_t + \nu e_a) \tag{4.6}$$

which is an expression for radial residual stresses in terms of cross-sectional areas of the rod and the bored-out axial hole.

4.3.2.2 Tangential Stresses

Figure 4.4 is a unit length free-body diagram of half the slug of material removed from the interior of the bar. Equilibrium of forces acting on the body gives

$$2r_{Pi} = 2 \int \sigma_t(\rho)d\rho \qquad (4.7)$$

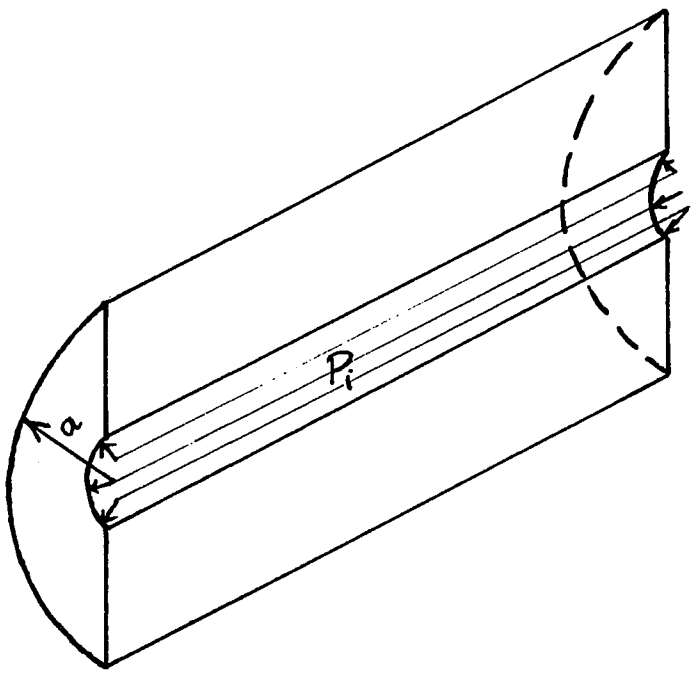

Figure 4.4. Free-body diagram of the bored-out slug.

Substituting expressions (4.4) and (4.5) for P_i and rearranging the resulting expression, the above equation becomes

$$\sigma_t(\rho)d\rho = \frac{E}{(1-\nu^2)}\frac{R^2-r^2}{2r}(e_t + \nu e_a) \tag{4.8}$$

Differentiation with respect to r results in

$$\sigma_t(r) = \frac{E}{(1-\nu^2)}\left[\frac{-R^2-r^2}{2r^2} - \Theta + \frac{R^2-r^2}{2r}\frac{d\Theta}{dr}\right] \tag{4.9}$$

where

$$\Theta = e_t + \nu e_a. \tag{4.10}$$

Multiplying the numerator and denominator by n and noting that

$$\frac{d\Theta}{dr} = \frac{d\Theta}{dA_r}\frac{dA_r}{d_r} = 2\pi r\frac{d\Theta}{dA_r} \tag{4.11}$$

equation (4.9) becomes

$$\sigma_t(r) = \frac{E}{(1-\nu^2)}\left[(A_R - A_r)\frac{de}{dA_r} - \frac{A_R + A_r}{2A_r}\Theta\right] \tag{4.12}$$

which is an expression for tangential residual stresses in terms of cross-sectional areas of the rod and the bored-out axial hole.

4.3.2.3 Longitudinal Stresses

Considering the slug of bored-out material again, it is assumed that upon removal of this material an axial force, F, is uniformly released from the boundaries of the remaining material. The force, F, on the removed material is given by

$$F = \int_0^r \sigma_a(\rho) dA_\rho \tag{4.13}$$

or

$$F = \int_0^r \sigma_a(\rho) \rho d\rho \tag{4.14}$$

Removal of such force relieves an axial stress from the remaining hollow cylinder such that:

$$\sigma_a' = \frac{F}{\pi(R^2 - r^2)} = \frac{E}{1-\nu^2}(e_a + \nu e_t) \tag{4.15}$$

where the second equality is obtained from equation (4.2). Substituting for F from equation (4.14), we get

$$2\ \sigma_a(\rho)\rho d\rho = \frac{E}{(1-\nu^2)}(R^2 - r^2)(e_a + \nu e_t) \tag{4.16}$$

Differentiation with respect to r results in

$$2r\sigma_a(r) = \frac{E}{1-\nu^2}\left[(-2r\lambda) + (R^2 - r^2)\frac{d\lambda}{dr}\right] \tag{4.17}$$

where

$$\lambda = e_a + \nu e_t. \tag{4.18}$$

Multiplying the numerator and denominator by π and noting that:

$$\frac{d\lambda}{dr} = \frac{d\lambda}{dA_r}\frac{dA_r}{dr} = 2\pi r\frac{d\lambda}{dA_r} \tag{4.19}$$

equation (4.17), after rearranging, becomes

$$\sigma_a(r) = \frac{E}{1-\nu^2}\left[(A_R - A_r)\frac{d\lambda}{dA_r} - \lambda\right] \tag{4.20}$$

Equation (4.20) relates the longitudinal residual stresses in the material to the cross-sectional areas of the rod and the bored-out axial hole.

4.3.3 Electro-chemical Machining

In conventional mechanical machining processes, a sharpened, hard cutting tool is passed over a softer workpiece to remove material as chips or shavings. In some situations, however, the damages inflicted on

the material due to such machining processes are not acceptable. Thermal damages, for example, could cause recovery to occur in some materials, altering the nature of properties such as the residual stresses [405]. Mechanical damages, on the other hand, are too destructive in situations such as sample preparation for microscopic observations. It is necessary, therefore, to remove material with minimum damage to the workpiece due to the removal process itself. As a result, a number of non-traditional machining processes have been developed for scientific and commercial operations which take advantage of techniques less harmful to the remaining piece [406]. Among these techniques, electric discharge machining (EDM), chemical machining (CHM), and electro-chemical machining (ECM) are the most widely-used material removal operations which use processes other than shearing off by physical contact.

The operating principles of processes such as chemical and electro-chemical machining are not newly invented but have been properly improved. Chemical etching, for example, has been used for decoration and printing purposes for many centuries [407]. More recently, since the advent of micro-electronics, the process has been used extensively to produce printed circuit boards in which the workpiece is purposely exposed to a corrosive medium in order to corrode all exposed areas.

The electro-chemical machining process is not new, either. The basis of its operation is the phenomenon of electrolysis, the laws of which were established by Faraday in 1833 [ ]. Electrolysis is the name given to the chemical process which occurs when an electric current is passed between two conductors dipped into a liquid solution. A typical example is that of two copper wires connected to a source of direct current and immersed in a solution of copper sulphate in water, Figure 4.5.

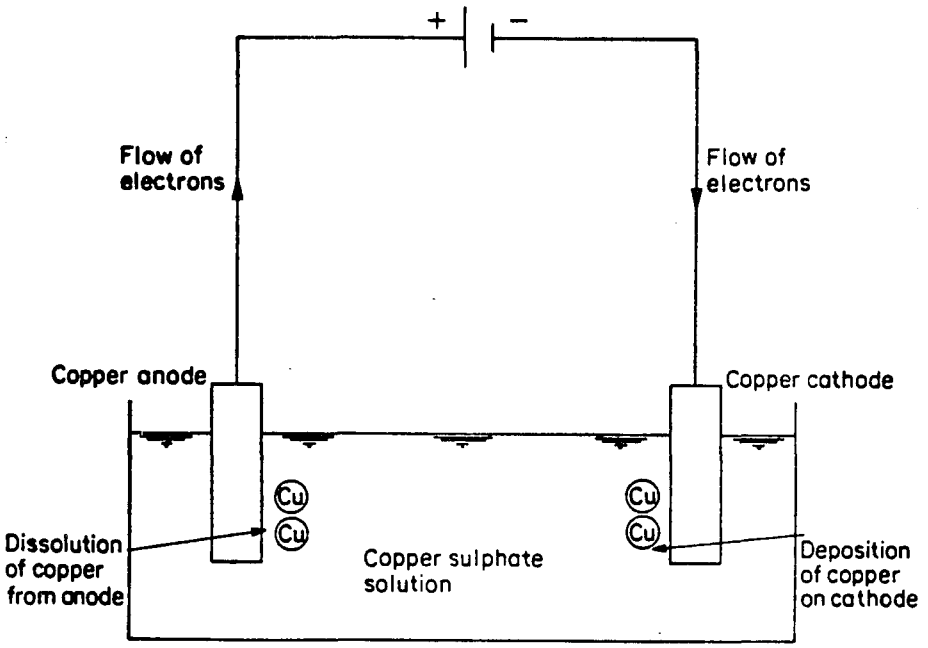

Figure 4.5. Electrolysis of copper sulphate solution.

During such a process, the overall cell reaction is the transfer of copper metal from the anode to the cathode. At the end of the experiment, the anodic wire will be found to have lost weight, while the cathodic wire will have increased in weight by an amount equal to that lost by the anodic wire. The results of this experiment, along with those of numerous others conducted by Faraday, led him to establish his two laws of electrolysis:

1) "The amount of any substance dissolved or deposited is directly proportional to the amount of electricity which has flowed," and
2) "The amounts of different substances deposited or dissolved by the same quantity of electricity are proportional to their chemical equivalent weights."

The mathematical description of the two laws is given as

$$m = \frac{AIt}{ZF} \tag{4.21}$$

where m is the mass dissolved from, or deposited upon, the metal by a current I passed for time t. A and Z are the atomic weight and valency of the reacting ions, respectively, and F is a universal constant known as Faraday's Constant. It is the amount of electric charge necessary to liberate one gram-equivalent (A/Z) of an ion in electrolysis. Its accepted common value is 96,500 C.

Equation (4.21) can be written in the form

$$\dot{m} = \frac{A}{ZF} I \tag{4.22}$$

which gives the mass removal rate, m, in terms of the process and material variables. Although the above equation is the theoretical mass removal rate, it is the rate obtained in practice in most cases. Some metals, however, dissolve in more than one valence state and therefore have mass removal rates different from theoretical values. It is known, for example, that copper dissolves in mono- and di-valent states in chloride [408]. Thus, depending on the metal and the electrolyte, the electro-chemical machining process may have to be calibrated for the mass removal rate.

4.4 EXPERIMENTAL STRESS MEASUREMENTS

4.4.1 Experimental Facilities and Materials

In order to conduct the residual stress experiments, small longitudinal holes had to be bored into the extruded specimens. In addition, the holes had to be made with minimum mechanical and thermal damage to the specimen. Therefore, mechanical drilling was avoided, and the electric discharge machining was chosen instead. The holes were bored using 2mm precision copper tube EDM electrodes. The final diameter of the holes was in the range of 1 to 1.5mm.

The experimental apparatus used for the residual stress measurements is shown in Figure 4.6. Two plastic tubes, which serve as discharge and delivery tubes for the electrolyte, were mounted on a laboratory stand, holding the specimen holder. The holder consisted of two brass electrode holders positioned together by four brass clamping plates. Small screws

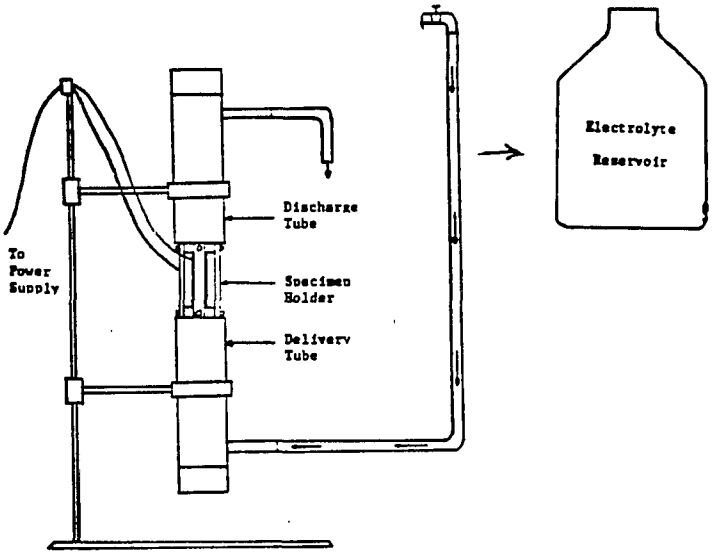

Figure 4.6. Electro-chemical machining apparatus.

were used to attach the clamping plates to the brass electrode holders. Two rubber O-rings or Teflon washers insulated the specimen from the electrode holders, which contained four holes around the electrode to allow the electrolyte to flow into the gap bwtween the electrode and the specimen. A solution of 75 volume percent phosphoric acid in water was used as the electrolyte for all experiments. Figures 4.7 and 4.8 are the schematic diagrams of the specimen holder and its cross-section, respectively.

Strain gauges used for the strain measurements were of the EA-09-031RB-120 type made by Micro-measurements Division of Measurements Group, Inc. These are a general-purpose family of strain gauges widely used in experimental stress analysis. These gauges are of open-faced construction with a 0.03mm tough, flexible polyimide film backing. The nominal resistance of the gauges were 120.0 ± 0.2% ohms and the gauge factor, specified by the manufacturer, was 2.01 ± 1.5% nominal. A 5-volt

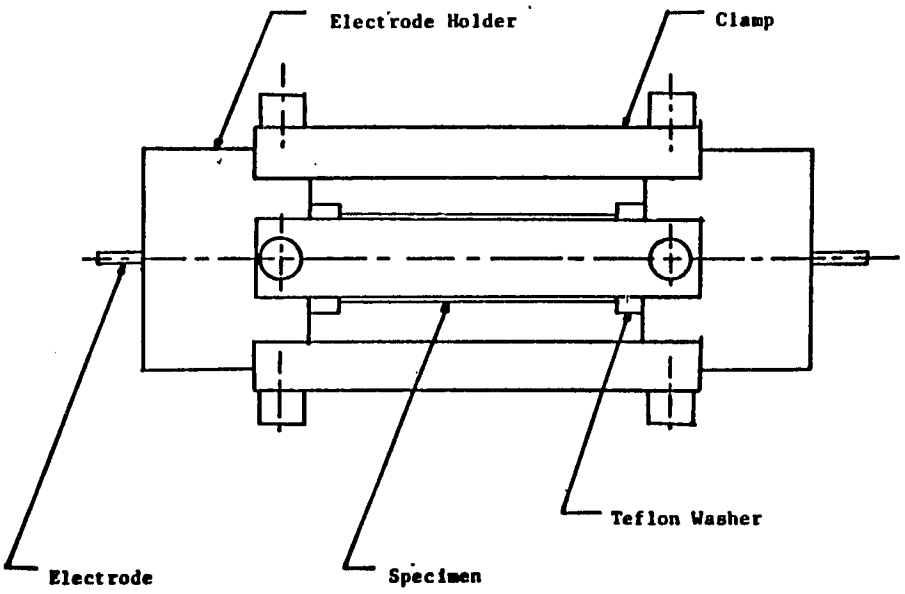

Figure 4.7. Schematic diagram of the specimen holder.

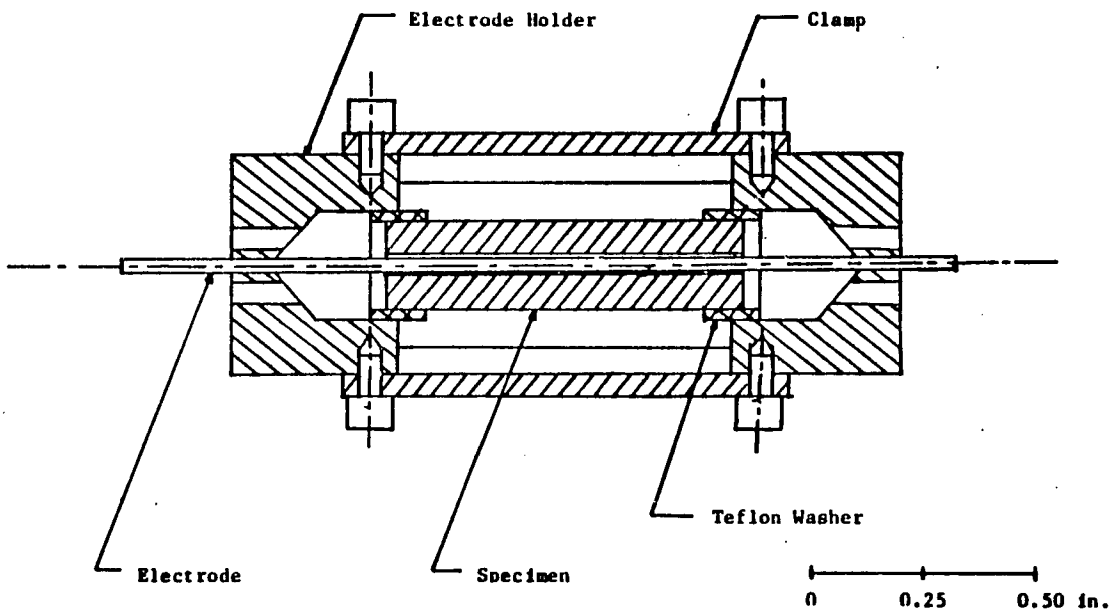

Figure 4.8. Cross-sectional view of the specimen holder.

power supply, an A/D converter, and a microcomputer were among the instruments used in the experiments. Two three-element rectangular rosettes of such gauges were used on each specimen in a manner described later in this chapter.

The materials used in this study were extruded billets of pure or combinations of OFHC copper, AL-20 Glidcop®, and AL-60 Glidcop®. Glidcop® is a class of copper alloys strengthened by various amounts of aluminum oxide dispersions. AL-20 Glidcop®, for example, contains .2 weight percent aluminum and 0.9 volume percent aluminum oxide, while the corresponding numbers for AL-60 Glidcop® are 16 and 2.7, respectively. Samples of several different extruded configurations were made available for residual stress experiments. Table 4.2 in the next section lists the initial dimensions of all test specimens.

4.4.2 Sample Preparation

Billets of extruded products were received from the Westinghouse Research & Development Center in Pittsburgh, Pennsylvania, where samples were extruded to a final diameter of 5.1mm. Specimens nominally 2.54 cm (1") in length were cut out of extruded products of AL-20 Glidcop®, AL-60 Glidcop®, and compounds of Glidcop®-clad copper. During the machining process, the samples were kept as cold as possible by pouring a liquid coolant over the exposed portion of each sample. As mentioned earlier, axial holes had to be bored in the specimens prior to the electrochemical experiments. This was done by electric discharge machining operation, since a closer tolerance and smaller holes were attainable. The final diameter of the holes were in the range of 1 to 1.5mm, Table 4.2.

TABLE 4.2. DIMENSIONS AND SPECIFICATIONS OF EXPERIMENTAL SPECIMENS

Specimen	Length (mm)	Percent Core	Material Grade	Hole Diameter (mm)
AL-20-1	25.35	100	AL-20	1.33
AL-20-2	25.20	100	AL-20	1.28
AL-60-1	24.87	100	AL-60	1.41
AL-60-2	25.63	100	AL-60	1.46
AL-20-50	25.09	50	AL-20	1.20
AL-20-75	24.91	75	AL-20	1.36
AL-60-90	25.12	90	AL-20	1.40
AL-60-50	25.54	50	AL-60	1.32
AL-60-75	24.93	75	AL-60	1.39
AL-60-90	25.60	90	AL-60	1.22

Finally, the surface of each specimen was thoroughly cleaned and strain gauges were mounted so that the middle element was aligned with the longitudinal axis of the specimen at this stage. The specimens were mounted on the ECM apparatus, and the work proceeded in a manner described in Section 4.4.4.

4.4.3 Calibration of Electro-chemical Machining

As mentioned in Section 4.3, although equation (4.22) could be used to determine the rate of mass removal in most cases, a more accurate result is obtained through actual experiments in which a known current is passed through the cell for different lengths of time and the mass removed after each run is measured. This was accomplished by using the experimental set-up shown in Figure 4.3, with the specimen as anode and the clamping plates as cathode.

A solution of 75 volume percent phosphoric acid in water was used as electrolyte and the calibration experiment was conducted for all three materials, namely copper Glidcop-60®, and Glidcop-20®. The mass removed after each run then was determined and liner equations were obtained; these relate the mass removed, m in mg, to time, t in minutes, for each material. The equation for copper, at a current of 0.6 amp, is

$$m = 18.4332t + 1.1325. \tag{4.23}$$

For Glidcop-20®, at the same current, the equation was found to be

$$m = 17.6382t + 1.2410, \tag{4.24}$$

and for Glidcop-60®, the equation is

$$m = 15.3116t + 0.9812. \tag{4.25}$$

4.4.4 Experimental Procedure

AL-20 Glidcop®, AL-60 Glidcop®, and copper-clad Glidcop® core specimens were prepared as explained in Section 4.4.2 and were mounted in the electro-chemical machining apparatus shown in Figure 4.3. A precision copper rod was used as cathode and was inserted in the axial hole through the brass electrode holders. Each gauge was made the active leg of a strain gauge bridge. After calibrating the bridges, a current of 0.6 amp was passed through the electro-chemical cell, which was made up of the specimen, the electrolyte, and the cathodic copper tube. The bridge input was 5 VDC and the amplified voltage change across the bridge was converted to digital signals by the A/D converter and recorded by the microcomputer every four minutes.

After each successful experiment, the quantities θ and λ of equations (4.10) and (4.18) were determined, and the mass removal rate was converted to area removal rate using the equation

$$m = \rho v = \rho AL. \tag{4.26}$$

After finding λ and θ in terms of the area removed, the data were smoothed using the least-square curve fitting technique, and the slopes $d\theta/dA$ and $d\lambda/dA$ were determined. Equations (4.6), (4.12), and (4.20)

then were used to determine the radial, tangential, and radial stresses, respectively. These results, along with the finite element results, are presented in the next chapter. Conclusive remarks with regard to the comparison of the experimental and numerical results are made in Chapter 6.

CHAPTER 5

RESULTS AND DISCUSSION

5.1 SIMULATION RESULTS

The results presented in this section are those of the finite element simulations obtained for extrusion ratios of 2.25, 4.0, and 7.5 in conjunction with two included die angles and four different compositions of core/clad materials. In all cases, simulations were started with the front end of the billet in the die. This corresponded to the tapered end of the billet in the actual extrusion experiments. Figure 5.1.1 shows this die and billet arrangement for the extrusion ratio of 2.25 and die angle of 45°, while the domain of the finite element problem is shown in Figure 5.1.2. Due to the low extrusion ratio, a smaller number of elements was used in the case of the extrusion ratio of 2.25.

Figure 5.1.3 is the deformed configuration of the original mesh in which the flow patterns indicate a tendency of a material element to move through the die faster the farther it is from the tool-workpiece interface. In addition, the deformed geometry shows less deformation of the elements near the leading end of the billet. This is expected and is due to the fact that that portion of the billet had been smaller in diameter and as a result had gone through less reduction than the rest of the configuration.

Figures 5.1.4, 5.1.5, and 5.1.6 show the distribution of radial, axial, and tangential stresses, respectively. The figures indicate that the effect of the die extends a little beyond the exit. In all cases,

there is a region after the die in which the stress components have no longitudinal variation and thus represent a steady state residual stress pattern. It is interesting to note, however, that the radial stresses remain compressive in both core and clad materials while the axial and tangential components exhibit radial variations which range from compression at the axis of symmetry (the core) to tension at the outer region (the clad). This phenomenon is consistent with the abovementioned observation that the center of the billet tends to extrude faster than the region near the outer surface.

Figure 5.1.7 shows the distribution of R-Z shear stress. As indicated in the figure, the magnitude of these stresses are very small compared to those of radial, axial, and tangential stresses. Variation of von Mises and Tresca equivalent stresses throughout the rod are shown in Figures 5.1.8 and 5.1.9, respectively. The magnitudes of the two effective stresses are almost identical. The variation of the principal stresses were also obtained and are presented in Figures 5.1.10 through 5.1.12.

Figures 5.1.13, 5.1.14, and 5.1.15 are contours of total radial, axial, and tangential strains, respectively, while the elastic components of these strains are shown in Figures 5.1.16 through 5.1.18. Comparison of the corresponding components of the total and elastic strains reveals that the magnitude of the elastic portion of the strains is insignificant relative to those of the total strains. This indicates that plastic strains dominate the elastic ones in a forming process such as hydrostatic extrusion. In fact, this is shown in Figures 5.1.19, 5.1.20, and 5.1.21, where the magnitude of the plastic strains is much greater than the elastic ones and only differ from the total strain components by a

slight amount.

Contours of radial and axial displacements are shown in Figures 5.1.22 and 5.1.23. The steady state of the extrusion process is again evident from the contours of radial displacements.

The foregoing presentation of the results was of those of extrusion ratio of 2.25 and included a die angle of 45°. A similar set of results, however, has been prepared for all cases of simulation mentioned earlier and are presented in the appendix.

The radial, axial, and tangential stresses of Figures 5.1.4 through 5.1.7 are presented for a compound of 50 volume percent core and extrusion ratio of 3.0. These are shown in Figures 5.1.24 through 5.1.26. Plots of each component are given for the core and the clad at two locations of the rod, namely the central axis and the outer row of elements. Again, it is clear that in all cases there is a region after the die in which the stress components have no longitudinal variation.

Figures 5.1.27 through 5.1.29 compare the radial distribution of stress components for two extrusion ratios of 2.25 and 7.5. It is evident that the magnitudes of the residual stresses generally correlate with the extrusion ratios and, therefore, the higher the extrusion ratio, the more significant the magnitude of the residual stresses would be. In the case of the axial stress, however, the trend reverses as we approach the surface. The plots also indicate the continuity of the stress patterns across the core/clad interface. This was expected and is due to the fact that both constituents of the composite rod have the same elastic properties and behave similarly. This is not the case, however, when the core material is different than the clad. A complete discussion of this phenomenon is presented in reference [ ].

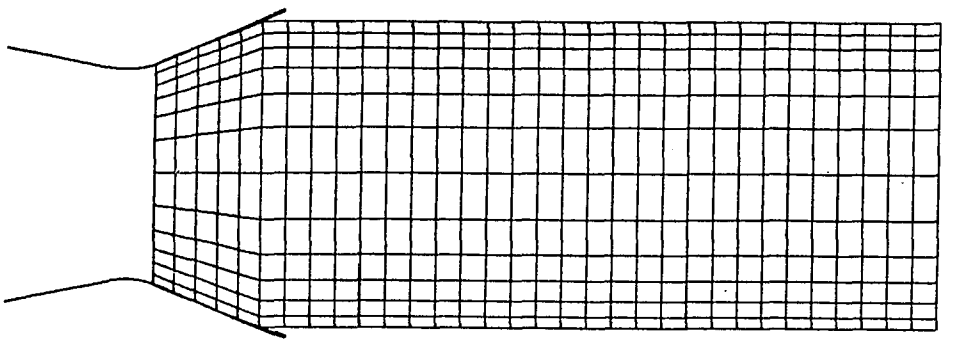

Figure 5.1.1 Die and billet configuration.
(α = 22.5° R = 2.25 % core = 100)

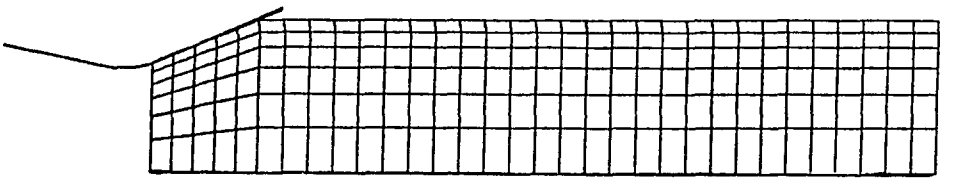

Figure 5.1.2 Domain of the finite element formulation.
(α = 22.5° R = 2.25 % core = 100)

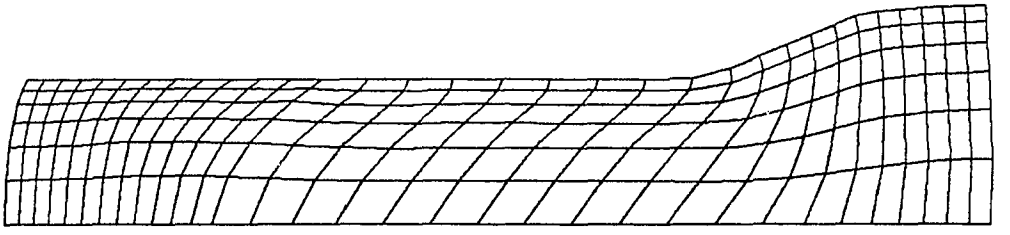

Figure 5.1.3 Deformed configuration.
(α = 22.5° R = 2.25 % core = 100)

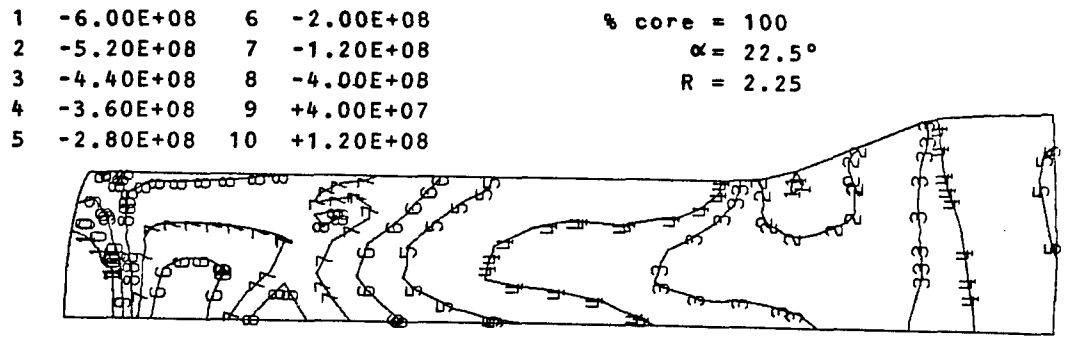

Figure 5.1.4 Distribution of radial stresses.

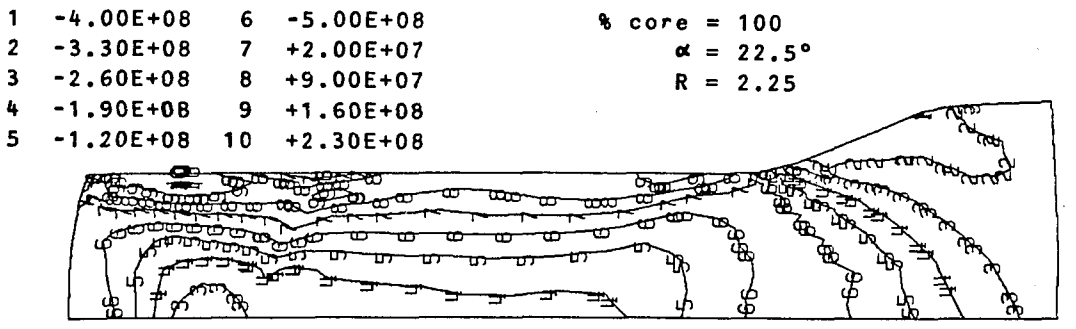

Figure 5.1.5 Distribution of axial stresses.

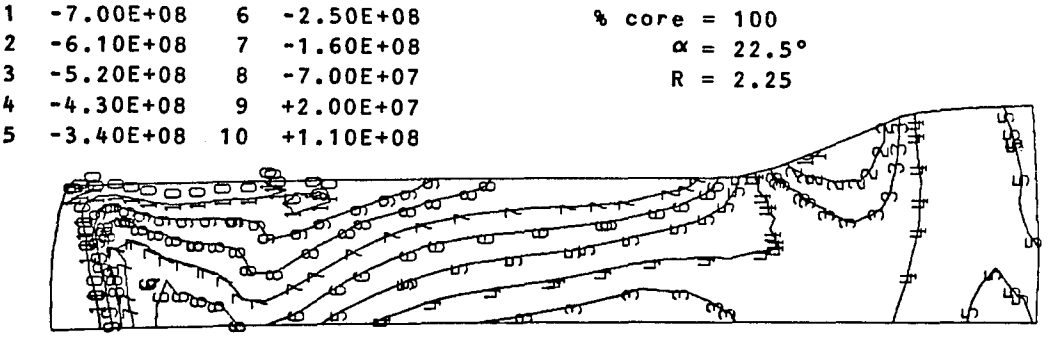

Figure 5.1.6 Distribution of tangential stresses.

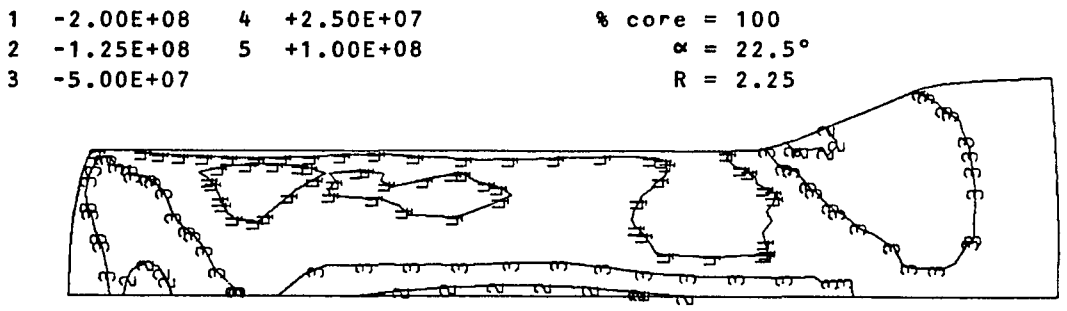

Figure 5.1.7 Distribution of shear stresses (r-z).

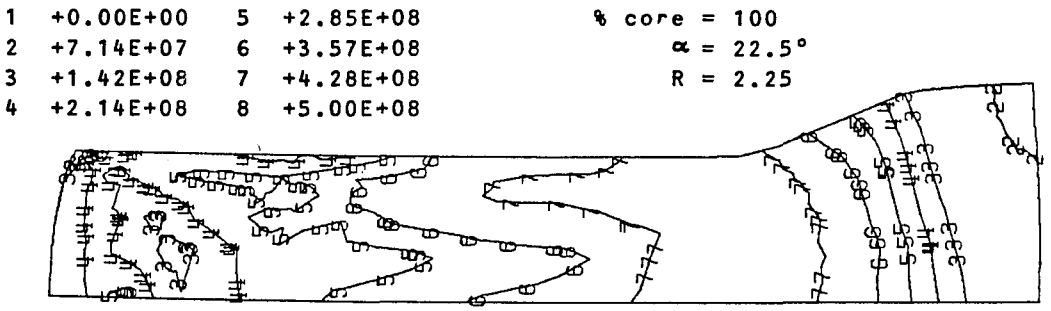

Figure 5.1.8 Distribution of Mises equivalent stresses.

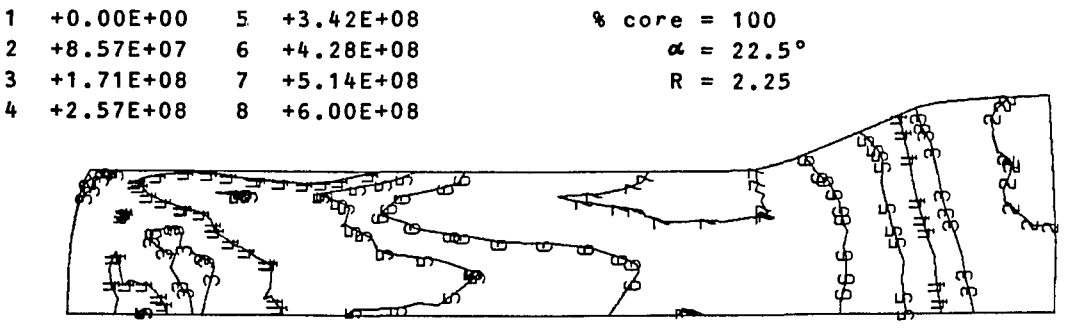

Figure 5.1.9 Distribution of Tresca equivalent stresses.

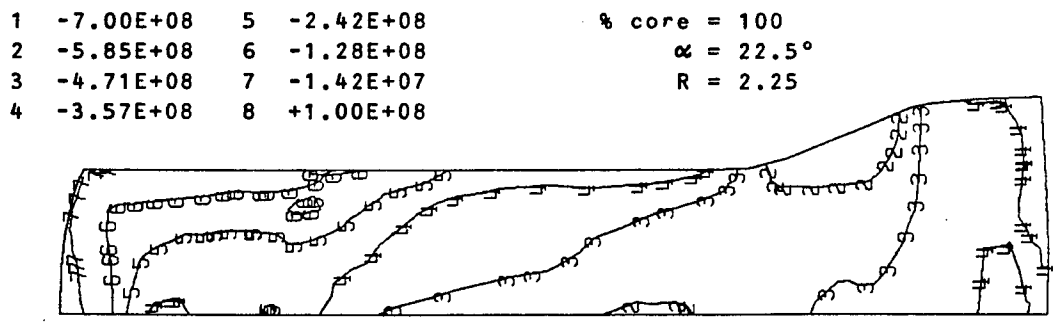

Figure 5.1.10 Distribution of minimum principal stresses.

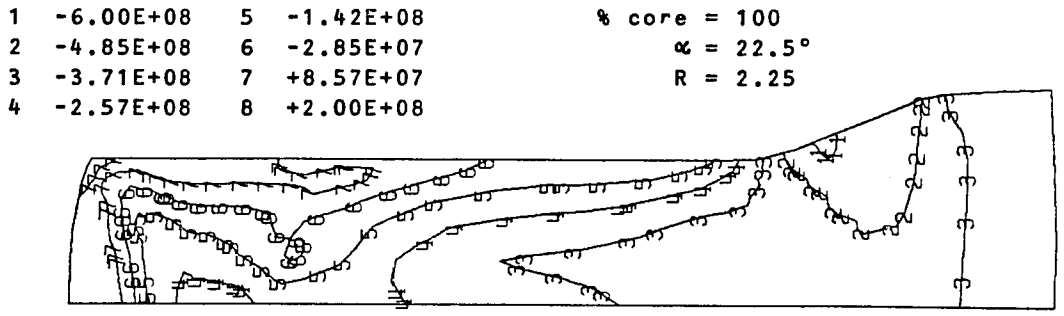

Figure 5.1.11 Distribution of intermediate principal stresses.

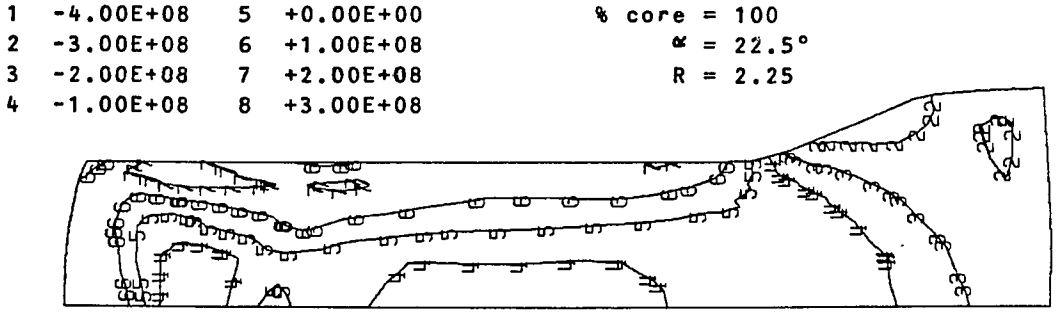

Figure 5.1.12 Distribution of maximum principal stresses.

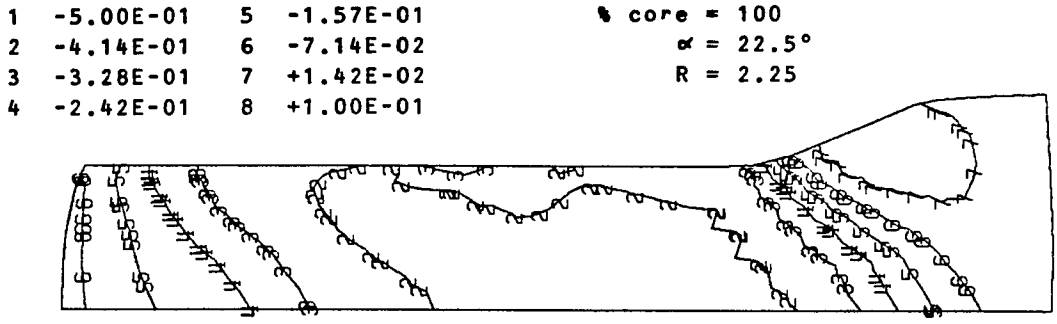

Figure 5.1.13 Contours of total radial strain.

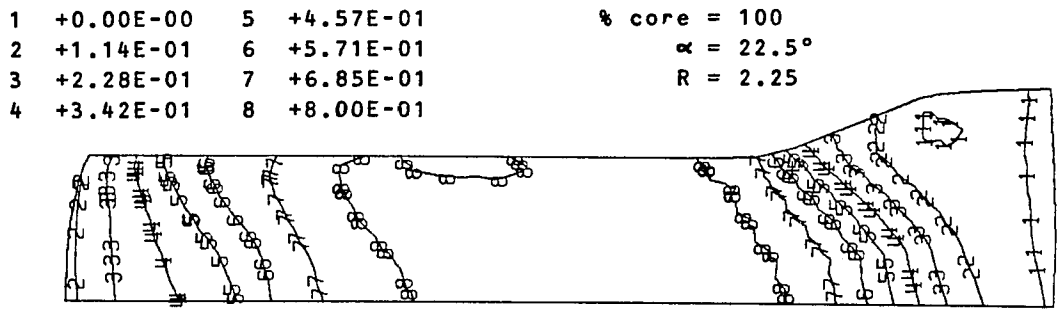

Figure 5.1.14 Contours of total axial strain.

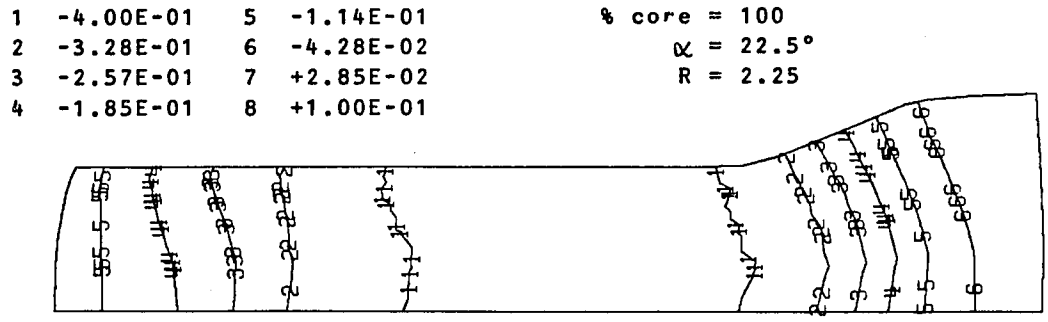

Figure 5.1.15 Contours of total tangential strain.

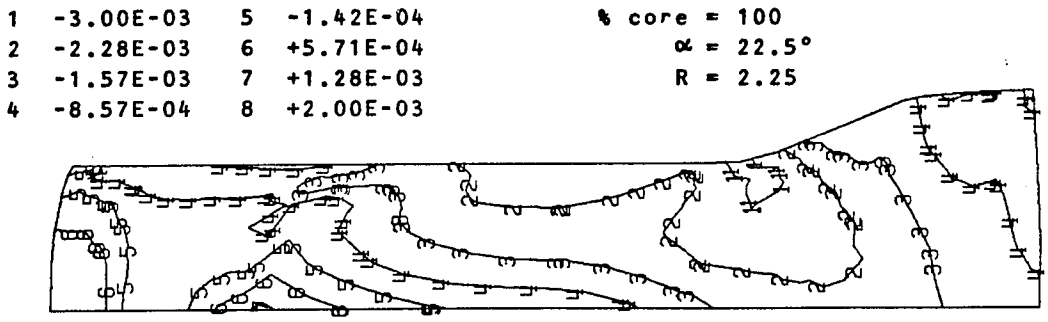

Figure 5.1.16 Contours of radial elastic strain.

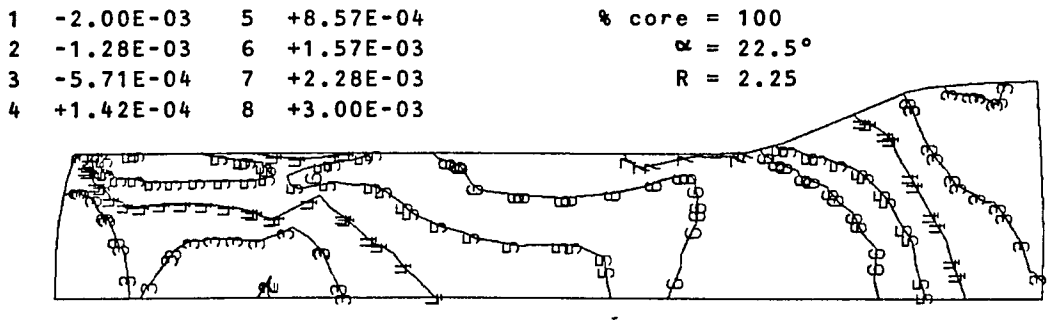

Figure 5.1.17 Contours of axial elastic strain.

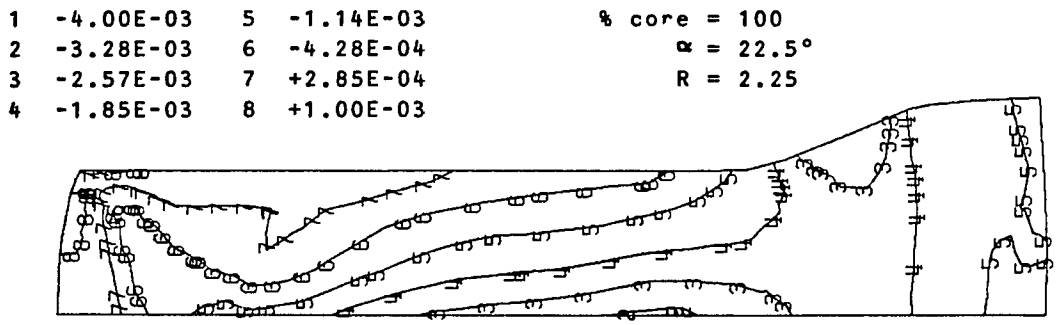

Figure 5.1.18 Contours of tangential elastic strain.

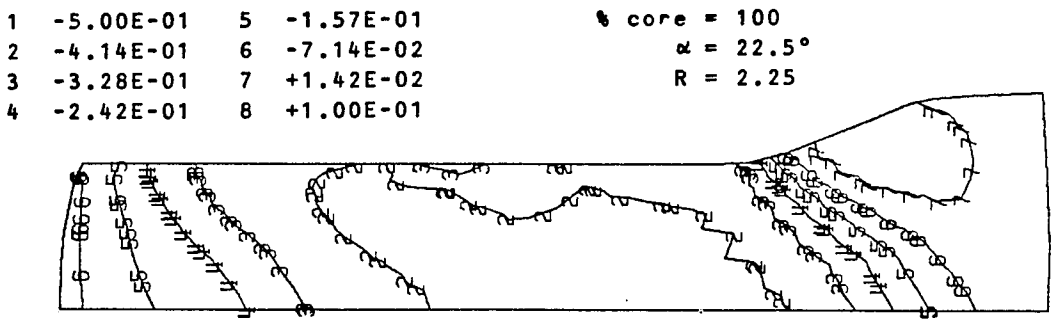

Figure 5.1.19 Contours of radial plastic strain.

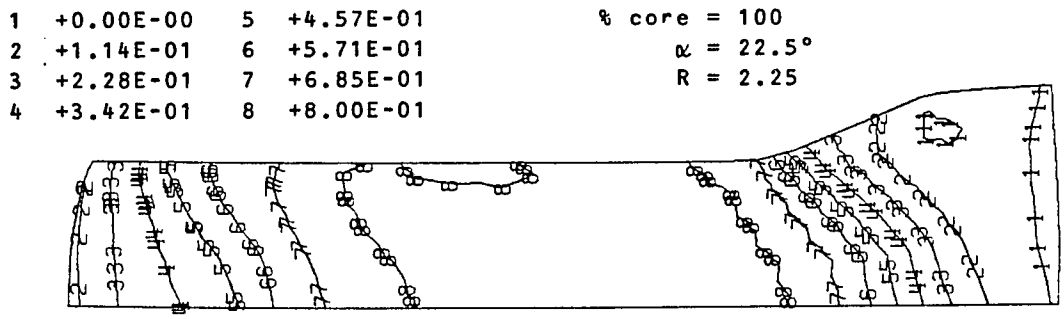

Figure 5.1.20 Contours of axial plastic strain.

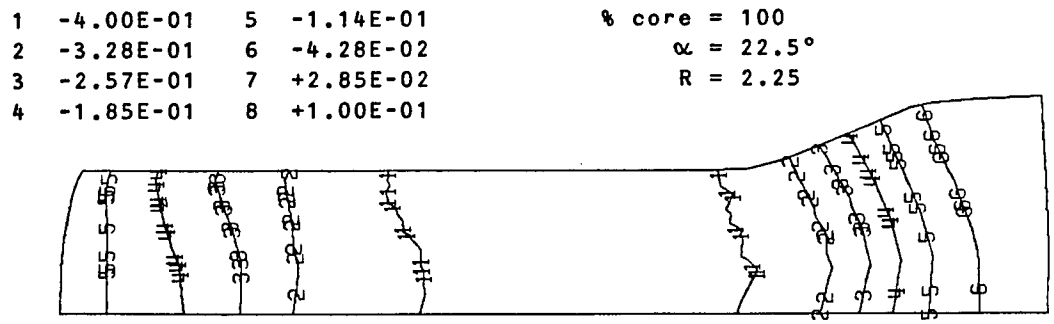

Figure 5.1.21 Contours of tangential plastic strain.

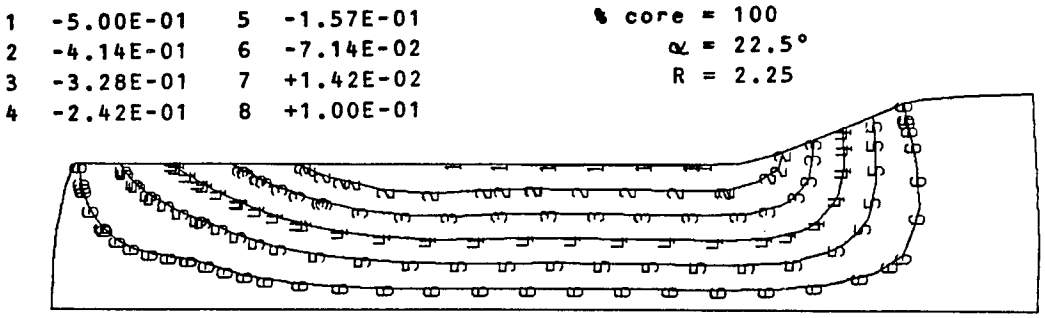

Figure 5.1.22 Contours of radial displacements.

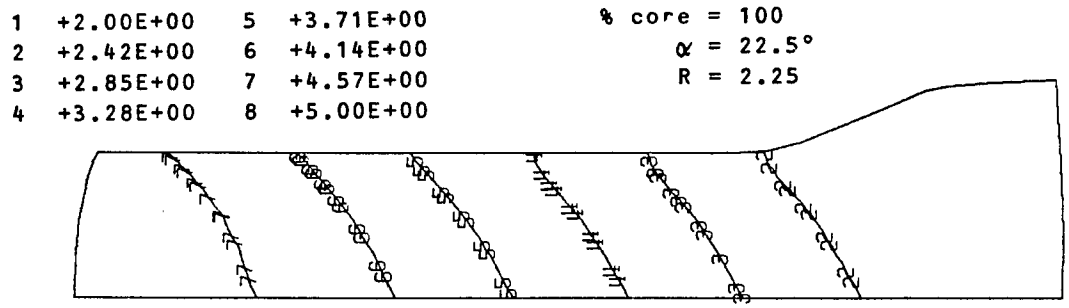

Figure 5.1.23 Contours of axial displacements.

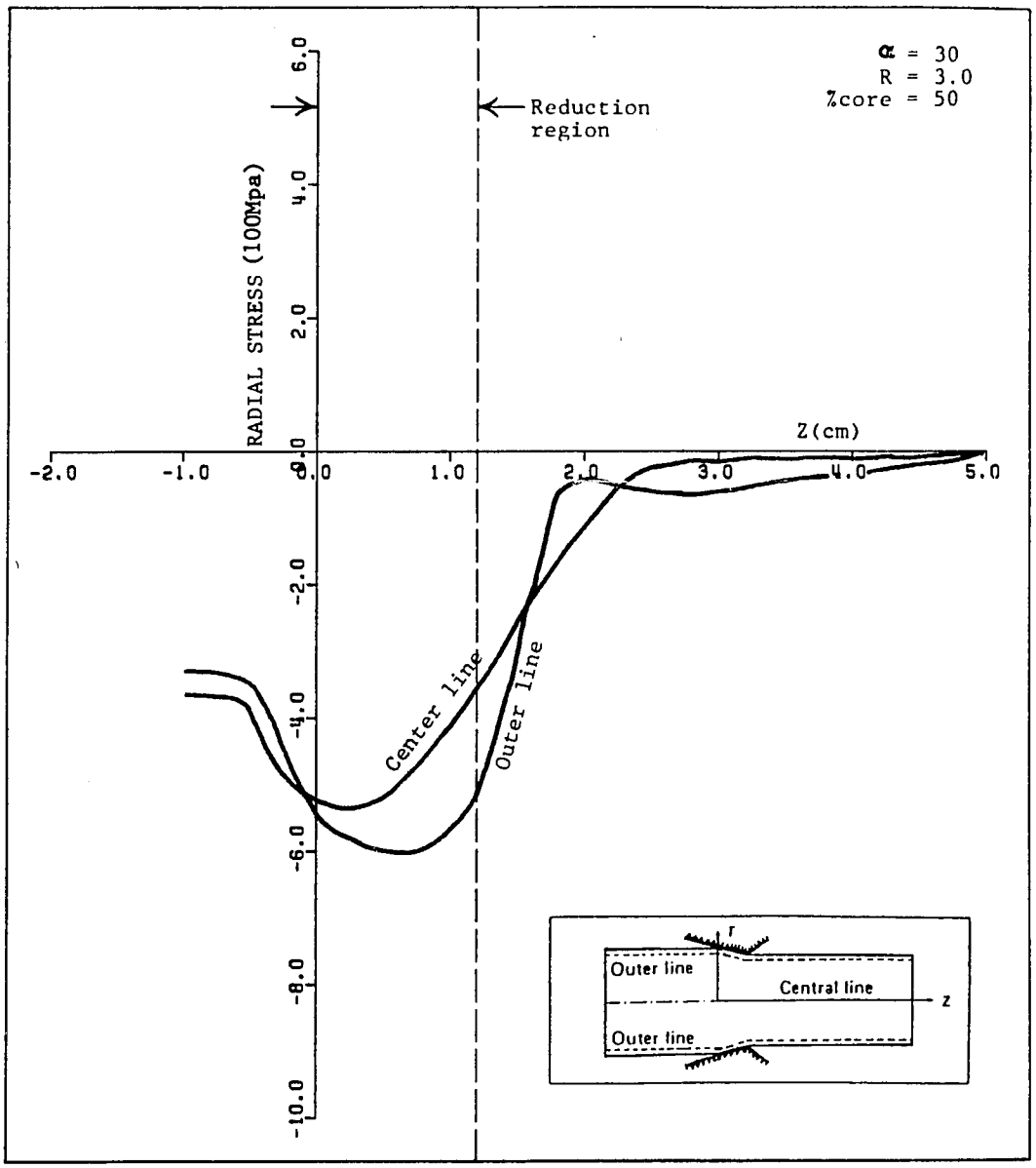

Figure 5.1.24 Axial distribution of radial stresses.

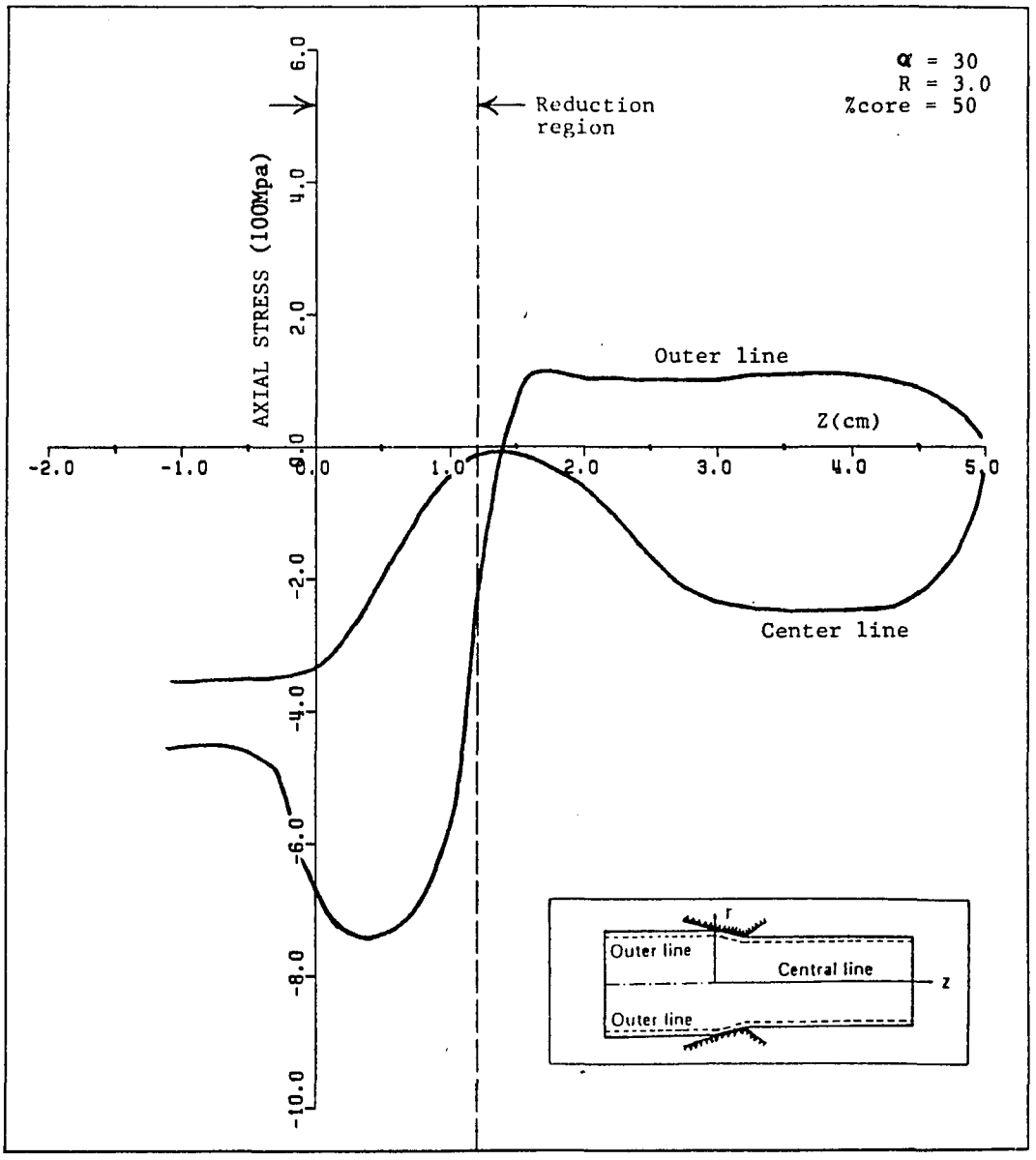

Figure 5.1.25 Axial distribution of axial stresses.

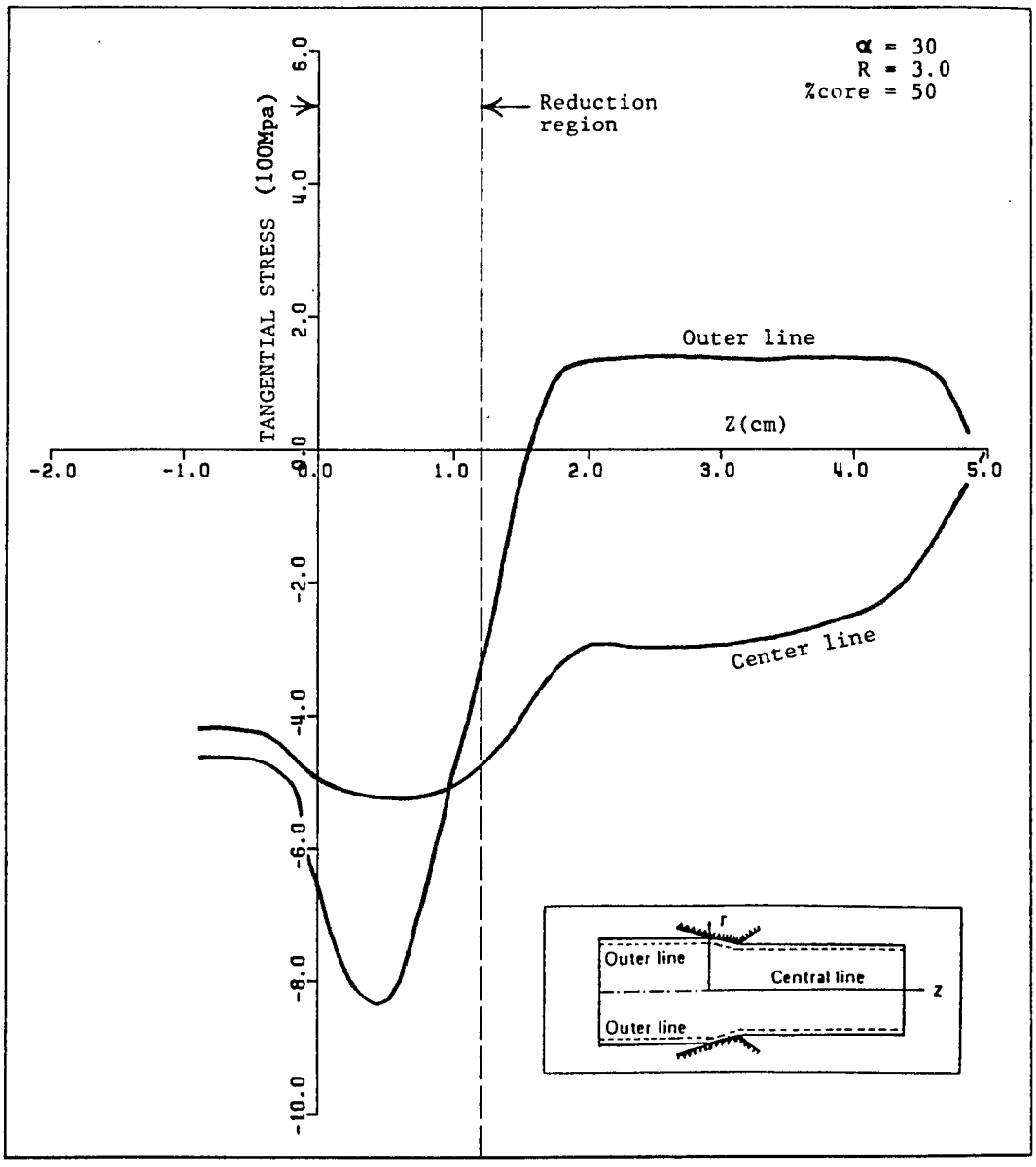

Figure 5.1.26 Axial distribution of tangential stresses.

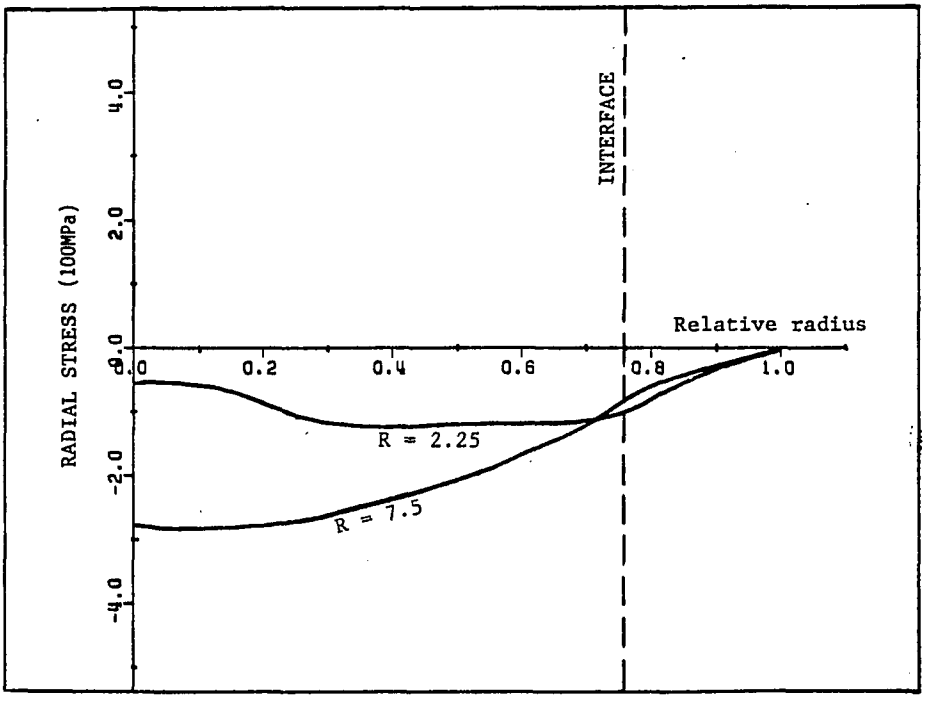

Figure 5.1.27 Radial distribution of radial stresses.

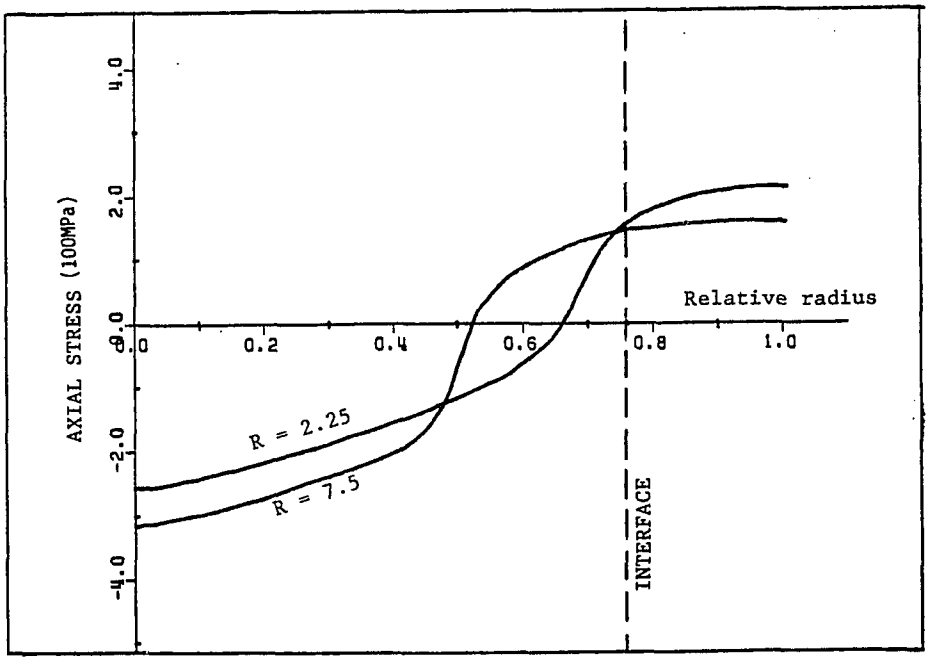

Figure 5.1.28 Radial distribution of axial stresses.

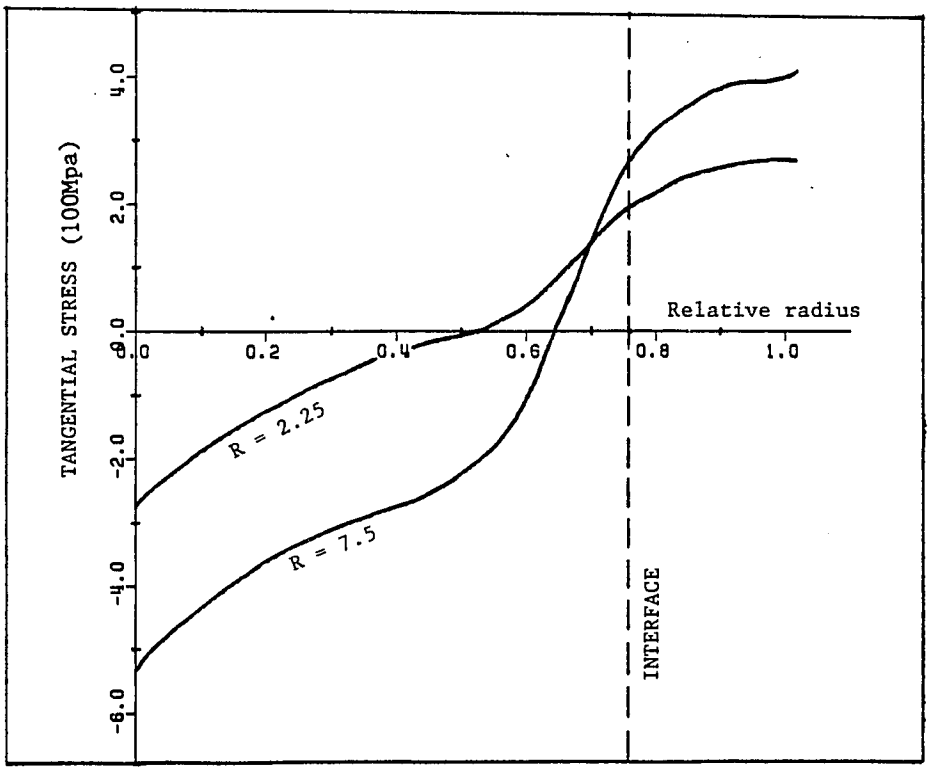

Figure 5.1.29 Radial distribution of tangential stresses.

In the simulation of the extrusion problem, the fluid pressure of the actual press was simulated as pressure boundary conditions on the back end and top of the billets. As the extrusion proceeded, the simulation process was stopped in due time to remove the load from that portion of the rod which had entered the die. In continuing the process, the cycle was repeated until the steady state was acquired. This condition is evident from Figure 5.1.30, in which the variation of the load factor is plotted against the displacement of the back end of the billet. Load factor is a coefficient that the program uses as a multiplier of the assigned load. After a peak in the load value, the breakthrough pressure, the magnitude of the pressure remains essentially constant. Small variation of the pressure is due to the minor lag in pressure compensation. As the billet moves forward, the volume of the chamber increases; as a result, the pressure drops only for the pump to compensate for the deficit amount.

Table 5.1 gives the numerical values of the breakthrough and steady-state pressure for all cases. The breakthrough pressure is generally higher than the steady state value and corresponds to the peak value of the load shown in Figure 5.1.30.

Figures 5.1.31 and 5.1.32 show the variations of extrusion pressure with extrusion ratio. For all four billet configurations, the relation between the steady state pressure and the natural logarithm of the extrusion is linear, which is consistent with the empirical equations presented in Chapter 2.

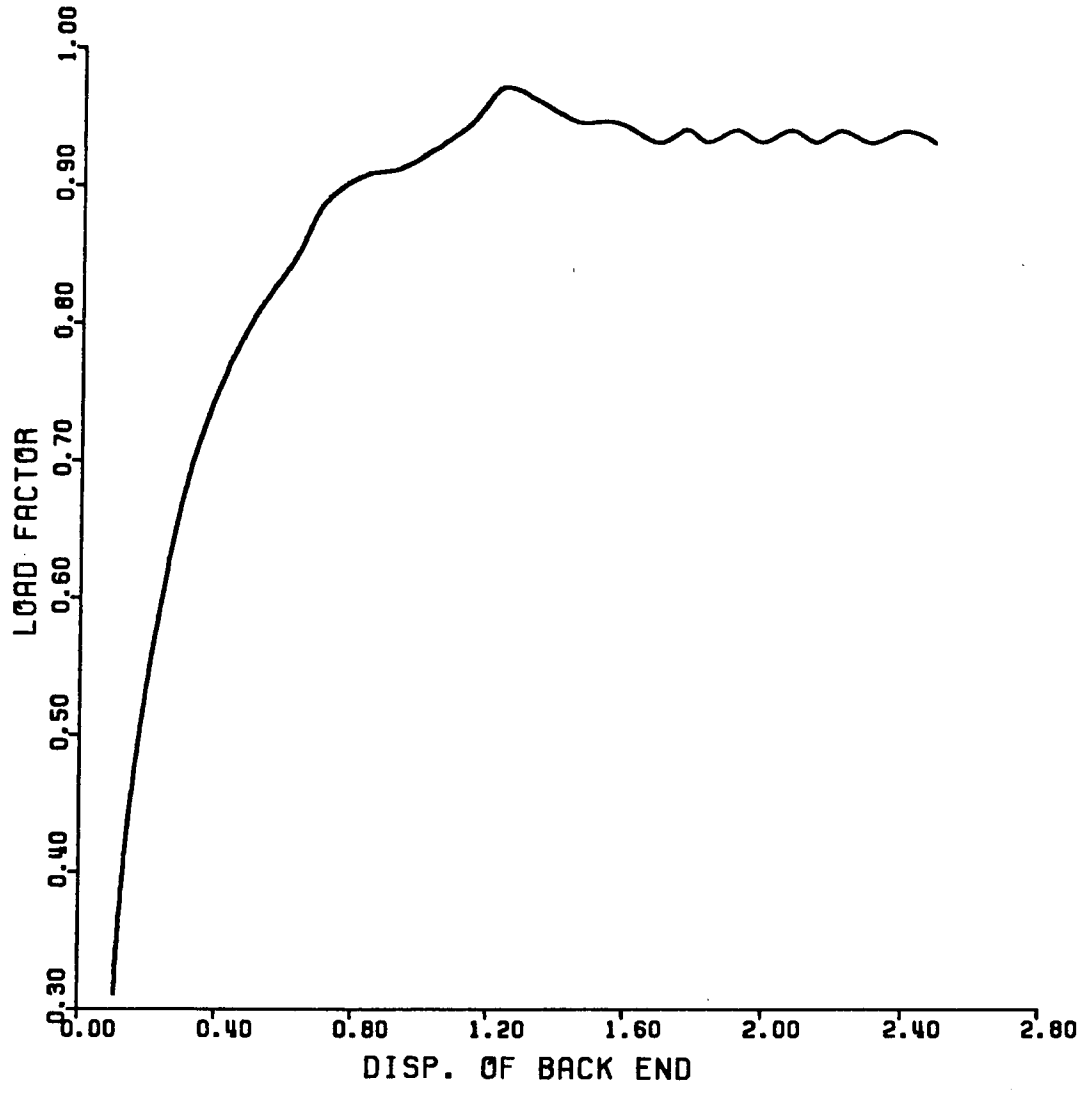

Figure 5.1.30 Pressure vs. displacement.

TABLE 5.1 BREAKTHROUGH AND STEADY-STATE EXTRUSION PRESSURES

Experiment Number	Die Cone Angle (Degrees)	Extrusion Ratio	Percent Core	Breakthrough Pressure (MPa)	Steady-state Pressure (MPa)
1	45	2.25	00	283	273
2	45	2.25	50	296	290
3	45	2.25	75	301	294
4	45	2.25	100	312	303
5	45	4.00	00	552	519
6	45	4.00	50	580	543
7	45	4.00	75	595	552
8	45	4.00	100	618	570
9	45	7.50	00	836	720
10	45	7.50	50	840	720
11	45	7.50	75	920	900
12	45	7.50	100	930	840
13	60	2.25	00	305	297
14	60	2.25	50	324	320
15	60	2.25	75	333	324
16	60	2.25	100	336	330
17	60	4.00	00	582	564
18	60	4.00	50	619	589
19	60	4.00	75	644	600
20	60	4.00	100	661	616
21	60	7.50	00	900	900
22	60	7.50	50	903	881
23	60	7.50	75	933	909
24	60	7.50	100	960	940

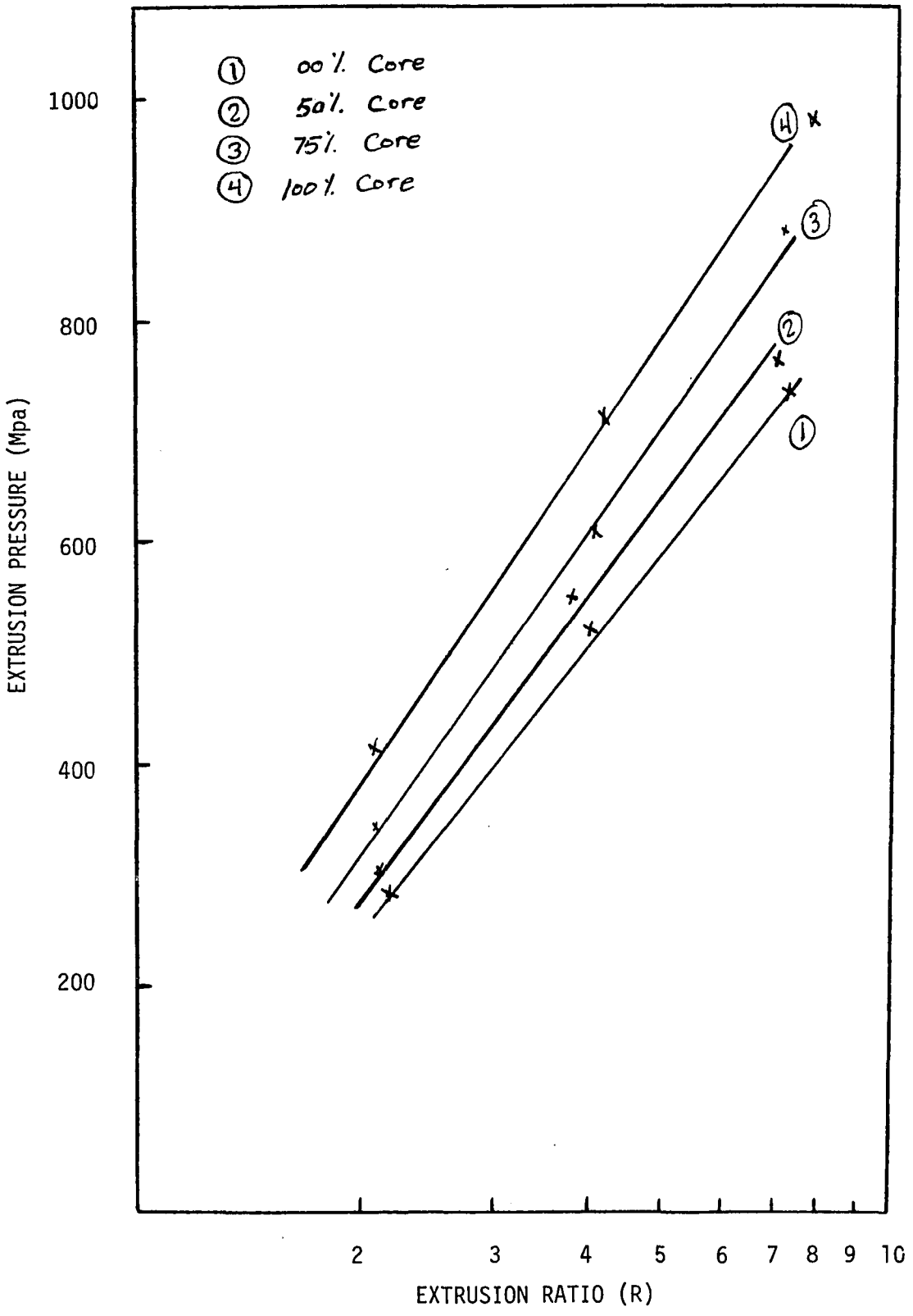

Figure 5.1.31 Variation of extrusion pressure with extrusion ratio. (Die angle = 45°)

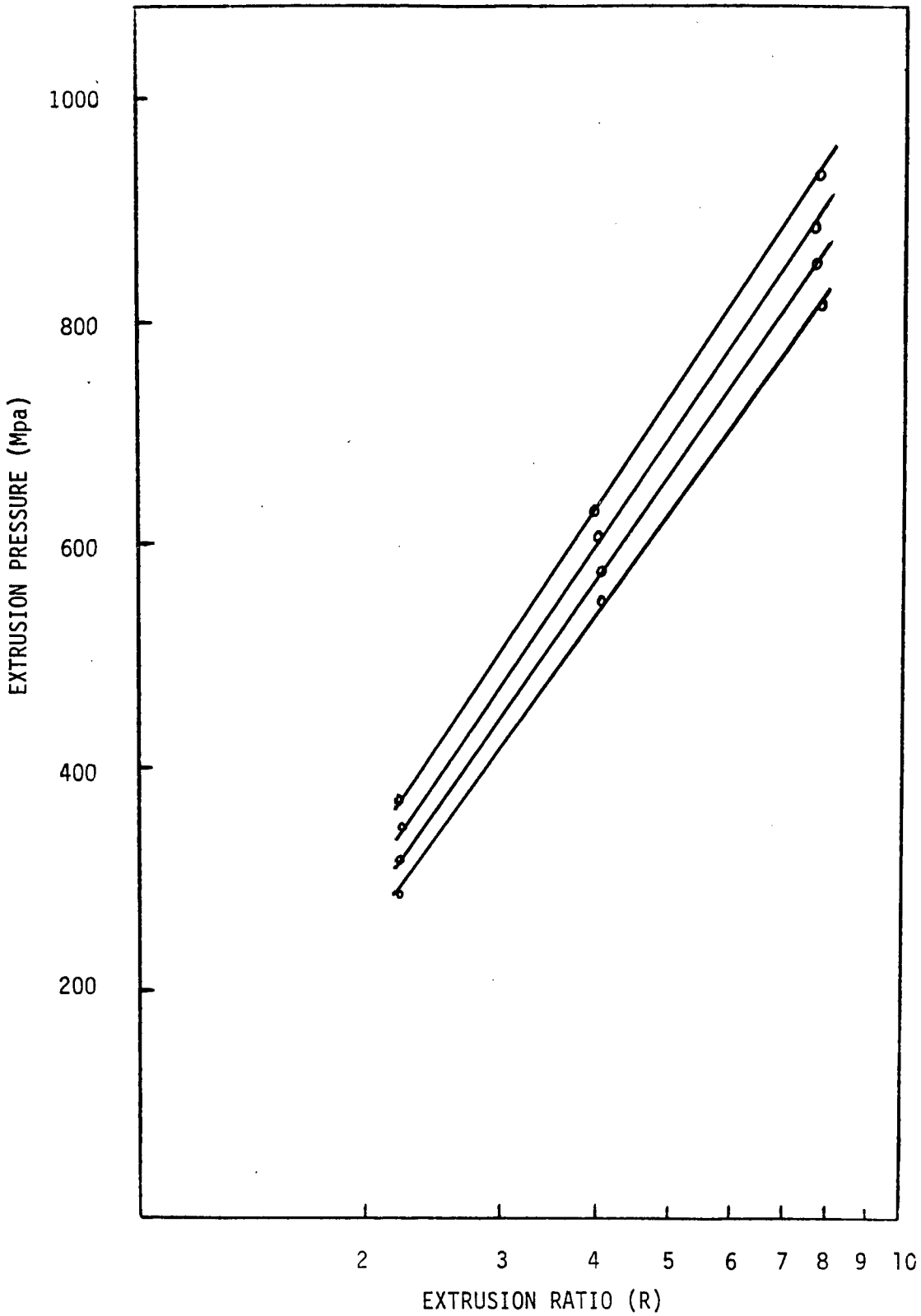

Figure 5.1.32 Variation of extrusion pressure with extrusion ratio. (Die angle = 60°)

5.2 EXPERIMENTAL RESULTS

Experimental results presented in this section consist of the hydrostatic extrusion pressure (steady state) presented in Table 4.1 and reproduced here as Table 5.2, as well as the residual stresses measured in extruded specimens, according to the procedure described earlier.

Figures 5.2.1 through 5.2.3 show the variation of stress components as a function of relative radius for the two cases of extrusion ratio of 3.0 and two different compounds. The dashed lines represent the 50% AL-20 Glidcop® clad with copper, while the solid line represents the 50% AL-60 Glidcop® core material. The results verify the residual stress patterns indicated by the numerical calculations. As indicated earlier, the continuity of the stress across the interface is because of the similarity between the two constituents. Little difference between the values for the two results is evident. This is probably due to the stress relief caused by deformation heating.

A comparison of the experimental and numerical results is by means of Figures 5.2.4 through 5.2.6, where the radial distribution of stress components are shown for two similar geometry and material configurations. The curves belong to composites of 50% core and extrusion ratio of 3, in conjunction with a 60° included die angle. The dashed lines represent the experimental results. It is clear that the magnitude of stresses is significantly different in two studies. Again, the radial stresses are compressive in both core and clad while the tangential and radial stresses are compressive in the core and tensile in the clad. In fact, the axial stress remains highly compressive along most of the radius of the product and becomes weakly tensile on the outer

surface. This behavior is explained by the requirement that zero total axial force should be transmitted at each cross-section in the steady state residual stress region. The integration of axial stress to obtain axial force emphasizes the importance of the contribution from the material far from the axis of symmetry, a point first made by Lee, Mallett, and McMeeking [ ].

Table 5.2 gives the experimental pressure values obtained during the experiments. The simulated values are generally higher than the experimental results reported. The explanation lies in the fact that during the extrusion process, most of the energy of deformation is converted into heat and, therefore, hot billets require smaller load to deform. On the other hand, the finite element simulation completely

TABLE 5.2. EXTRUSION PARAMETER-EXTRUSION PRESSURE DATA

Experiment Number	Material Grade	Extrusion Ratio	Percent Core	Extrusion Pressure (Mpa)
AL-20-1	AL-20	3.0	100	285
AL-20-2	AL-20	2.0	100	270
AL-60-1	AL-60	3.0	100	298
AL-60-2	AL-60	2.0	100	278
AL-20-50	AL-20	3.0	50	260
AL-20-75	AL-20	3.0	75	268
AL-60-90	AL-20	3.0	90	305
AL-60-50	AL-60	3.0	50	283
AL-60-75	AL-60	3.0	75	305
AL-60-90	AL-60	3.0	90	312

Die angle: 60°
Lubricant: Lanolin
Pressurizing Fluid: Castor Oil

ignores the temperature effect and, consequently, no consideration heat is incorporated into the numerical results.

5.3 EFFECT OF THE PROCESS VARIABLES

The effect of the process variables and material composition on the extrusion pressure is clear from the results of previous sections. In fact, Figures 5.1.31 and 5.1.32 show the variation of extrusion pressure with extrusion ratio. As the figures indicate, for a given die angle the extrusion pressure increases linearly with the natural logarithm of the extrusion ratio, i.e., the higher the extrusion ratio, the higher the extrusion pressure. It is also evident that the pressure increases with an increase in volume of the core material. This is expected and is due to the fact that the core material is harder than the copper cladding and therefore, it requires more pressure to extrude.

The effect of die angle on the pressure can be seen from Table 5.1. At all extrusion ratios, the extrusion pressure is higher for a die angle of 60° than its corresponding value for a die angle of 45°. Unfortunately, this final point cannot be concluded from the experimental results since all experiments were conducted at a die angle of 60°. In practice, however, the smaller die angle may have some inverse effect, as this decrease would be offset by the increase in friction due to the greater length of the low-angle die for the same extrusion ratio.

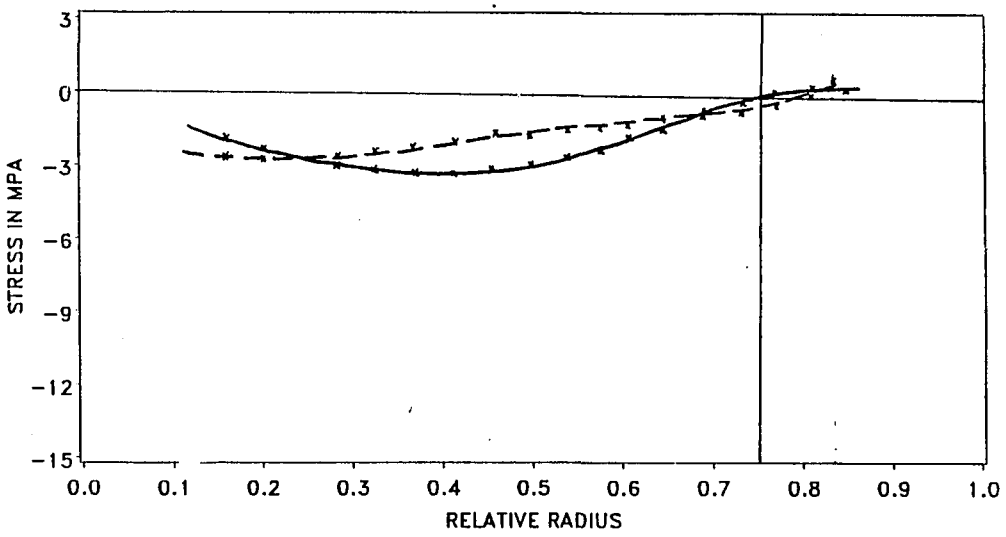

Figure 5.2.1 Radial distribution of radial stresses.

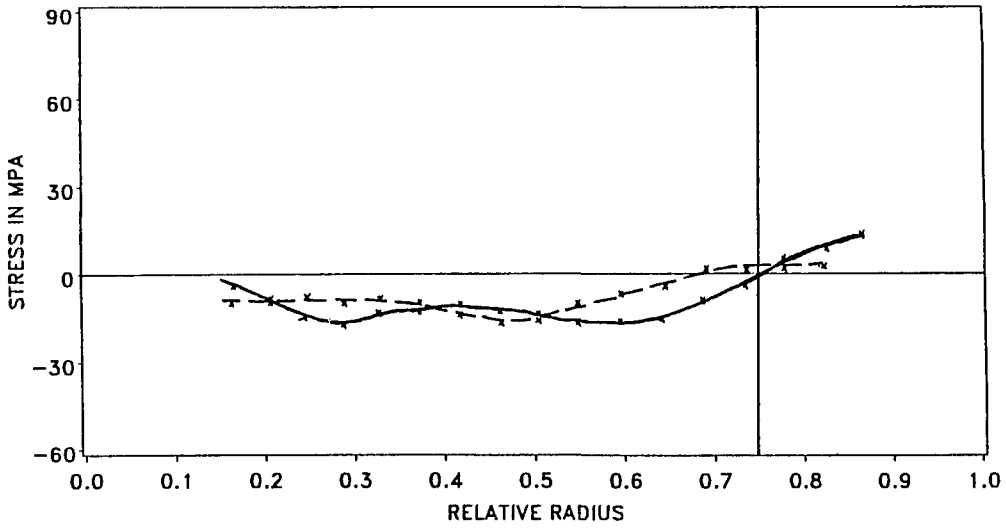

Figure 5.2.2 Radial distribution of axial stresses.

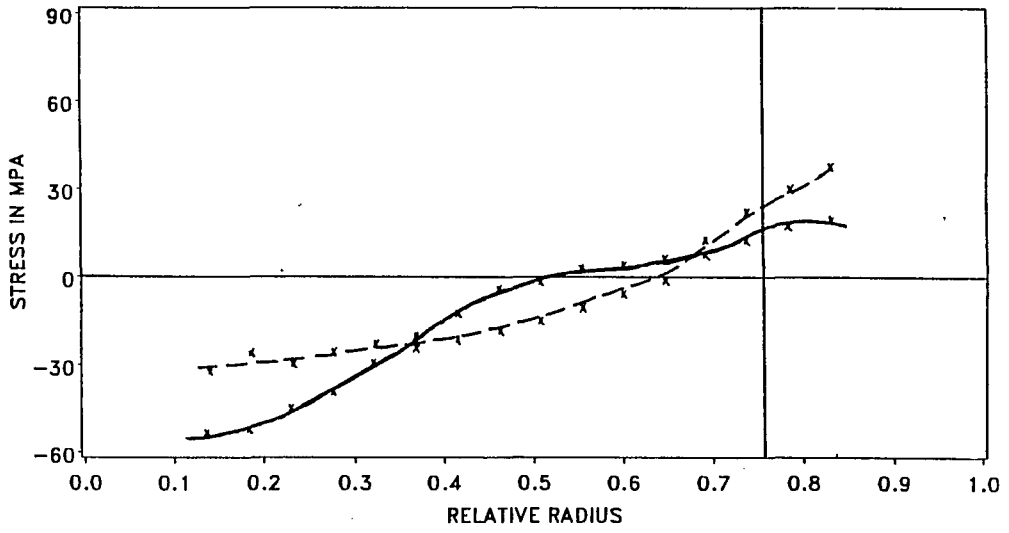

Figure 5.2.3 Radial distribution of tangential stresses.

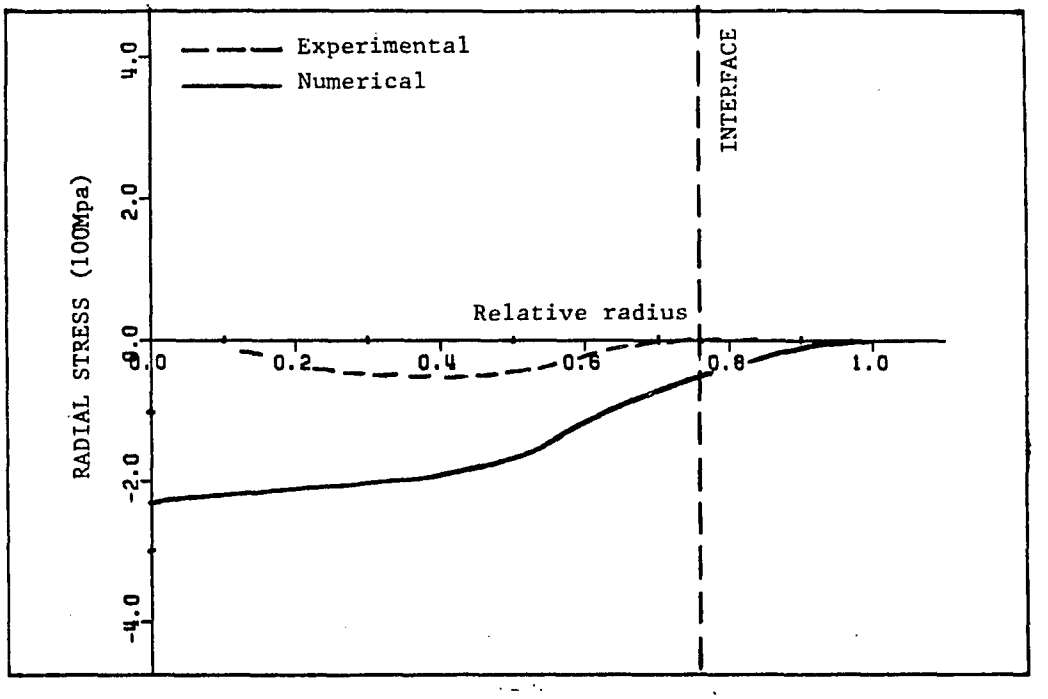

Figure 5.2.4 Radial distribution of radial stresses.

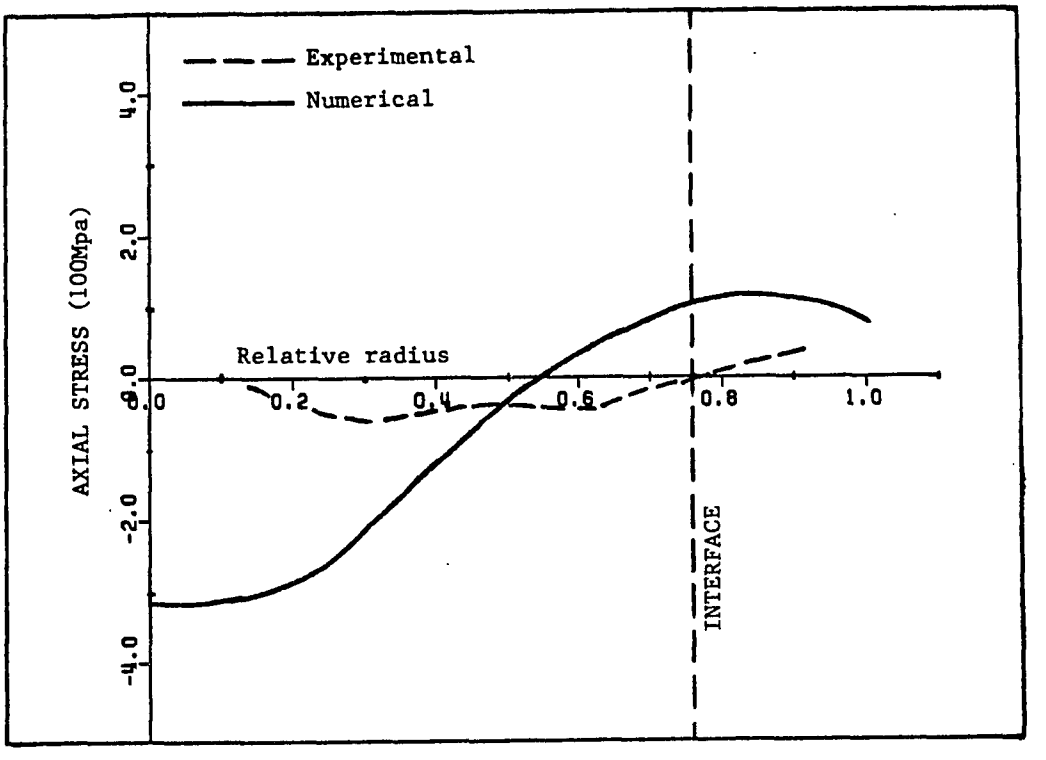

Figure 5.2.5 Radial distribution of axial stresses.

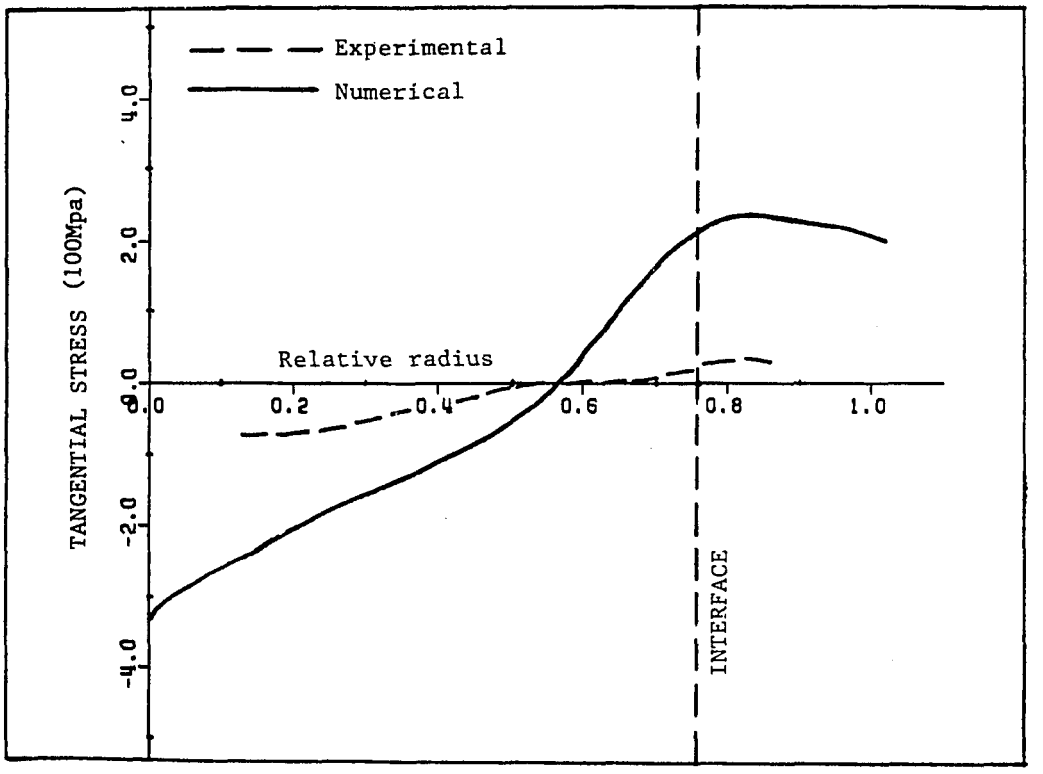

Figure 5.2.6 Radial distribution of tangential stresses.

CHAPTER 6

CONCLUSIONS

6.1 EXTRUSION PRESSURE

Extrusion pressure results obtained show that the extrusion pressure increases linearly with the natural logarithm of the extrusion ratio. Also, higher pressure values are associated with higher die angles. The simulation results are generally greater than the experimental results.

6.2 RESIDUAL STRESSES

Radial residual stresses are compressive throughout the thickness of the product, while the axial and tangential components of stress are compressive in the core and tensile in the clad. The magnitude of the radial stresses, however, is smaller than that of the axial and tangential stresses.

The simulation values obtained for all components of residual stresses are higher than in the experimental results. The trend in most is the same.

The results indicate the continuity of the stress patterns across the interface. This is due to the similarity in the constituents.

REFERENCES

101 Pearson, C.E., Extrusion of Metals, John Wiley & Sons, Inc., London, pp. 5-9, 1944.

102 Peters, F.P., "Producing Lead for Chemical Equipment," Met. Ind., vol. 56, pp. 436-438, 1940.

103 "Collected Experimental Papers of P.W. Bridgman," Harvard University Press, 1964.

104 Hydrostatic Extrusion--Theory and Applications, N. Inoue and M. Nishihara, Eds., Elsevier, London, 1985, p. 1.

105 Fuchs, F.J., The Wire Journal, Oct. 1960, pp. 105-113.

106 Vodar, B. and J. Kieffer, The Mechanical Behavior of Materials Under Pressure, Edited by H.H.D. Pugh, Applied Science Publishers, 1971, pp. 1-53.

107 Beresner, B.J., L.R. Veveshchagin, Yu. N., Izv. Akad. Nank SSSR, Otdl. Tech. Nank, 5 , 1957, pp. 48-55.

108 Vodar and Kieffer, Ibid.

109 Laue, K. and H. Stenger, Extrusion, American Society for Metals, Ohio, p. 5, 1981.

110 Butler, L.H., "The Effect of Lubricants on the Growth of Surface Contact Areas During Plastic Deformation of Metals," J. Inst. Metals, 89:116, 1960.

111 Williams, C.G., "Mechanism of the Action of Extreme Pressure Lubricants, Proc. Royal Society, 212A, p. 512, 1952.

112 Leland, J.F. and J.W. Helms, "Troubles with Cold Extrusion May Be Traced to Lubrication," SAE Journal, p. 43, Nobember 1954.

113 Laue and Stenger, Ibid., p. 89.

114 Ibid.

115 Ibid., p. 98.

116 Massat, H. and B. Vodar, "Forming and Extrusion Apparatus with Accurate Pressure Control Up to 20 kbar," Hydrostatic Extrusion, H.L.D. Pugh, Ed., Mechanical Engineering Publications, London, pp. 59-71, 1974.

201 Bridgman, P.W., Physics of High Pressure, Int. Textbooks of Exact Sciences, Gr. Bells and Sans, Ltd., London, 1949.

202 "Collected Experimental Papers of P.W. Bridgman," Ibid.

203 Hydrostatic Extrusion--Theory and Applications, Ibid. Nishihara,

204 Beresner and Veveshchagin, Ibid.

205 Vodar and Kieffer, Ibid.

206 Nishihara, M., K. Tanaka and T. Muramatsu, Proc. 75h Japan Cong. Test. Mat., vol. 7, p. 154, 1964.

207 Nishihara, M., et. al, Proc. 8th Japan Cong. Test. Mat., vol. 8, p. 73, 1965.

208 Nishihara, M., K. Tanaka, S. Yamamoto and Y. Yamaguchi, J. Soc. Materials Science, Japan, vol. 16, pp. 169-173, 1967.

209 Nishihara, M., K. Tanaka, S. Yamamoto and Y. Yamaguchi, Proc. 10th Japan Cong. Test. Mat., vol. 10, pp. 50-53, 1967.

210 Nishihara, M., and K. Izawa, Science and Engineering Review of Doshisha University, vol. 9, pp. 41-64, 1968.

211 Nishihara, M., Preprints, NEL/AIRAPT International Conference on Hydrostatic Extrusion, Univ. Stirling, Scotland, 1973, pp. 33-81.

212 Fuchs, Ibid.

213 Green, D., Journal of the Institute of Metals, vol. 100, pp. 295-300, 1972.

214 Black, J.T. and W.G. Voorhes, Journal of Engineering for Industry, Trans. ASME, vol. 100, pp. 37-42, 1978.

215 Avitzur, B., The Wire Journal, pp. 73-80, July 1975.

216 Nishihara, M., T. Matsushita and Y. Yamaguchi, Preprints, 14th Annual Meeting of European High Pressure Research Group, Dublin, Ireland, Sept. 6-8, 1976.

217 Inoue, N., and M. Nishihara, Hydrostatic Extrusion, Chapter 2, Elsevier, London, 1985.

218 Ibid., pp. 21-40.

219 Johnson, W. and H. Kudo, The Mechanics of Metal Extrusion, Manchester University Press, 1962.

220 Ewing, D.J.F., J. Mech. Phys. Solids, vol. 15, pp. 105-114, 1967.

221 Collins, I.F., Proc. Roy. Soc. London, A-303, pp. 217-338, 1968.

222 Osakada, K. and Y. Niimi, Int. J. Mech. Sci., vol. 17, pp. 241-254, 1975.

223 Yamaguchi, M., T. Matsushita, M. Nuguchi, and T. Fujita, Proc. 1972 Japanese Spring Conf. Tech. Plasticity, Nagoya, May 11-13, pp. 69-72

224 Johnson and Kudo, Ibid.

225 Hydrostatic Extrusion--Theory and Applications, p. 13.

226 Avitzur, B., R. Wu, S. Talbert and Y.T. Chou, "Criterion for Prevention of Core Fracture During Extrusion of Bimetal Rods," J. Eng. Ind., Trans. ASME Series B, vol. 104, pp. 293-304, 1982.

227 Lowenstein, P.W. and W.B. Tuffin, "Metallurgical Bonding of Dissimilar Metals by Co-extrusion," Met. Eng. Quart, vol. 4, pp. 26-31, 1964.

228 Blazynski, T.Z. and M. Matin, "The Response of Implosively Prewelded Arrays of Rods to Processing by Hydrostatic Extrusion," J. Mech. Work. Technol., vol. 6, pp. 291-302, 1982.

229 Dull, D., E.B. Kendall and L. Raymond, "Ti-Be Composite Produced by Co-extrusion of Powder," Materials Technology - An Interamerican Approach for the 70s, ASME, United Engineering Center, New York, 1970.

230 Johnsson, S., "Recent Developments in Hydrostatic Extrusion," Wire World Intl., vol. 11, pp. 23-27, 1969.

231 Alexander, J.M., "Hydrostatic Extrusion--The State of the Art," CME, vol. 9, pp. 108-111, 1973.

232 Pacheco, L.A. and J.M. Alexander, "On the Hydrostatic Extrusion of Copper-covered Aluminum Rods," Numerical Methods in Industrial Forming Processes, J.F.T. Pittman, R.D. Wood, J.M. Alexander and O.C. Zeinkeiwicz, Eds., Pineridge Press, Swansea, U.K., pp. 205-216, 1982.

233 K. Osakada, M. Limb and P.B. Mellor, "Hydrostatic Extrusion of Composite Rods with Hard Cores," Int. J. Mech. Sci., vol. 15, pp. 291-307, 1973.

234 Hartley, C.S., "Upper Bound Analysis of Extrusion of Axisymmetric Piecewise Homegeneous Tubes," Int. J. Mech. Sci., vol. 15, pp. 651-663, 1973.

235 Lee, E.H., R.L. Mallett and R.M. McMeeking, "Stress and Deformation Analysis of Metal Forming Processes," Numerical Modeling of Manufacturing Processes, PVP-PB-025, R.F. Jones, Jr., H. Armen and J.T. Fond, Eds., ASME, New York, pp. 19-33, 1977.

236 Alexander, J.M. and B. Lengyel, Hydrostatic Extrusion, Mills and Boon, London, 1971.

237 Alexander, J.M. and C.S. Hartley, "On the Hydrostatic Extrusion of Copper-covered Aluminum Rods," Hydrostatic Extrusion, H. L7, D. Pugh, Ed., Mechanical Engineering Publications, London, pp. 72-78, 1974.

238 Lugosi, R., C.S. Hartley and A.T. Male, "The Influence of Interfacial Shear Yield Strength on the Deformation Mechanics of an Axi-Symmetric Two-Component System," Westinghouse Research Lab. Tech. Document No. 77-1D4-PROEN-P1, 1977.

239 Hartley, C.S. and R. Srinivasan, "Constitutive Equations for Large Plastic Deformation of Metals," J. Eng. Mat. Technol., vol. 105, pp. 162-167, 1983.

240 Avitzur, B., "Analysis of Wire Drawing and Extrusions Through Conical Dies of a Large Cone Angle," J. Eng. Ind., Trans. ASME Series B, vol. 87, pp. 89-96, 1965.

241 Avitzur, B., "Hydrostatic Extrusion," J. Eng. Ind. Trans. ASME Series B, vol. 87, pp. 487-493, 1965.

242 Osakada, K., J. Nakano and K. Mori, "Finite Element Method for Rigid-plastic Analysis of Metal Forming--Formulation for Finite Deformation," Int. J. Mech. Sci., vol. 24, pp. 459-468, 1982.

243 Avitzur, B., Metal Forming: Processes and Analysis, Tata-McGraw-Hill, New Delhi, 1977.

244 Osakada, K. and P.B. Mellor, Int. J. Mech. Sci., vol. 15, pp. 291-307, 1973.

245 Prager, W. and P.G. Hodge, Jr., Theory of Perfectly Plastic Solids, Chapman & Hall, Ltd., London, 1951.

246 Avitzur, B., "The Production of Bi-metal Rod and Wire," The Wire Journal, vol. 3, pp. 42-49, 1970.

301 McHenry, D., "A Lattice Analogy for the Solution of Plane Stress Problems," J. Inst. Civ. Eng., vol. 21, pp. 59-82, 1943.

302 Newmark, N.M., "Numerical Methods of Analysis in Bars, Plates, and Elastic Bodies," Numerical Methods in Analysis in Engineering, L.E. Grintner, Ed., Macmillan, 1949.

303 Hrenikoff, A., "Solution of Problems in Elasticity by the Framework Method," J. Appl. Mech., A8, pp. 169-175, 1941.

304 Turner, M.J., R.W. Clough, H.C. Martin, and L.J. Topp, "Stiffness and Deflection Analysis of Complex Structures," J. Aero. Sci., 23:9, pp. 805-823, 1956.

305 Clough, R.W., "The Finite Element in Plane Stress Analysis," Proc. 2nd ASCE Conf. on Electronic Computation, Pittsburgh, Pa., Sept. 1960.

306 Melosh, R.J., "Structural Analysis of Solids," Proc. ASCE, ST4, pp. 205-223, Aug. 1963.

307 Zienkiewicz, O.C. and Y.K. Cheung, "Finite Elements in the Solution of Field Problems, The Engineer, pp. 507-510, 1965.

308 Wilson, E.L. and R.E. Nickell, "Application of Finite Element Method to Heat Conduction Analysis," Nucl. Eng. Design, vol. 4, pp. 1-11, 1966.

309 Visser, W., "A Finite Element Method for the Determination of Non-stationary Temperature Distribution and Thermal Deformations," Proc. Conf. on Matrix Methods in Structural Mechanics, Air Force Inst. Tech., Wright-Patterson Air Field Base, Ohio, 1965.

310 Ghaboussi, J. and E.L. Wilson, "Flow of Compressible Fluids in Elastic Media," Int. J. Num. Meth. Eng., vol. 5, pp. 419-442, 1973.

311 ABAQUS: A General Purpose Nonlinear Finite Element Program, Hibbit, Karlsson, and Sorensen, Inc., 1982.

312 Chandra, A. and S. Mukherjee, "Boundary Element Formulations for Large Strain--Large Deformation Problems of Viscoplasticity," Int. J. Solids Structures, 20:1, pp. 41-53, 1984.

313 Osias, J.R. and J.L. Swedlow, "Finite Elasto-plastic Deformation: I-Theory and Numerical Examples," Int. J. Solids Structures, vol. 10, pp. 321-339, 1974.

314 Lee, E.H., "Elasto-plastic Deformation at Finite Strains," J. Appl. Mech., vol. 36, pp. 1-6, 1969.

315 Hibbit, H.D., P.V. Marcal, and J.R. Rice, "A Finite Element Formulation for Problems of Large Strain and Large Displacement," Int. J. Solids Structures, vol. 6, pp. 1069-1086, 1970.

316 Nagtegaal, J.C. and J.E. De Jong, "Some Computational Aspects of Elastic-plastic Large Strain Analysis," Int. J. Num. Meth. Eng., vol. 17, pp. 15-41, 1981.

317 Turner, M.J., E.H. Dill, H.C. Martin, and R.J. Melosh, "Large Deflections of Structures Subjected to Heating and External Loads," J. Aerospace Sci., vol. 27, pp. 97-102, 1960.

318 Nemat-Nasser, S., "Decomposition of Strain Measures and Their Rates in Finite Deformation Elastoplasticity," Int. J. Solids Structures, vol. 15, pp. 155-166, 1979.

319 Lee, E.H. and R.M. McMeeking, "Concerning Elastic and Plastic Components of Deformation," Int. J. Solids Structures, vol. 16, pp. 715-721, 1980.

320 Lee, E.H., "Analyses of the Propagation of Plane Elastic-plastic Waves of Finite Strain," J. Appl. Mech., vol. 34, pp. 931-936, 1967.

321 Lee, E.H., R.L. Mallett, and R.M. McMeeking, "Stress and Deformation Analysis of Metal Forming Processes," Numerical Modeling of Manufacturing Processes, PVP-PB-025, R.F. Jones, H. Armen, and J.T. Fong, Eds., ASME, pp. 19-33, 1977.

322 McMeeking, R.M. and J.R. Rice, "Finite Element Formulations for Problems of Large Elastic-plastic Deformation," Int. J. Solids Structures, vol. 11, pp. 601-616, 1975.

323 Lee, E.H. and R.L. Mallett, "Stress and Deformation Analysis of the Metal Extrusion Process," Comp. Meth. in Appl. Mech. Engr., vol. 10, pp. 339-353, 1977.

324 ABAQUS: Theory Manual, Ibid.

325 Lubarda, V.A. and E.H. Lee, "A Correct Definition of Elastic and Plastic Deformation and Its Computational Significance," J. Appl. Mech., vol. 48, 35-40, 1981.

326 Yamada, Y., N. Yoshimura, and T. Sakurai, "Plastic Stress Strain Matrix and Its Application for the Solution of Elastic-plastic Problems by the Finite Element Method," Int. J. Mech. Sci., vol. 10, 1968.

327 Ramm, E., "Strategies for Tracing the Nonlinear Response Near Limit Points," Nonlinear Finite Element Analysis in Structural Mechanics, W. Wundelich, E. Stein, and K.J. Bathe, Eds., Springer-Verlag, Berlin, 1981.

401 Lovic, W.R., N.C. Iyer, and A.T. Male, "Deformation Processing by Hydrostatic Co-extrusion: Status Report," Westinghouse R & D Center Report No. 81-2D4-CODEF-R1, 1981.

402 Sachs, G., "Der Nachwies innerer Spannungen in Stangen und Rohren," Z. Metall., vol. 19, pp. 352-357, 1927.

403 Lambert, J.W., "A Method of Deriving Residual Stress Equations," Experimental Stress Analysis, vol. 12, pp. 91-96, 1954.

404 Timoshenko, S. and Goodier, Theory of Elasticity, New York, McGraw-Hill, 1951.

405 Kato, B. and H. Aoki, "Residual Stresses in Cold Formed Tubes," J. of Strain Analysis, vol. 13, pp. 193-204, 1978.

406 Springborn, R.K., Ed., Non-traditional Machining Processes, ASME, Dearborn, Mich., 1967.

407 Hoare, J. and M. LaBoda, "Electrochemical Machining," Techniques of Electrochemistry, Vol. 3, E. Yeager and A.J. Salkind, Eds., John Wiley & Sons, New York, pp. 48-104, 1978.

408 McGeough, J.A., Principles of Electrochemical Machining, Chapman & Hall, London, 1974.

VITA

Mohammad Dehghani was born on August 22, 1955, in Tehran, Iran. After completing primary and secondary education in Tehran's high schools, he joined the Iranian armed forces in November 1975.

In June 1977 he entered Louisiana State University in Baton Rouge, Louisiana. He earned his B.S. degree in December 1980 and his M.S. degree in August 1982, both in Mechanical Engineering. He then began the Ph.D. program in Mechanical Engineering.

DOCTORAL EXAMINATION AND DISSERTATION REPORT

Candidate: Mohammad M. Dehghani

Major Field: Mechanical Engineering

Title of Dissertation: Computer Simulation of Hydrostatic Co-Extrusion of Bimetallic Compounds

Approved:

Major Professor and Chairman

Dean of the Graduate School

EXAMINING COMMITTEE:

Thomas P. Zacharias

Date of Examination:

June 29, 1987